DRAW RESONANCE INSTABILITY IN COEXTRUSION FIBER SPINNING

By

WOEI-SHYONG LEE

A DISSERTATION PRESENTED TO THE GRADUATE SCHOOL
OF THE UNIVERSITY OF FLORIDA IN PARTIAL FULFILLMENT
OF THE REQUIREMENTS FOR THE DEGREE OF
DOCTOR OF PHILOSOPHY

UNIVERSITY OF FLORIDA

1993

UNIVERSITY OF FLORIDA LIBRARIES

This dissertation is dedicated to my parents and my wife for their understanding, love, and patience, and to my daughter for the joy she has brought to my life.

ACKNOWLEDGMENTS

I wish to express my thanks and appreciation to my advisor Professor Chang-Won Park for his constant guidance throughout this research and for his invaluable help in doing the experiments and writing this dissertation. Also, I would like to thank Dr. Do-Young Yoon and Mr. Kun-Sang Yoon for their help during this work. I would also like to thank Professor Narayanan, Professor Fricke, Professor Johns and Professor Walker as members of the supervisory committee for their advice and support.

I wish to thank Dr. Walker of the Department of Physics at University of Florida, US Department of Engery, National Science Foundation and Electric Power Research Institutite for their supporting this work. I also acknowledge the support given by Drs. K. C. H. Yi and N. J. Maraschin of Union Carbide Corporation and Drs J. Harmon of the Department of Physics at University of Florida for providing the materials for the experiments. I am grateful to Dr. Fricke for allowing me using the rheogoniometer and Mr. Zaman for his help in measuring the rheological properties of materials.

Finally, I would like to extend my thanks to all the people in the department main office, accounting office, other laboratories and machine shop who have been helpful and kind.

TABLE OF CONTENTS

page

ACKNOWLEDGMENTS iii

LIST OF TABLES vi

LIST OF FIGURES vii

ABSTRACT xi

CHAPTERS

1 INTRODUCTION 1

- 1.1 Description of Fiber Spinning 1
- 1.2 Definition of Draw Resonance 4
- 1.3 Instabilities in Fiber Spinning Flow 5
- 1.4 Coextrusion 6
- 1.5 Scope of this Study 7

2 STEADY FLOW ANALYSIS 10

- 2.1 Introduction 10
- 2.2 Problem Formulation and Scalings 11
  - 2.2.1 Spinning Equations 13
  - 2.2.2 Constitutive Equations 14
  - 2.2.3 Scalings and Dimensionless Governing Equations 15
- 2.3 Boundary Conditions 17
- 2.4 Steady State Solutions 20
- 2.5 Effect of Hoop Stress 32
- 2.6 Effect of Initial Shear Stress 34
- 2.7 Effect of Shear Viscosity Ratio M 37
- 2.8 Summary and Conclusion 43

3 LINEAR STABILITY ANALYSIS 45

- 3.1 Introduction 45
- 3.2 Stability of Isothermal Newtonian Fiber Spinning Flow 46
- 3.3 Stability of Isothermal UCM Fiber Spinning Flow 47

3.4 Stability of Two-Phase Fiber Spinning Flow 47
3.5 Results and Discussion 51
3.6 Summary and Conclusion 69

4 DRAW RESONANCE EXPERIMENTS 71

4.1 Introduction 71
4.2 Experiment Materials 72
4.3 Coextrusion Fiber Spinning 81
4.4 Results and Discussion 84
4.5 Summary and Conclusion 98

5 FABRICATION OF PLASTIC OPTICAL FIBERS 100

5.1 Introduction 100
5.2 New Processing 102
5.3 Optical Fiber Spinning 105
  5.3.1 Experiments 105
  5.3.2 Styrene Core Fibers 106
  5.3.3 Modification of the Spinning Equipment 107
  5.3.4 Styrene-Hexyl Methacrylate Copolymer 107
  5.3.5 Polysiloxanes 109
  5.3.6 Uniformity of Fiber Radius 111
5.4 Summary and Conclusion 111

6 SUMMARY AND CONCLUSION 112

APPENDICES

A THE FINITE DIFFERENCE APPROACH OF EIGENVALUE PROBLEMS 115

B THE MAXIMUM DRAW RATIO 123

C COMPUTER PROGRAMS 126

REFERENCE LIST 143

BIOGRAPHICAL SKETCH 148

LIST OF TABLES

Table page

1 Values of λ^1 for isothermal, Newtonian spinning at Dr=20.21 48

2 Values of λ^1 for differential values of discretisation points (De=0.02, Dr=30, t_0=10.0, M=1.0) 52

3 Real and imaginary parts of first four eigenvalues at the critical Dr^* (f=0.2, De=0.015, t_0=10.0, M=1.0) 62

4 The properties of experiment materials 74

LIST OF FIGURES

Figure page

1 Schematic of fiber spinning process 3

2 Schematic of coextrusion fiber spinning 12

3 Draw ratio as a function of inverse axial force at $De=0.02$, $M=1$, $t_0=10$; a: $G=0.023$, $Dr=60$; b: $G=0.064$, $Dr=60$; c: $G=0.046$, $Dr=71$ 24

4 Inverse axial force as a function of Deborah number, De:
  (a) $Dr=20$, $t_0=10$ (asymptotic solution, $G\rightarrow 0$: 1. $De=0.046$, 2. $De=0.047$, 3. $De=0.050$) 26
  (b) $Dr=30$, $t_0=10$.(asymptotic solution, $G\rightarrow 0$: 1. $De=0.031$, 2. $De=0.032$, 3. $De=0.033$) 27

5 Inverse axial force as a function of Deborah number, De at different draw ratios when $f=0.2$, $t_0=10$, $M=1$ 29

6 Steady state axial velocity profiles:
  (a) $Dr=30$, $De=0.02$, $t_0=10$, $M=1$ 30
  (b) $Dr=40$, $De=0.02$, $t_0=10$, $M=1$ 31

7 Normal stress distribution along the flow direction at different initial values of normal stress:
  (a) $f=0.2$, $Dr=30$, $De=0.02$, $t_0=10$, $M=1$ 35
  (b) $f=0.5$, $Dr=30$, $De=0.02$, $t_0=10$, $M=1$ 36

8 Shear stress distribution along the flow direction at different initial values of shear stress:
  (a) $f=0.2$, $Dr=30$, $De=0.02$, $t_0=10$, $M=1$ 38
  (b) $f=0.5$, $Dr=30$, $De=0.02$, $t_0=10$, $M=1$ 39

9 Steady state axial velocity profiles at different initial values of shear stress:
  (a) $f=0.2$, $Dr=30$, $De=0.02$, $t_0=10$, $M=1$ 40
  (b) $f=0.5$, $Dr=30$, $De=0.02$, $t_0=10$, $M=1$ 41

10 Draw ratio as a function of inverse axial force at different shear viscosity ratios; De=0.02, t_0=10 42

11 Variation of the real part of the first eigenvalue with draw ratio for various Deborah numbers at f=0.5, t_0=10, M=1 53

12 Critical draw ratio as a function of Deborah number for various f at t_0=10, M=1 (maximum attainable Dr for (a) f=0.2(Max); (b) f=0.2(Asymptote); (c) f=0.5 and 1.0) 55

13 Draw ratio as a function of inverse axial force (f=0.2, De=0.02, t_0=10, M=1) 57

14 Draw ratio as a function of inverse axial force for various Deborah numbers (f=0.2, t_0=10, M=1) 59

15 Inverse axial force as a function of Deborah number for various draw ratios (f=0.2, t_0=10, M=1) 61

16 Neutral-stability curve for f=0.2, t_0=10, M=1. Values of λ^1_{imag} indicated on curve 64

17 Period of the first normal mode at critical conditions. Values of λ^1_{imag} indicated on curve 65

18 Dimensionless period as a function of residence time for various f at t_0=10 and M=1 67

19 Critical draw ratio as a function of Deborah number for various M at f=0.2, t_0=10, compared with that for f=1.0(UCM), M=1 and t_0=10; curves: neutral-stability curves, straight lines: maximum draw ratio locus 68

20 Shear viscosity function η versus shear rate $\dot{\gamma}$ of linear low-density polyethylene at 200°C: (○) HS-7028; (□) DMDA-8320, and low-density polyethylene at 145°C: (Δ) DYNH-1; (✶) Alathon-1540 76

21 Shear stress τ_{12} versus shear rate $\dot{\gamma}$ of linear low-density polyethylene at 200°C: (○) HS-7028; (□) DMDA-8320, and low-density polyethylene at 145°C: (Δ) DYNH-1; (✶) Alathon-1540 77

22 Normal stress difference N_1-N_2 versus shear rate $\dot{\gamma}$ of linear low-density polyethylene at 200°C: (O) HS-7028; (☐) DMDA-8320, and low-density polyethylene at 145°C: (Δ) DYNH-1; (✶) Alathon-1540 78

23 Normal stress function $\Psi_1-\Psi_2=(N_1-N_2)/\dot{\gamma}^2$ versus shear rate $\dot{\gamma}$ of linear low-density polyethylene at 200°C: (O) HS-7028; (☐) DMDA-8320, and low-density polyethylene at 145°C: (Δ) DYNH-1; (✶) Alathon-1540 79

24 Schematic of coextrusion fiber spinning system 82

25 Schematic of coextrusion die 83

26 Variation of fiber diameter with increasing draw ratio; (f=0.23, draw span L=3 cm) 85

27 Period t^* of draw resonance versus L/w_0 for the coextrusion of
(a) LLDPE(HS-7028)/LDPE(DYNH-1): (O) 100% HS-7028; (—) Newtonian theory; (☐) 20% DYNH-1; (Δ) 50% DYNH-1; (✶) 80% DYNH-1 87
(b) LLDPE(HS-7028)/LDPE(Alathon-1540): (O) 100% HS-7028; (—) Newtonian theory; (☐) 20% Alathon-1540; (Δ) 50% Alathon-1540; (✶) 80% Alathon-1540 88
(c) LLDPE(HS-7028)/LDPE: (O) 100% HS-7028; (—) Newtonian theory; (☐) 50% DYNH-1; (Δ) 50% Alathon-1540 89

28 The maximum-to-minimum diameter ratio as a function of draw ratio for the combination of 20%–LDPE(DYNH-1)/80%–LLDPE(HS-7028) at three different draw spans: (O) L=3 cm; (☐) L=6 cm; (Δ) L=10 cm 92

29 Variation of the maximum-to-minimum diameter ratio for three combinations of
(a) LDPE(DYNH-1)/LLDPE(HS-7028) 93
(b) LDPE(Alathon-1540)/LLDPE(HS-7028) 94
at different draw spans: (O) L=3 cm; (☐) L=6 cm; (Δ) L=10 cm

30 Critical draw ratio as a function of skin-layer flow rate fraction for different combinations at different draw spans: (O) L=3 cm; (☐) L=6 cm; (Δ) L=10 cm. Core: LLDPE(HS-7028); Skin: LDPE (—: Alathon-1540, ------ : DYNH-1) 95

31 Critical draw ratio as a function of skin-layer flow rate fraction for different combinations at *L*=6 cm:
(1) Core:LLDPE(HS-7028); Skin:LDPE(Alathon-1540)
(2) Core:LLDPE(DMDA-8320);Skin:LDPE(Alathon-1540)
(3) Core:LLDPE(HS-7028); Skin:LDPE(DYNH-1)
(4) Core:LLDPE(DMDA-8320);Skin:LDPE(DYNH-1) 97

32 Experimental set-up for the spinning of plastic optical fibers 103

33 Batch reactor attachment for the plastic optical fiber spinning 108

34 Maximum attainable draw ratio as a function of Deborah number for *f*=0.2,0.5 and 1.0 at t_0=10.0 (—), and true maximum draw ratio as a function of Deborah number for *f*=0.2 at t_0=10.0 (-----) 125

Abstract of Dissertation Presented to the Graduate School
of the University of Florida in Partial Fulfillment of the
Requirements for the Degree of Doctor of Philosophy

DRAW RESONANCE INSTABILITY IN COEXTRUSION FIBER SPINNING

By

Woei-Shyong Lee

August 1993

Chairperson: Dr. Chang-Won Park
Major Department: Chemical Engineering

The draw resonance instability of a bicomponent coextrusion fiber spinning has been studied theoretically and experimentally. For the theoretical analysis a simple model has been adopted in which a Newtonian and an upper-convected Maxwell fluid is the core and the skin layer, respectively. This model is chosen to investigate a two-phase flow in which the two fluids have quite different extensional rheology. The results indicate that the viscoelastic skin layer has a stabilizing influence in which the onset of draw resonance of a Newtonian fluid is delayed to a higher draw ratio by the coextrusion. An unexpected behavior of the coextrusion flow is predicted in that the highest draw ratio for a stable coextrusion spinning can be larger than that of the single-phase spinning of either fluid (Newtonian or upper-convected Maxwell) under certain conditions. In the experimental study a linear low-density polyethylene and a low-density polyethylene were used as the core and the skin, respectively. These materials have been chosen to simulate the flow situation considered in the theoretical investigation. While the theoretical model is too simple to provide a quantitative agreement with the experiment, various aspects of the experimental observations appear to be in qualitative agreement with the theoretical predictions.

A novel processing method has been developed for the fabrication of plastic optical fibers in which a modified coextrusion fiber spinning technique is used. Lab scale experiments have demonstrated that the new method is capable of fabricating defect-free clad fibers using several different types of materials. The new method is possible because the mechanics of the bicomponent spinning flow is controlled by the viscoelastic cladding material under typical spinning conditions as the process modeling study has indicated.

CHAPTER 1
INTRODUCTION

1.1 Description of Fiber Spinning

An important industrial process for manufacturing artificial fibers is called the fiber spinning process in which a polymer material is continuously extruded downward through a spinneret or through a die to form an extrudate of circular (or noncircular) cross section. Somewhere downstream of the spinneret the extrudate is pulled by a take-up machine to form a thin filament. The technique of spinning synthetic fibers has made significant progress during the past thirty years. New spinning processes, as well as new varieties of man-made fibers, have been developed. For a given fiber-forming material, different spinning techniques can sometimes produce fibers having markedly improved physical and/or mechanical properties. The fiber industry has therefore made continuous efforts to modify existing processes and develop new ones. There have been two recent developments in fiber spinning technology: the production of "shaped" fibers and the production of "coextrusion" (or bicomponent) fibers. A shaped fiber is one whose cross section is noncircular. A coextrusion fiber consists of two different components, extruded side by side. Each of them has its advantages over fibers made in the conventional way.

One of the conventional types of spinning processes is commonly known as "melt spinning" in which a fiber can be made by extruding molten polymer and allowing the thread to solidify. In melt spinning, fluid elements are subjected to a strong elongational flow. Unlike shearing flows, the elongational flows generally constitute a free-boundary problem. The elongational flow of a fiber spinning process has been given substantial attention in the last three decades, due to the increasing importance of the economics of synthetic fiber production and the quality of the product. The typical characteristic of the elongational flows including the melt spinning can be found in the monographs by Ziabicki (1976), Petrie (1979), and Denn (1980).

The melt spinning process is shown schematically in Figure 1. The fiber-forming zone consists of three regions: die swell region, draw-down region and solid region. Die swell is caused by the stress relaxation as the material leaves the confining geometry of die or spinneret. Viscoelasticity of polymers typically results in a much larger die swell than purely viscous materials. The dependence of the die swell on rheological properties and on the die geometry is quite complicated, and the theoretical prediction of the die swell is as yet incomplete. Many experimental results have shown that for a given polymer at a given temperature die swelling increases as output rate increases, and as die length and die diameter decrease (Bergonzoni and DiCresce, 1966). The die swell region is followed by the draw-down region in which the molten polymer is drawn to a fine filament as the axial velocity increases to the predetermined take-up velocity. Because of the die swell the fiber diameter near the spinneret can not be predicted accurately. However, this region of uncertainty is restricted to a small region within a few spinneret diameters of the die exit, and most of the spinning length corresponds to the draw-down region. In the analyses of the fiber spinning flow, therefore, the initial filament diameter is typically taken as either the maximum observed value or the spinneret diameter itself. The location of the point of solidification may be controlled precisely by rapid quenching with blowing air, a water bath or a chill roll.

At the early stage of the analyses, researchers usually have neglected any interactions between the fiber and the surrounding medium (i.e., air). Under these assumptions the flow is isothermal and no shear or normal stresses act on the filament

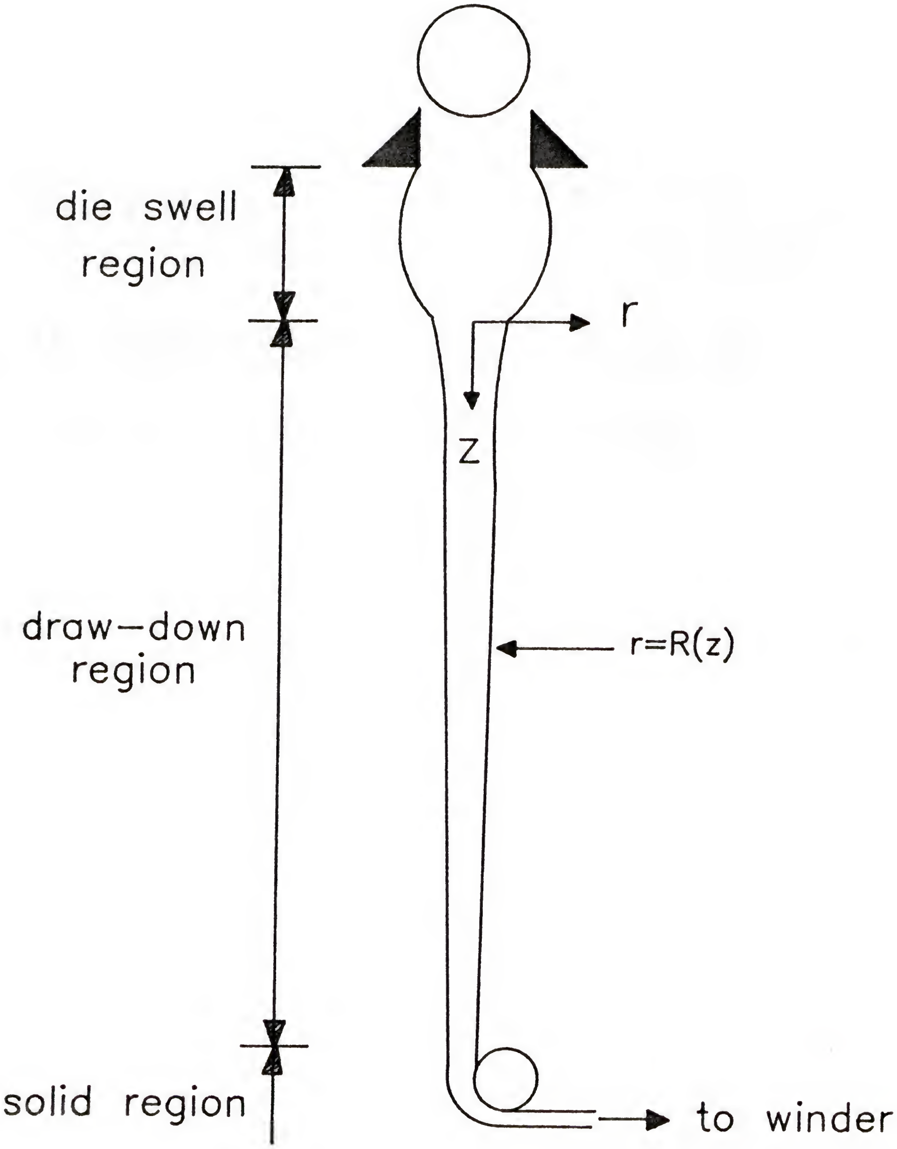

Figure 1. Schematic of fiber spinning process

boundary (Matovich and Pearson, 1969; Shah and Pearson, 1972a, 1972b; Spearot and Metzner, 1972; Donnelly and Weinberger, 1975; Denn, Petrie and Avenas, 1975; Fisher and Denn, 1975a, 1975b, 1976; Chang and Denn, 1979, 1980; Chang, Denn and Geyling, 1981; Kase and Nakajima, 1980; Larson, 1983). A nonisothermal analysis may simulate the real situation more closely. However, the inclusion of energy equation coupled with the equation of motion only makes the system to be more complicated without seriously affecting the fundamental characteristics of the fiber spinning flow (Kase and Matsuo, 1965, 1967; Shah and Pearson, 1972a, 1972b; Nakamura, et al., 1972, 1974; Fisher and Denn, 1977; Gupta and Metzner, 1982).

The most important aspect of the fiber spinning flow is that the fiber is slender and its diameter varying slowly in the flow direction. This allows an asymptotic analysis which result in a one-dimensional representation of the fiber spinning flow (Schultz and Davis, 1982, 1984a; Park, 1990).

1.2 Definition of Draw Resonance

When polymer melts are subjected to fast drawing processes such as fiber spinning, extrusion coating, or film casting, an instability phenomenon called "draw resonance" is often encountered in which the fiber radius (or the film thickness) and the take-up force fluctuate periodically. This instability occurs when the draw ratio, which is defined as the ratio of the take-up to the extrusion velocity, is greater than a certain critical value and the fluctuation is observed to be sustained with a well-defined period and amplitude. The terminology of "draw resonance" was coined by Christensen (pp.752, 1962): "Surging, or draw resonance, is defined as a non-uniformity of gauge, or coating weight, in the machine direction," and its periodic nature was first described by Miller (pp.137, 1963): "Sustained periodic fluctuation of fiber radius (or film thickness) which occurs above a certain critical take-up velocity (or draw ratio)." The draw resonance has been studied extensively ever since due to its industrial importance. Among the various drawing processes, the fiber spinning has been studied most extensively probably because its geometry is simpler than the other processes. Despite their geometric differences, however, the development and understanding of the fiber spinning process is directly applicable to extrusion coating and film casting processes since the mathematical descriptions in modeling these processes are analogous.

The theory of draw resonance was first developed independently by Kase and Matsuo (1965, 1967) and by Pearson and Matovich (1969). These analyses were carried out for an isothermal spinning of a Newtonian fluid under the assumption that the inertia, gravity, and surface tension effects were negligible. Their results predicted that the critical draw ratio for the onset of draw resonance is 20.21. The theory was then extended to power law fluids and viscoelastic fluids (Denn et al., 1975; Fisher and Denn, 1976; Phan-Thien, 1978, 1987; Petrie, 1979; Larson, 1983; Phan-Thien and Caswell, 1986; Gupta et al., 1986; Mackay and Petrie, 1992). These studies have shown that the shear thinning behavior of polymeric fluids has a destabilizing effect whereas the viscoelasticity has a stabilizing effect. The theoretical predictions are generally in reasonable agreement with many experimental observations at least qualitatively (Christensen, 1962; Donnelly and Weinberger, 1975; Matsumoto and Bogue, 1978; Chang and Denn, 1979; Demay and Agassant, 1985). A thorough survey of numerous studies on the subject was given in a review paper by Petrie and Denn (1976), and an updated list of references can be found in more recent papers by Denn (1980, 1983) and Mewis and Petrie (1987).

1.3 Instabilities in Fiber Spinning Flow

Many different types of instabilities are encountered in polymer processing. From a practical standpoint it is important to identify the parameters which dictate the instability and to understand the instability behaviors as affected by the parameters.

In the fiber spinning process, there may be three different types of instabilities; melt fracture, draw resonance and fiber breakage. The melt fracture phenomenon, which results in surface roughness, is common to most extrusion processes. This instability occurs if an excessive shear stress is imposed on the polymer flow. Although it is generally agreed that this instability may be related to the stick-slip phenomenon at the polymer-metal interface (i.e., die surface), theoretical understanding of it is only at the seminal stage at the present time. Such melt fracture often limits the output rate of a fiber spinning system, since successful spinning usually requires a smooth extrudate.

The other types of spinning instability arise not from the shear flow in the die but from the free-boundary flow in the drawing region between the spinneret and the take-up point. The draw resonance, in which the fiber diameter fluctuates periodically, may be a kinematic instability as it is predicted without all external and surface forces except the viscous force. Only the polymers with a very low viscoelasticity are susceptible to this instability since a large viscoelasticity may alter the flow kinematics significantly.

The polymers with a large viscoelasticity exhibit fiber breakage instead of draw resonance. Since the breakage may occur as the stress imposed on the fiber exceeds the cohesive strength of the material, it may not be an instability phenomenon in a fluid mechanical sense.

In this thesis, the major emphasis is on the theoretical and experimental investigation of the draw resonance.

1.4 Coextrusion

All the analyses described in section 1.2 are for a "single-phase" flow, and few studies have been devoted to a "multi-phase" flow. A multi-phase flow refers to a flow situation in a coextrusion process; two or more polymers are processed simultaneously to produce composite materials such as multilayer films or cladded fibers (e.g., optical fibers). The coextrusion process has been known for many years and has been broadly used for numerous applications in the plastics industry. Nevertheless, there exist relatively few fundamental studies on the subject (Han, 1975; Waters and Keeley, 1987). As was indicated in many studies on single-phase fiber spinning, the characteristics of draw resonance (i.e., critical draw ratio, amplitude and period) depend on the fluid rheology. Thus, a unique flow situation is encountered in coextrusion processes when the rheological properties of the constituent polymers are quite different from one another.

One such example may be the coextrusion of a linear low-density polyethylene and a low-density polyethylene. The former is known to be very prone to draw resonance whereas the latter is not. The spinnability of a low-density polyethylene is typically limited by the breakage of spinline as the stress in the melt may exceed the cohesive strength of the material (Ziabicki, 1976). The difference in the stability behaviors of the two materials may result from the fundamental differences in their rheological properties. A low-density polyethylene, which has a high degree of long chain branching, has a larger relaxation time than a linear low-density polyethylene. Consequently, the former tends to show a distinct strain hardening behavior when subjected to an elongational flow whereas the latter does not (Chang and Lodge, 1972; Spearot and Metzner, 1972; Minoshima and White, 1986a, 1986b). If these two materials are coextruded, their flow mechanics may be strongly influenced by the rheological interactions of the two materials.

1.5 Scope of this Study

This thesis is a theoretical and experimental study of the fundamentals of a two-phase coextrusion fiber spinning. In chapter 2 one-dimensional equations are presented for the steady flow of a two-phase coextrusion fiber spinning. As pointed out previously, the one-dimensional equations are obtained as a result of an asymptotic analysis in which the aspect ratio of the slender fiber is the small parameter. Simple constitutive models (Newtonian and upper-convected Maxwell models) are chosen to represent the two-phase system so that the competing influence of viscous and viscoelastic forces is investigated. Some discussions and computations are also given to explain the boundary conditions which have been used for the present analysis.

In chapter 3 the stability of the steady flow to an infinitesimal disturbance is investigated. The stability criteria are given by the neutral-stability curves not only for the single-phase flow (Newtonian or upper-convected Maxwell fluids) but also for the two-phase flow (the combination of a Newtonian and a UCM fluid). Considering the periodic nature of the draw resonance, the linear stability analysis is useful and informative.

In chapter 4 experimental investigation of the draw resonance is presented. A linear low-density polyethylene and a low-density polyethylene have been used for the study as the core and the skin layer, respectively. This choice of materials has been made to simulate the flow situation considered in the theoretical investigation. The theoretical model is too simple to expect a quantitative agreement with the experiment. Nevertheless, various aspects of the experimental observations appear to be in qualitative agreement with the predictions of the linear stability analysis. The results in fact show similarities in various trends. The critical draw ratios, the ratios of fiber maximum to minimum radius, and periods are measured and analyzed. The results show that the core-layer material is stabilized when the skin-layer material is a viscoelastic material. This observation may be of important industrial implication.

In chapter 5, a modified coextrusion fiber spinning process is applied to fabricate plastic optical fibers using non-conventional materials. Initially the experiment was conducted specifically for the on-going efforts to develop radiation hard scintillating optical fibers for the Superconducting Super Collider. This new approach was then extended to make plastic optical fibers using various polymeric materials which cannot be formed into optical fiber by the conventional process technique of thermal-drawing. As the major emphasis of the experiments was on the processing aspects, little attention has been given to monitoring the optical properties of the fiber thus fabricated.

The summary and conclusion of this dissertation are finally given in chapter 6.

CHAPTER 2
STEADY FLOW ANALYSIS

2.1 Introduction

The fiber spinning process has been investigated to date from several different aspects; steady-state characteristics, stability behaviors and the die swell under applied axial force. The early investigations focused on the single-phase fiber spinning of isothermal Newtonian fluid (Kase and Matsuo, 1965, 1967; Matovich and Pearson, 1969). During the last several decades, the reaserchers have considered the power-law fluid and various viscoelastic models (Shah and Pearson, 1972c; Denn, Petrie and Avenas, 1975; Ishihara and Kase, 1976; Petrie, 1978). The essential difficulty in analyzing the motion of a viscoelastic liquid is the choice of the constitutive equation. The constitutive or rheological equation of state is the relation between stress and deformation of a material. Petrie (1979) states: "We do not know what equations we should be solving but are interested in the way the choice of constitutive equation interacts with the dynamics and affects the mathematical problem to be solved (pp.2)."

The first theoretical analysis on the two-phase fiber spinning flow was conducted by Park (1990). As in his study, the present analysis also adopts a simple system in which a Newtonian and an upper-convected Maxwell fluid are assumed to be the core and the skin layer, respectively. This simple model is chosen to investigate a rather extreme situation where the two fluids have quite different rheological properties. It is assumed that the flow is isothermal and that only viscous and viscoelastic forces are important thus neglecting the influence of inertia, gravity, and surface tension.

The present analysis is limited to the draw-down region where the fluids are stretched forming a thin fiber. In this region the change of the fiber radius with the flow direction is very small. Consequently, one-dimensional approximation is applied at the outset in which the axial velocity, pressure, and stress fields are assumed to be independent of the radial coordinate. The one-dimensional approximation was proven to be valid in the draw-down region by asymptotic analyses (Schultz and Davis, 1982; Park, 1990, 1991) and numerical simulations (Fisher, Denn and Tanner, 1980; Keunings, Crochet and Denn, 1983). Throughout the analysis the shear viscosity ratio of the core layer and skin layer is assumed to be unity while the relaxation time of the skin layer as well as its flow rate fraction are varied.

An asymptotic analysis for the steady flow under the prescribed conditions has been given for the case in which the applied stress (or draw force) is infinitely large compared to the elastic shear modulus of the skin-layer material (Park, 1990). The result of the asymptotic analysis is extended here to include the steady state solutions for a finite draw force. The steady state solution serves as a base flow for the linear stability analysis presented in the next chapter. The steady state solutions indicate that the viscoelasticity of the skin layer plays a significant role in determining the overall mechanics of the flow. Thus, a strong influence of the viscoelasticity may be also anticipated on the stability of the flow even when the flow rate of the skin layer may be smaller than that of the Newtonian core layer.

2.2 Problem Formulation and Scalings

The schematic of a bicomponent fiber spinning flow is shown in Figure 2. The core layer and skin layer are assumed to be a Newtonian and an upper-convected Maxwell fluid, respectively. The region of interest for this analysis is limited to the draw-down region where the materials are stretched under the applied axial tension. The one-dimensional approximation is adopted at the outset in which the flow is assumed to be

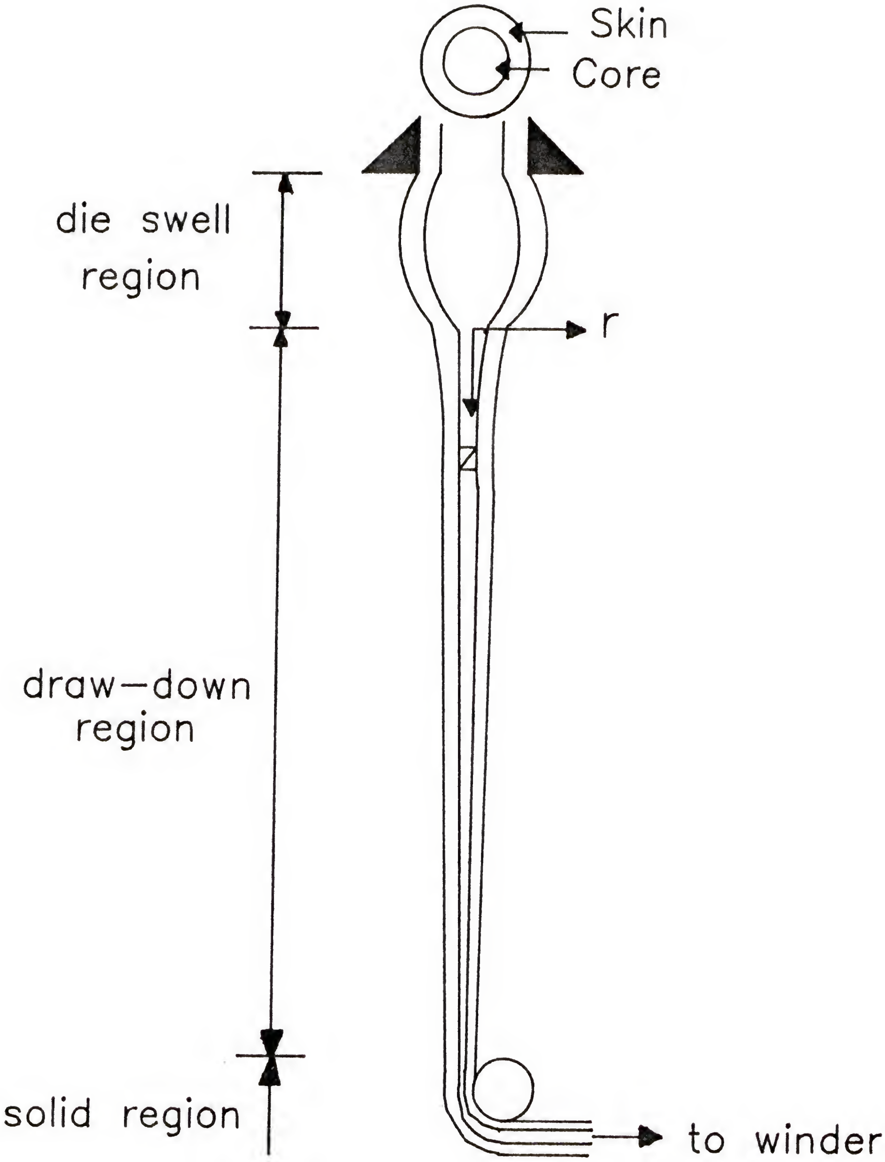

Figure 2. Schematic of coextrusion fiber spinning

isothermal and axisymmetric. Under this assumption, the stress and axial velocity are uniform over the cross-section of the fiber at each axial locations. This approximation is known to be invalid in the immediate vicinity of the die exit where the extrudate swell occurs. However, the extrudate swell is restricted to a very small region and the one-dimensional flow is quickly approached within about two radii from die exit. Thus, the extrudate swell region may be excluded from the analysis without causing a serious problem. Therefore, the origin of the system is taken to be approximately at the point just below the extrudate swell region in which the rate of change of fiber diameter with the axial distance is very small (dR/dz<<1). In most of the studies on melt spinning the same approach has been taken regarding the origin of the coordinate system.

2.2.1 Spinning Equations

Under the assumption that the gravity, inertia, and surface tension are negligible compared with viscous and viscoelastic forces, the continuity equation and the momentum equation are given as follows:

$$\frac{\partial A}{\partial t}+\frac{\partial}{\partial z}(Aw)=0 \tag{2.1}$$

$$\frac{\partial}{\partial z}\left[fA\left\{(\tau_{zz}^{s}-\tau_{rr}^{s})-\frac{1}{2}(\tau_{\theta\theta}^{s}-\tau_{rr}^{s})\right\}+(1-f)A\left\{(\tau_{zz}^{c}-\tau_{rr}^{c})-\frac{1}{2}(\tau_{\theta\theta}^{c}-\tau_{rr}^{c})\right\}\right]=0 \tag{2.2}$$

Here A is the cross-sectional area of the fiber, w the axial velocity in the flow direction. The τ_{ij} represent the extra stresses in the radial rr, circumferential $\theta\theta$, and axial zz directions, and the superscripts s and c denote the skin and core layer, respectively. The fraction of skin-layer flow rate is expressed by f. The two terms in the first curly bracket of (2.2) are the axial tension born by the upper-convected Maxwell skin layer while the two terms in the second curly bracket of (2.2) are the axial tension in the Newtonian core layer.

2.2.2 Constitutive Equations

The rheological expressions are needed to describe the relationships between stresses and deformation for the skin and core material. For a uniaxial elongational flow, the velocity gradient tensor ($\nabla \underline{v}$) and the rate-of-deformation tensor $\underline{\underline{D}}$ are expressed as

$$(\nabla \underline{v}) = \underline{\underline{D}} = \begin{bmatrix} -\frac{1}{2}\frac{\partial w}{\partial z} & 0 & 0 \\ 0 & -\frac{1}{2}\frac{\partial w}{\partial z} & 0 \\ 0 & 0 & \frac{\partial w}{\partial z} \end{bmatrix} \tag{2.3}$$

Here the $\underline{\underline{D}}$ is defined by $\frac{1}{2}[(\nabla \underline{v}) + (\nabla \underline{v})^T]$. Since off-diagonal elements of $\nabla \underline{v}$ are zero, $\nabla \underline{v} = \underline{\underline{D}}$. For the Newtonian core layer and the upper-convected Maxwell skin layer, the constitutive equations are written as

$$\underline{\underline{\tau}}^c = 2\mu^c \underline{\underline{D}} \tag{2.4}$$

$$\underline{\underline{\tau}}^s + \lambda \left\{ \frac{\partial \underline{\underline{\tau}}^s}{\partial t} + (\underline{v} \bullet \nabla)\underline{\underline{\tau}}^s - (\nabla \underline{v})^T \bullet \underline{\underline{\tau}}^s - \underline{\underline{\tau}}^s \bullet (\nabla \underline{v}) \right\} = 2\mu^s \underline{\underline{D}} \tag{2.5}$$

where λ is the relaxation time of the upper-convected Maxwell fluid; μ^c and μ^s are the shear viscosities of the Newtonian and the upper-convected Maxwell fluid. These material parameters, λ, μ^c, and μ^s, are constant in the given constitutive models.

The substitution of Eq.(2.3) into Eqs.(2.4) and (2.5) gives the radial *rr*, circumferential *θθ*, and axial *zz* components of the constitutive equations for the core layer and skin layer as

$$\tau^c_{rr} = -\mu^c \frac{\partial w}{\partial z}\ ,\quad \tau^c_{\theta\theta} = -\mu^c \frac{\partial w}{\partial z}\ ,\quad \tau^c_{zz} = 2\mu^c \frac{\partial w}{\partial z} \tag{2.6,2.7,2.8}$$

$$\tau^s_{rr} + \lambda\left(\frac{\partial \tau^s_{rr}}{\partial t} + w\frac{\partial \tau^s_{rr}}{\partial z} + \tau^s_{rr}\frac{\partial w}{\partial z}\right) = -\mu^s \frac{\partial w}{\partial z} \tag{2.9}$$

$$\tau^s_{\theta\theta} + \lambda\left(\frac{\partial \tau^s_{\theta\theta}}{\partial t} + w\frac{\partial \tau^s_{\theta\theta}}{\partial z} + \tau^s_{\theta\theta}\frac{\partial w}{\partial z}\right) = -\mu^s \frac{\partial w}{\partial z} \tag{2.10}$$

$$\tau^s_{zz} + \lambda\left(\frac{\partial \tau^s_{zz}}{\partial t} + w\frac{\partial \tau^s_{zz}}{\partial z} - 2\tau^s_{zz}\frac{\partial w}{\partial z}\right) = 2\mu^s \frac{\partial w}{\partial z} \tag{2.11}$$

2.2.3 Scalings and Dimensionless Governing Equations

The scalings for the nondimensionalization are as follows:

$$(r,z)\sim(R_0,L),\qquad t\sim\frac{L}{w_0},\qquad w\sim w_0,\qquad A\sim A_0,\qquad \tau\sim\frac{F}{A_0}$$

where R_0 is the radius of the fiber at z=0 and L is the draw span; w_0 and A_0 are the average axial velocity and the cross-sectional area at the origin (z=0); F is the axial draw force applied at the take-up (z=1). Under these scalings, the dimensionless continuity equation remains the same as equation (2.1) if the variables in (2.1) are considered to be dimensionless. Combining the Eqs (2.2), (2.6), (2.7), and (2.8), the momemtum equation is given in a dimensionless form as

$$\frac{\partial}{\partial z}\left[fA\left\{(\tau_{zz}-\tau_{rr})-\frac{1}{2}(\tau_{\theta\theta}-\tau_{rr})\right\}+3(1-f)GMA\frac{\partial w}{\partial z}\right]=0 \tag{2.12}$$

The superscripts *s* are dropped here for convience as all stress components appearing in the equations are for the skin layer.

The constitutive equations for the upper-convected Maxwell fluid are given by

$$\tau_{zz}+De\left(\frac{\partial\tau_{zz}}{\partial t}+w\frac{\partial\tau_{zz}}{\partial z}-2\tau_{zz}\frac{\partial w}{\partial z}\right)=2G\frac{\partial w}{\partial z} \tag{2.13}$$

$$\tau_{rr}+De\left(\frac{\partial\tau_{rr}}{\partial t}+w\frac{\partial\tau_{rr}}{\partial z}+\tau_{rr}\frac{\partial w}{\partial z}\right)=-G\frac{\partial w}{\partial z} \tag{2.14}$$

$$\tau_{\theta\theta}+De\left(\frac{\partial\tau_{\theta\theta}}{\partial t}+w\frac{\partial\tau_{\theta\theta}}{\partial z}+\tau_{\theta\theta}\frac{\partial w}{\partial z}\right)=-G\frac{\partial w}{\partial z} \tag{2.15}$$

Here the time dependence is preserved as they will be used in the following chapter.

The dimensionless parameters appearing in the above equations are defined as follows:

Deborah number	$De=\frac{\lambda w_0}{L}$
Shear viscosity ratio	$M=\frac{\mu^c}{\mu^s}$
Dimensionless inverse axial force	$G=\frac{\mu^s A_0 w_0}{FL}$
Skin-layer flow rate fraction	$f=\frac{Q_S}{Q_T}$

Here Q_S and Q_T are the flow rate of the skin layer and the total flow rate, respectively.

A rigorous derivation of the one-dimensional Equations (2.1), (2.12), (2.13), (2.14) and (2.15) can be found in Park (1990) in which the method of asymptotic expansions is applied in the small parameter ε which is defined as the ratio of the radial to axial characteristic length scales R_0/L. The most significant assumption in deriving Equations (2.1), (2.12), (2.13), (2.14) and (2.15) may be the radial uniformity of the extra normal stresses in the skin layer. While the velocity independence of the radial coordinate arises naturally from the asymptotic analysis, there is no clear indication that the extra normal stresses in the skin layer are radially uniform. If the initial stress condition at z=0 is independent of r, however, the stress field becomes radially uniform for all z. Thus, for simplicity, it has been assumed that the stress field of the skin layer is also independent of the radial coordinate. This assumption may not be a severe restriction considering the successes of many theoretical analyses built on the same assumption for single-phase flows.

2.3 Boundary Conditions

At the origin of the draw-down region, the cross-sectional area of the fiber and the axial velocity are given as A_0 and w_0, respectively. The take-up velocity and the draw force cannot both be specified. If the take-up velocity is fixed, then there exists a corresponding force which is necessary to obtain the prescribed take-up velocity. Here the applied force at the take-up point is adjusted so that the desired value of the final fiber radius (or the axial velocity at z=L) is obtained. Thus, the boundary conditions of the cross-sectional area and the velocity of the fiber are described as

$$A = A_0 \qquad \text{at} \quad z = 0 \tag{2.16}$$

$$w = w_0 \qquad \text{at} \quad z = 0 \tag{2.17}$$

$$w = w_L \qquad \text{at} \quad z = L \tag{2.18}$$

After nondimensionalization using the scalings described in section 2.2.3, the cross-sectional area and the velocity conditions at the both ends of the fiber are given in dimensionless form as

$$A = 1 \qquad \text{at } z = 0 \tag{2.19}$$

$$w = 1 \qquad \text{at } z = 0 \tag{2.20}$$

$$w = Dr \qquad \text{at } z = 1 \tag{2.21}$$

Here *Dr* is the draw ratio defined as the ratio of the take-up to the extrusion velocity $w(1)/w(0)$ (or the ratio of the initial to the final cross-sectional area of the fiber).

One underlying assumption in specifying these velocity conditions is that no-slip occurs at the interface between the two fluids; that is, the velocity is uniform over the entire cross-section of the fiber. The normal stresses, on the other hand, are discontinuous across the fluid-fluid interface although they are radially uniform within each layer. The two terms in the curly bracket of Eq.(2.12) represent the axial tension born by the skin layer whereas the last term in (2.12) is the axial tension in the Newtonian core. Unless the draw ratio or the Deborah number is very small, the tension in the viscoelastic skin layer is typically much greater than that in the Newtonian core; that is, most of the tension on the spinline is supported by the skin layer.

In addition to the velocity conditions, the stress state at z=0 needs to be specified for the viscoelastic skin layer. The initial stress condition accounts for the strain history of the fluid to that point, and we assume that it is given as

$$\tau_{zz}(0) = t_0 \tag{2.22}$$

$$\tau_{rr}(0) = t_0 - 1 \tag{2.23}$$

$$\tau_{\theta\theta}(0) = \tau_{rr}(0) \tag{2.24}$$

Here the value of t_0 is an arbitrary constant. Although the numerical assignment for this value is arbitrary, numerical calculations have shown that the mechanics of the flow is rather insensitive to the value of t_0 (see section 2.6). For most of the calculations presented in this study, numerical value of 10 was assigned to t_0.

While arbitrary values can be assigned to τ_{rr} and $\tau_{\theta\theta}$ regardless of τ_{zz}, it was chosen that $\tau_{rr} = t_0 - 1$ and $\tau_{\theta\theta} = \tau_{rr}$ for all the results throughout this thesis. For a single-phase flow of an upper-convected Maxwell fluid (i.e., f=1), specification of τ_{rr} at z=0 happens to be unnecessary since its value is determined to be $\tau_{zz}(0) - 1$ by the axial force balance. Thus, the choice of $\tau_{rr}(0) = t_0 - 1$ for the two-phase flow corresponds to the situation that the upper-convected Maxwell fluid in the two-phase flow experiences the same strain history as its single-phase flow. It may be a sound choice for the comparison between single- and two-phase flows. As pointed out previously, however, the flow mechanics is not seriously affected by the numerical value of t_0 or by any other choice of τ_{rr}. In section 2.6, the negligble influence of t_0 is discussed in detail.

The initial value of $\tau_{\theta\theta}$ is chosen to be the same as $\tau_{rr}(0)$ in order to drop the ($\tau_{\theta\theta} - \tau_{rr}$) term in Equation (2.12). This term accounts for the hoop stress resulting from the concentric core-skin structure of the flow. As will be shown in section 2.5, the spinning flow is also insensitive to the initial value of the hoop stress. Thus, the given choice again does not seriously affect the conclusions of the present study. Furthermore, when $\tau_{rr}(0) - \tau_{\theta\theta}(0)$, it can be shown from (2.14) and (2.15) that $\tau_{\theta\theta} = \tau_{rr}$ for all z. Thus the momentum equation (2.12) is simplified to

$$\frac{\partial}{\partial z}\left[fA(\tau_{zz} - \tau_{rr}) + 3(1-f)GMA\frac{\partial w}{\partial z} \right] = 0 \qquad (2.25)$$

This equation is more convenient than (2.12) for the comparison between single- and two-phase flow. If f is set to zero, Equation (2.25) is reduced to the one for a

Newtonian single-phase flow. If $f=1$, on the other hand, the well-known equation for the spinning of an upper-convected Maxwell fluid is recovered.

The system of Equations (2.1), (2.13),(2.14) and (2.25) along with the boundary conditions (2.19) through (2.23) is to be solved throughout all this work. The specific choices for the boundary conditions may appear to restrict the flow situation to a very specific case. Due to the insensitivity of the flow mechanics to the initial stress condition, however, the present results in fact represent the general situation of the two-phase flow. Further justification of the initial stress condition is given in sections 2.5 and 2.6, and an unexpected interesting implication of (2.24) is also discussed in section 2.5.

2.4 Steady State Solutions

At steady state the time derivatives $\partial/\partial t$ are set to zero, and the steady system to be solved becomes

$$\frac{d}{dz}(A^{ss}w^{ss})=0 \tag{2.26}$$

$$\frac{d}{dz}\left[fA^{ss}(\tau_{zz}^{ss}-\tau_{rr}^{ss})+3(1-f)GMA^{ss}\frac{dw^{ss}}{dz}\right]=0 \tag{2.27}$$

$$\tau_{zz}^{ss}+De\left(w^{ss}\frac{d\tau_{zz}^{ss}}{dz}-2\tau_{zz}^{ss}\frac{dw^{ss}}{dz}\right)=2G\frac{dw^{ss}}{dz} \tag{2.28}$$

$$\tau_{rr}^{ss}+De\left(w^{ss}\frac{d\tau_{zz}^{ss}}{dz}+\tau_{rr}^{ss}\frac{dw^{ss}}{dz}\right)=-G\frac{dw^{ss}}{dz} \tag{2.29}$$

The boundary conditions are

$$A^{ss}(0)=1 \tag{2.30}$$

$$w^{ss}(0) = 1 \tag{2.31}$$

$$w^{ss}(1) = Dr \tag{2.32}$$

$$\tau_{zz}^{ss}(0) = t_0 \tag{2.33}$$

$$\tau_{rr}^{ss}(0) = t_0 - 1 \tag{2.34}$$

The integration of (2.26) and (2.27) results in

$$A^{ss}w^{ss} = 1 \tag{2.35}$$

$$\tau_{zz}^{ss} - \tau_{rr}^{ss} = \frac{1}{f}\left[w^{ss} - 3(1-f)GM\frac{dw^{ss}}{dz}\right] \tag{2.36}$$

A simple manipulation of (2.28) and (2.29) using (2.35) and (2.36) yields the following set of nonlinear differential equations for numerical integration:

$$\frac{dw^{ss}}{dz} = u^{ss} \tag{2.37}$$

$$\frac{du^{ss}}{dz} = \frac{1}{3(1-f)GMDe} - \frac{u^{ss}}{w^{ss}}\left(\frac{1}{De} + u^{ss}\right) + \frac{u^{ss}}{(1-f)M}\left(\frac{2}{3G} - \frac{f}{Dew^{ss}} - \frac{f\tau_{zz}^{ss}}{Gw^{ss}}\right) \tag{2.38}$$

$$\frac{d\tau_{zz}^{ss}}{dz} = \frac{1}{Dew^{ss}}\left[2u^{ss}(G + De\tau_{zz}^{ss}) - \tau_{zz}^{ss}\right] \tag{2.39}$$

Here superscripts *ss* denotes the steady state, and the new variable u^{ss} represents the derivative dw^{ss}/dz.

Using the boundary conditions at z=0 (i.e., Equations (2.31), (2.33),(2.34)), the initial value of u^{ss} (i.e., dw^{ss}/dz) is derived from (2.36) as

$$u^{ss} = \frac{dw^{ss}}{dz} = \frac{1}{3GM} \qquad \text{at } z = 0 \tag{2.40}$$

Using the boundary conditions (2.31), (2.33) and (2.40), Equations (2.37), (2.38) and (2.39) can be integrated numerically to determine w^{ss} and τ_{zz}^{ss} for specified values of *f*, *M*, *De* and t_0. Once w^{ss} and τ_{zz}^{ss} are determined, A^{ss} and τ_{rr}^{ss} follow from (2.35) and (2.36). The fourth order Runge-Kutta-Gill method was used for the integration.

The inverse axial force *G* is not a prescribed parameter. Instead the draw ratio *Dr* is specified at z=1 (Equation (2.32)). Thus, the value of *G* is determined by a shooting method so that the boundary condition (2.32) is satisfied. In Figures 3, the draw ratio *Dr* is given as a function of *G* for various *f* (f=0, 0.2, 0.5, and 1.0) as M=1, De=0.02, and t_0=10. For a Newtonian single-phase flow (i.e., f=0), an analytic expression is known for the relationship between *Dr* and G^{NW}:

$$Dr = \exp\left(\frac{1}{3G^{NW}}\right) \tag{2.41}$$

or

$$G^{NW} = \frac{1}{3\ln Dr} \tag{2.42}$$

Here G^{NW} is the inverse axial force for the Newtonian fluid, which is defined as $G^{NW} = \mu^c A_0 w_0 / FL$. Using the definition of *G* for the two-phase flow given in page 16, Equation (2.41) can be rewrtiien as

$$Dr = \exp\left(\frac{1}{3GM}\right) \tag{2.43}$$

Thus, when the stability of the flow is not considered, we may say that a Newtonian fluid can be stretched indefinitely as the draw force is increased. On the other hand, Upper-convected Maxwell fluid cannot be stretched indefinitely since the draw force becomes infinity beyond a certain draw ratio. The maximum obtainable draw ratio, which is 51 for *De*=0.02, is predicted analytically by the asymptotic theory (see Appendix B). In a single-phase flow of either a Newtonian or an upper-convected Maxwell (UCM) fluid (f=0.0 and 1.0, respectively), the draw ratio increases monotonically with increasing draw force. However, the relationship between *Dr* and *G* is shown to be not necessarily monotonic for two-phase flows as indicated in Figure 3. For the prescribed condition (i.e., *M*=1, *De*=0.02 and t_0=10), the curve for f=0.5 follows the monotonic trend of the single-phase UCM fluid approaching *Dr*=49 as $G \to 0$. When f=0.2, however, *Dr* reaches a maximum value of about 71 (point **c** of Figure 3) before the infinite-stress asympotote (*Dr*=50) is approached. Thus, when *Dr* is between 50 and 71, there exist two steady state solutions for f=0.2 (e.g., points **a** and **b** of Figure 3 for *Dr*=60).

The existence of the maximum draw ratio at a finite *G* for a small value of f seems physically conceivable. When the draw ratio is small, the viscous force dominates the flow mechanics whereas the viscoelastic force does when the draw ratio is large. Thus, a transition may occur from a viscous force dominant mode to a viscoelastic force dominant mode as the draw force (or the draw ratio) is increased. For a relatively large value of f (e.g., f=0.5 in Figure 3), the transition may occur at a draw ratio which is smaller than the asymptotic value for $G \to 0$. Consequently, *Dr* increases monotonically with decreasing *G*. If f is small, on the other hand, the viscous force is dominant until the draw ratio is much larger than the value predicted by the asymptotic theory (f=0.2 curve in Figure 3). As the draw force is further increased, the viscoelastic force becomes significant acting against further stretching of the fluid resulting in a maximum *Dr* at a finite value of *G*.

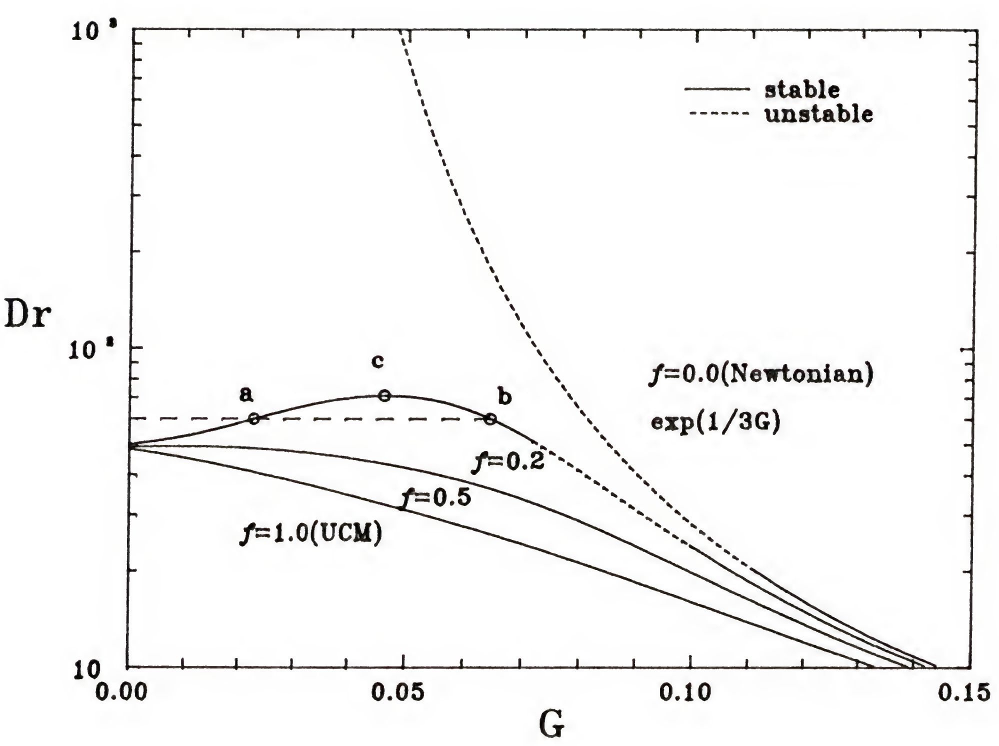

Figure 3. Draw ratio as a function of inverse axial force at De=0.02, M=1, t_0=10; a: G=0.023, Dr=60; b: G=0.064, Dr=60; c: G=0.046,Dr=71

This behavior of the coextrusion flow has an interesting implication; that is, the highest draw ratio for a stable spinning can be larger than that of the single-phase spinning flow of either fluid if the region **bc** in Figure 3 happens to be stable. It may be noted that the Newtonian single-phase flow is unstable when $Dr>20.21$ (Pearson and Matovich,1969). As will be discussed in Chapter 3, the low-G branch of the multiple steady solutions (i.e., the portion of the $f=0.2$ curve where $G<0.05$ including point **a**) is shown to be always unstable. The high-G branch of the solution, on the other hand, is either stable when De is large or goes through two transitions with increasing Dr when De is small. Thus, when De is large enough so that the high-G branch solution is stable without the two transitions, it is possible to obtain a much higher draw ratio with coextrusion than obtainable with either the UCM fluid or the Newtonian fluid.

Similar implication may be expressed using a different type of plot. In Figure 4a and 4b, the inverse axial force G is plotted as a function of Deborah number De at two different draw ratios $Dr=20$ and 30, respectively. The scale of inverse axial force G in Figure 4 is normalized by the value for the Newtonian single-phase flow case, Eq.(2.42):

$$\frac{G}{G^{NW}} = 3G \ln Dr \tag{2.44}$$

In Figure 4, a draw ratio of 20 is chosen for an illustration purpose because it corresponds to the limiting draw ratio of a Newtonian fluid for stability (Pearson and Motovich, 1969; Denn, Petrie and Avenas, 1975).

These figures represent the maximum value of De beyond which the given draw ratio ($Dr=20$ or 30) is unattainable. In Figure 4a for $Dr=20$, the maximum De for $f=1.0$ is 0.046. This value indicates that an upper-convected Maxwell fluid whose De is larger than 0.046 can not be drawn beyond $Dr=20$. Thus, if Dr is desired to be 20, the material time constant should be small enough so that De is smaller than 0.046. When $f=0.5$, the

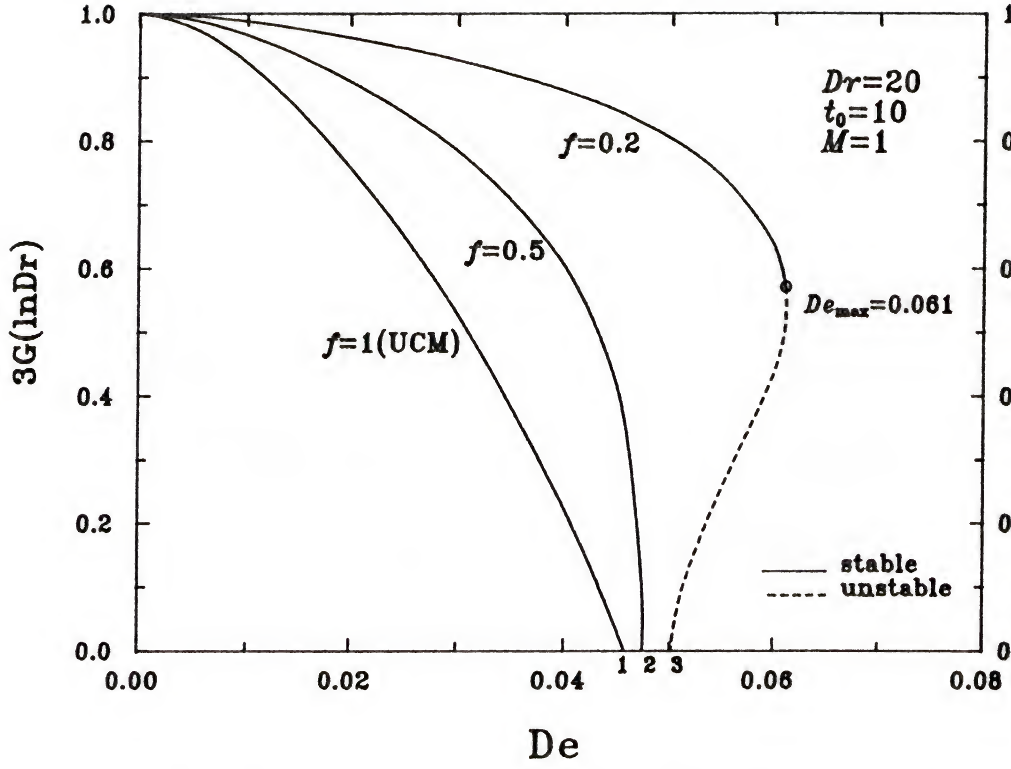

Figure 4. Inverse axial force as a function of Deborah number, *De*: (a) *Dr*=20, t_0=10.(asymptotic solution, $G \rightarrow 0$: 1. *De*=0.046, 2. *De*=0.047, 3. *De*=0.050); (b) *Dr*=30, t_0=10.(asymptotic solution, $G \rightarrow 0$: 1. *De*=0.031, 2. *De*=0.032, 3. *De*=0.033).

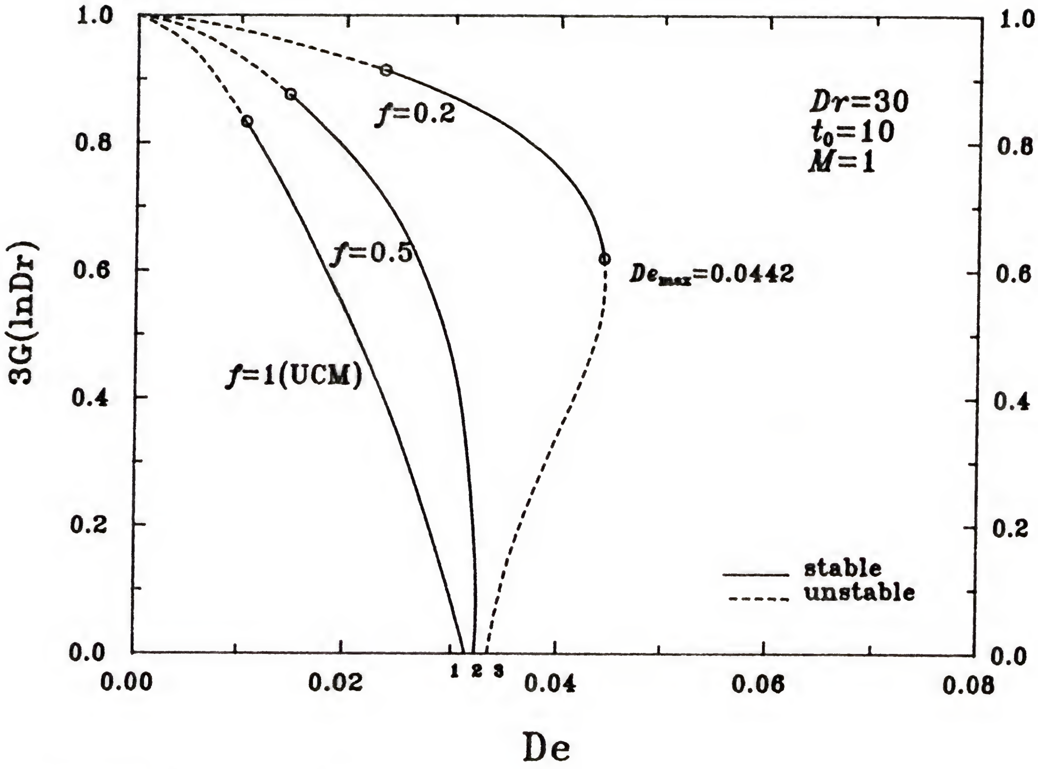

Figure 4. (continued).

maximum *De* for *Dr*=20 is allowed to be only slightly larger (i.e., 0.047). When *f*=0.2, however, *De* can be as high as 0.061 which is substantially larger than 0.046. Thus, in a coextrusion flow, an upper-convected Maxwell fluid can be drawn to a higher draw ratio than with a single-phase flow. Similar behavior is described in Figure 4b for *Dr*=30.

An analytic expression for the maximum Deborah number at a given draw ratio is given in the work of Park (1990):

$$De_{\max} = \left(D_r + \frac{k}{2} \ln\left[\frac{|D_r - k|^3 |1-k^3|}{|D_r^3 - k^3| |1-k|^3} \right] - k\sqrt{3}\left\{ \tan^{-1}\left(\frac{2D_r + k}{k\sqrt{3}}\right) - \tan^{-1}\left(\frac{2+k}{k\sqrt{3}}\right) \right\} - 1 \right)^{-1}.$$

$$\text{where} \quad k = \sqrt[3]{1 - \frac{1}{t_0 f}} \qquad (2.45)$$

When *f*=1 and t_0=1, this expression is reduced to $De_{\max}=1/(Dr-1)$ which is for the single-phase flow of UCM fluid as derived by Denn, Petrie and Avenas (1975).

The computaional results of the present analysis are shown to be very close to the prediction of the analytic expression supporting the accuracy of the present numerical calculation.

The multi-valuedness of the coextrusion flow at *f*=0.2 represented in Figure 3 is also manifested in Figures 4a and 4b. When *De* is between 0.050 and 0.061, two steady solutions exist for *Dr*=20 and *f*=0.2; that is the lower and the higher *G* solutions which is similar to **a** and **b** of Figure 3. In Figure 5 a similar plot is given but for various values of *Dr* when *f* is fixed at 0.2. It appears that the multi-valuedness persists over a broad range of *Dr*.

In Figure 6, the steady state velocity profiles are given as a function of the axial coordinate *z* for *M*=1, *De*=0.02 and t_0=10 at two different values of draw ratio (*Dr*=30

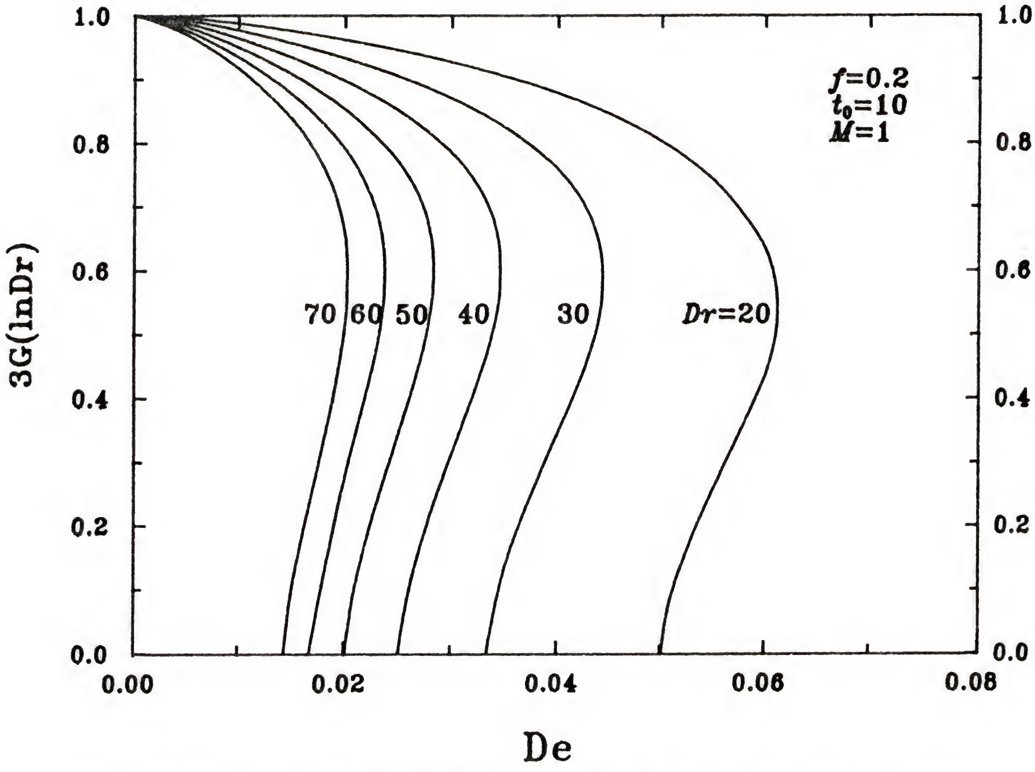

Figure 5. Inverse axial force as a function of Deborah number, *De* at different draw ratios when f=0.2, t_0=10, M=1.

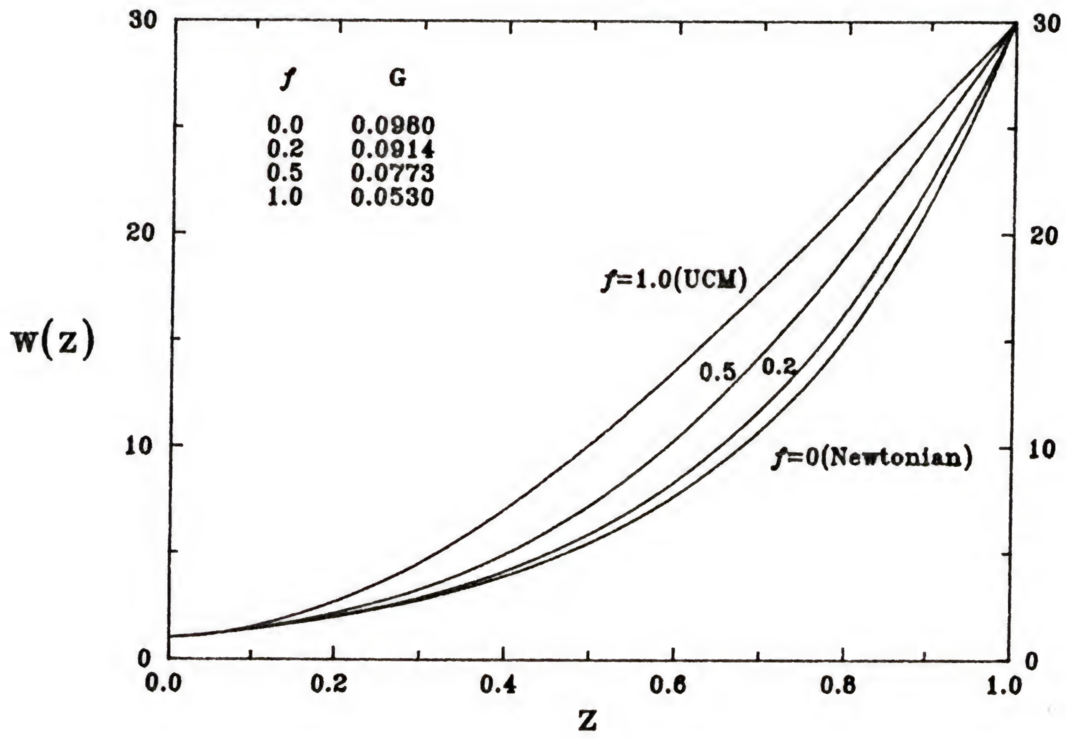

Figure 6. Steady state axial velocity profiles: (a) *Dr*=30, *De*=0.02, t_0=10, *M*=1; (b) *Dr*=40, *De*=0.02, t_0=10, *M*=1.

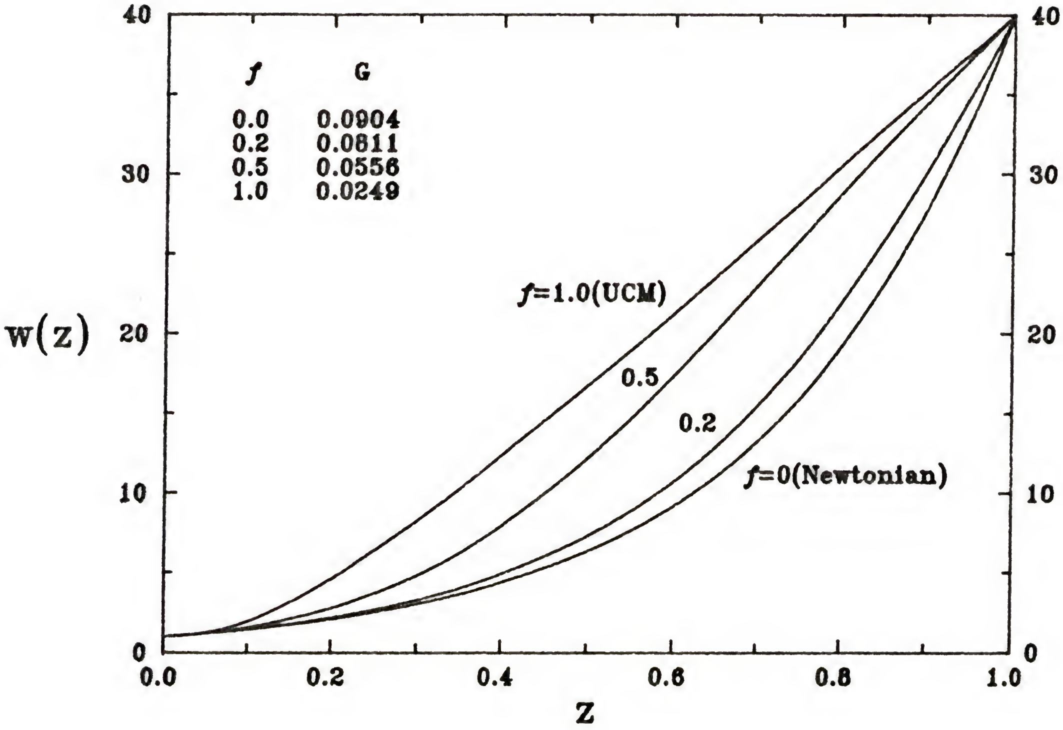

Figure 6. (continued).

and 40). It is indicated in the figures that the velocity profiles for large f (f=1.0 and 0.5) become more linear with increasing Dr as the viscoelasticity effect of the skin layer become more significant. According to the theory of single-phase flows, the UCM fluid flow is stable at both Dr=30 and 40 whereas the Newtonian flow is unstable. Thus, it may be of interest to determine whether the two-phase flows are stable or not at these draw ratios.

2.5 Effect of Hoop Stress

The difference $\tau_{\theta\theta} - \tau_{rr}$ in Equation (2.12) accounts for the hoop stress resulting from the concentric core-skin structure of the two-phase flow. Although $\tau_{\theta\theta}$ and τ_{rr} satisfy the same differential equation (2.14) and (2.15), they are not necessarily the same. However, if the initial conditions for $\tau_{\theta\theta}$ and τ_{rr} are the same or if the isotropic pressure in the skin layer is assumed to be radially uniform, the hoop stress term in (2.12) is dropped since either condition results in $\tau_{\theta\theta} = \tau_{rr}$ for all z.

In the presence of the hoop stress, the set of equations to be solved for the steady state is as follows:

$$\frac{d}{dz}(A^{ss}w^{ss}) = 0 \tag{2.26}$$

$$\frac{d}{dz}\left[fA^{ss}\left\{ (\tau_{zz}^{ss} - \tau_{rr}^{ss}) - \frac{1}{2}(\tau_{\theta\theta}^{ss} - \tau_{rr}^{ss}) \right\} + 3(1-f)GMA^{ss}\frac{dw^{ss}}{dz} \right] = 0 \tag{2.46}$$

$$\tau_{zz}^{ss} + De\left(w^{ss}\frac{d\tau_{zz}^{ss}}{dz} - 2\tau_{zz}^{ss}\frac{dw^{ss}}{dz} \right) = 2G\frac{dw^{ss}}{dz} \tag{2.28}$$

$$\tau_{rr}^{ss} + De\left(w^{ss}\frac{d\tau_{zz}^{ss}}{dz} + \tau_{rr}^{ss}\frac{dw^{ss}}{dz} \right) = -G\frac{dw^{ss}}{dz} \tag{2.29}$$

$$\tau_{\theta\theta}^{ss} + De\left(w^{ss}\frac{d\tau_{\theta\theta}^{ss}}{dz} + \tau_{\theta\theta}^{ss}\frac{dw^{ss}}{dz} \right) = -G\frac{dw^{ss}}{dz} \tag{2.47}$$

The intergration of the steady equations (2.26) and (2.46) associated with the boundary conditions (2.30)-(2.34) gives

$$A^{ss}w^{ss} = 1 \tag{2.35}$$

$$(\tau_{zz}^{ss} - \tau_{rr}^{ss}) - \frac{1}{2}(\tau_{\theta\theta}^{ss} - \tau_{rr}^{ss}) = \frac{1}{f}\left[w^{ss} - 3(1-f)GM\frac{dw^{ss}}{dz} \right] \tag{2.48}$$

Using (2.35) and (2.48) followed by a simple manipulation of (2.28), (2.29), and (2.47) gives the following first order differential equations

$$\frac{dw^{ss}}{dz} = \frac{1}{3(1-f)GM}\left[w^{ss} - f(T^{ss} - \frac{1}{2}E^{ss}) \right] \tag{2.49}$$

$$\frac{d\tau_{zz}^{ss}}{dz} = \frac{1}{Dew^{ss}}\left[\frac{2(G + De\tau_{zz}^{ss})}{3(1-f)GM}\left\{ w^{ss} - f(T^{ss} - \frac{1}{2}E^{ss}) \right\} - \tau_{zz}^{ss} \right] \tag{2.50}$$

$$\frac{dT^{ss}}{dz} = \frac{1}{Dew^{ss}}\left[\frac{(3G - DeT^{ss} + 3De\tau_{zz}^{ss})}{3(1-f)GM}\left\{ w^{ss} - f(T^{ss} - \frac{1}{2}E^{ss}) \right\} - T^{ss} \right] \tag{2.51}$$

$$\frac{dE^{ss}}{dz} = \frac{1}{Dew^{ss}}\left[\frac{-DeE^{ss}}{3(1-f)GM}\left\{ w^{ss} - f(T^{ss} - \frac{1}{2}E^{ss}) \right\} - E^{ss} \right] \tag{2.52}$$

The appropriate boundary conditions for the above equations are

$$w^{ss}(0) = 1 \tag{2.31}$$

$$\tau_{zz}^{ss}(0) = t_0 \tag{2.33}$$

$$T^{ss}(0)=\tau_{zz}^{ss}(0)-\tau_{rr}^{ss}(0)=1 \tag{2.53}$$

$$E^{ss}(0)=\tau_{\theta\theta}^{ss}(0)-\tau_{rr}^{ss}(0)=\text{arbitrary constant.} \tag{2.54}$$

Here the two variables T^{ss} and E^{ss} are the first normal stress $T^{ss}=\tau_{zz}^{ss}-\tau_{rr}^{ss}$ and the hoop stress $E^{ss}=\tau_{\theta\theta}^{ss}-\tau_{rr}^{ss}$. The above system (Eqs.(2.49)~(2.52)) can be integrated by using fourth order Runge-Kutta-Gill method along with the boundary conditions (2.31), (2.33), (2.53), and (2.54). The initial values of the hoop stress $E^{ss}(0)$ can be given arbitrarily.

The results of the computation show that the steady state solutions for the axial velocity and the stress profiles have no significant difference when the initial value of $E^{ss}(0)$ is varied. Figure 7 shows the hoop stress distributions along flow direction at two different skin flow rate ratios (f=0.2 and 0.5) when all other paramertes are specified as Dr=30, De=0.02, M=1, t_0=10. The initial hoop stresses are varied at −10, −2, 0, 2, and 10, respectively. In spite of the difference in the initial hoop stress condition all the hoop stress profiles quickly approach to zero indicating the negligible importance of hoop stress in fiber spinning flow. Consequently, the system we are dealing with may not be seriously affected by the initial hoop stress. Thus, the initial stress condition $\tau_{\theta\theta}(0)=\tau_{rr}(0)$ which is used in the present computation should not seriously diminish the generality of the current study.

2.6 Effect of Initial Shear Stress

The boundary conditions for the axial velocity described in section 2.3 are straightforward. The specification of the initial stress state of the viscoelastic skin layer, however, is somewhat ambiguous since it is not a measurable quantity. In case of a purely viscous fluid, the initial stress state does not depend on the previous strain history and the specification of it is not necessary. The stress state of viscoelastic fluids, on the other hand, depends on the upstream condition due to their memory effect. Therefore, if the stress state at z=0 is to have strong influence on the downstream dynamics of the fiber

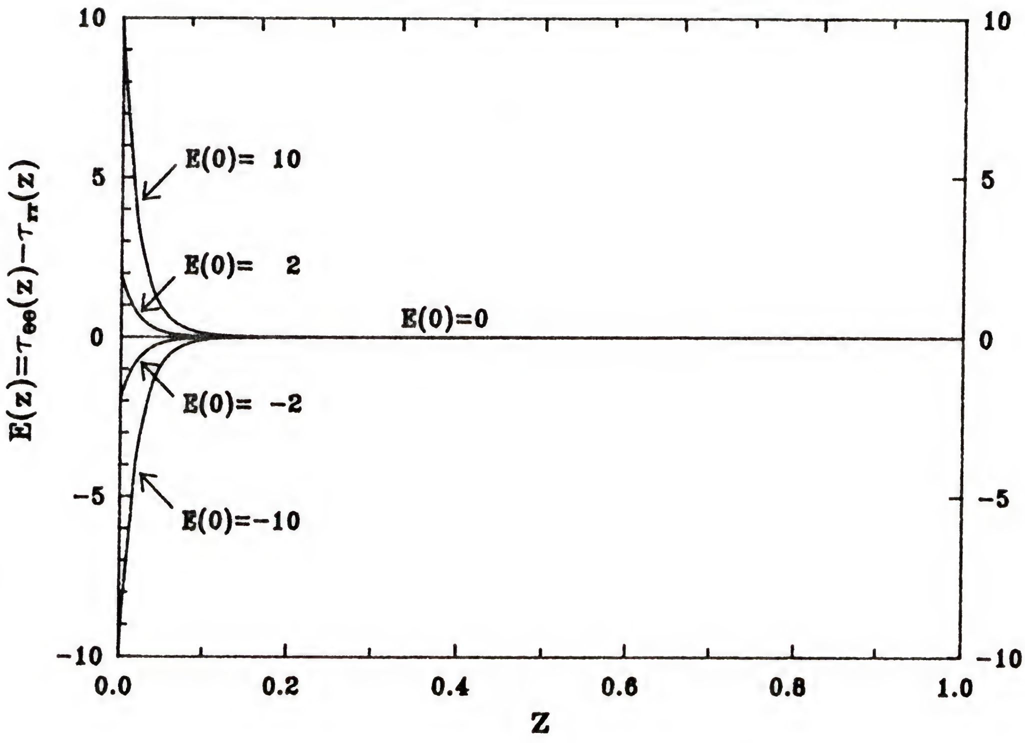

Figure 7. Normal stress distribution along the flow direction at different initial values of normal stress: (a) f=0.2, Dr=30, De=0.02, t_0=10, M=1; (b) f=0.5, Dr=30, De=0.02, t_0=10, M=1

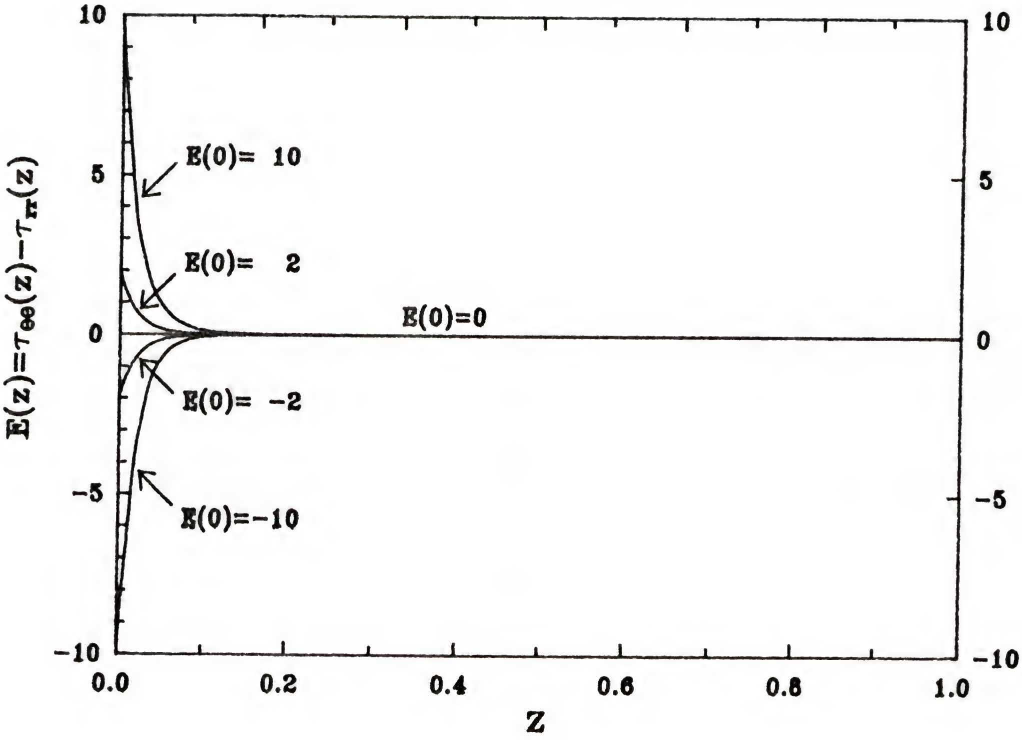

Figure 7. (continued).

spinning flow, it will be necessary to consider the strain history of the material inside the die. In this section, influence of initial stress condition (especially to value of t_0) on the overall dynamics of the fiber spinning flow is investigated by integrating the system equations for various values of t_0.

The axial normal stress distributions for two-phase coextruded fiber (Newtonian and UCM) at different combinations (f=0.2, 0.5) are plotted in Figure 8a and 8b, respectively. It is apparent from the figure that the influence of the initial stress is restricted to a rather small region near the die exit (up to $z \cong 0.1$) and it has only negligible influence in most of the draw-down region. This behavior is conceivable considering the fact that the fiber spinning flow is a "strong flow" in which the deformation of the material is near exponential. Consequently, within a short downstream distance, the old strain history is completely overwhelmed by the strong downstream conditions (Larson, 1988).

The velocity distributions given in Figure 9a and 9b also reflect the negligible influence of the initial stress condition. Obviously, the influence of the initial stress state will persist over a longer distance if t_0 is extremely large.

2.7 Effect of Shear Viscosity Ratio *M*

The shear viscosity ratio M is one of the parameters which affects the flow system. For the two-phase fiber spinning flow, the draw ratio as a function of inverse axial force is plotted for different values of M (Figure 10). It may be easier to consider that changing the value of M is equivalent to changing the shear viscosity of the Newtonian core layer while that of the viscoelastic skin is fixed. That is, the value of M is decreased as the shear viscosity of the Newtonian core decreases. At the given conditions (De=0.02, t_0=10), the Dr-G curves for M=1 and f=0.2, 0.5 (curve 2 and 5 in Figure 10) have been discussed in section 2.4.

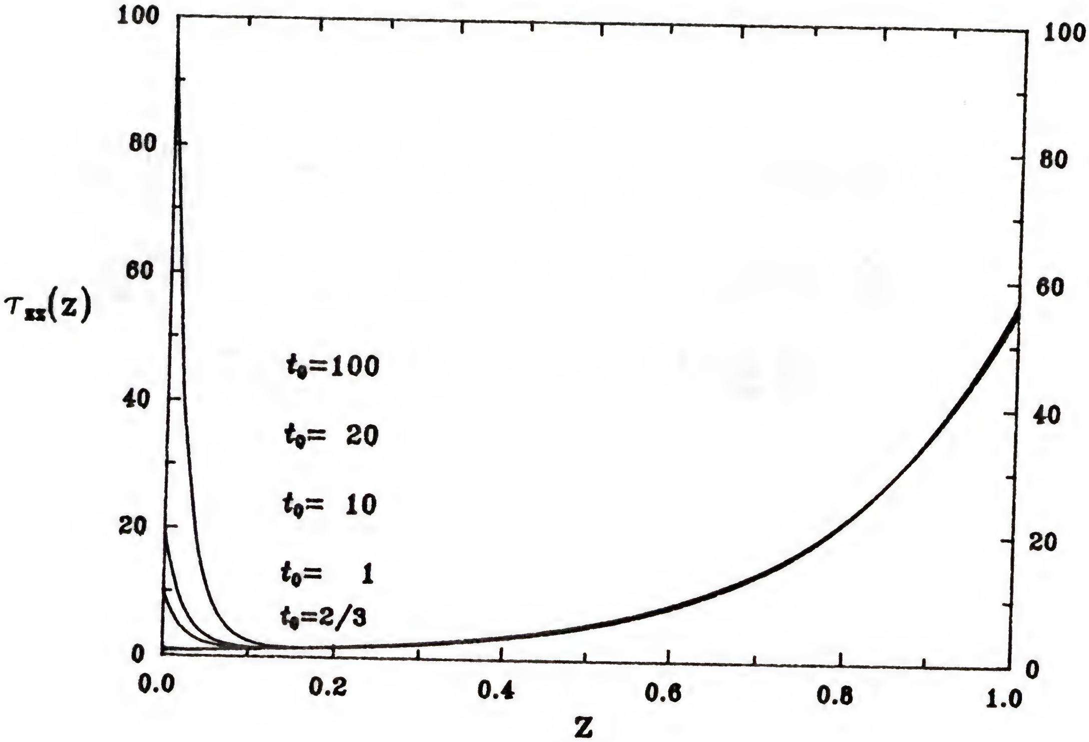

Figure 8. Shear stress distribution along the flow direction at different initial values of shear stress: (a) f=0.2, Dr=30, De=0.02, t_0=10, M=1; (b) f=0.5, Dr=30, De=0.02, t_0=10, M=1.

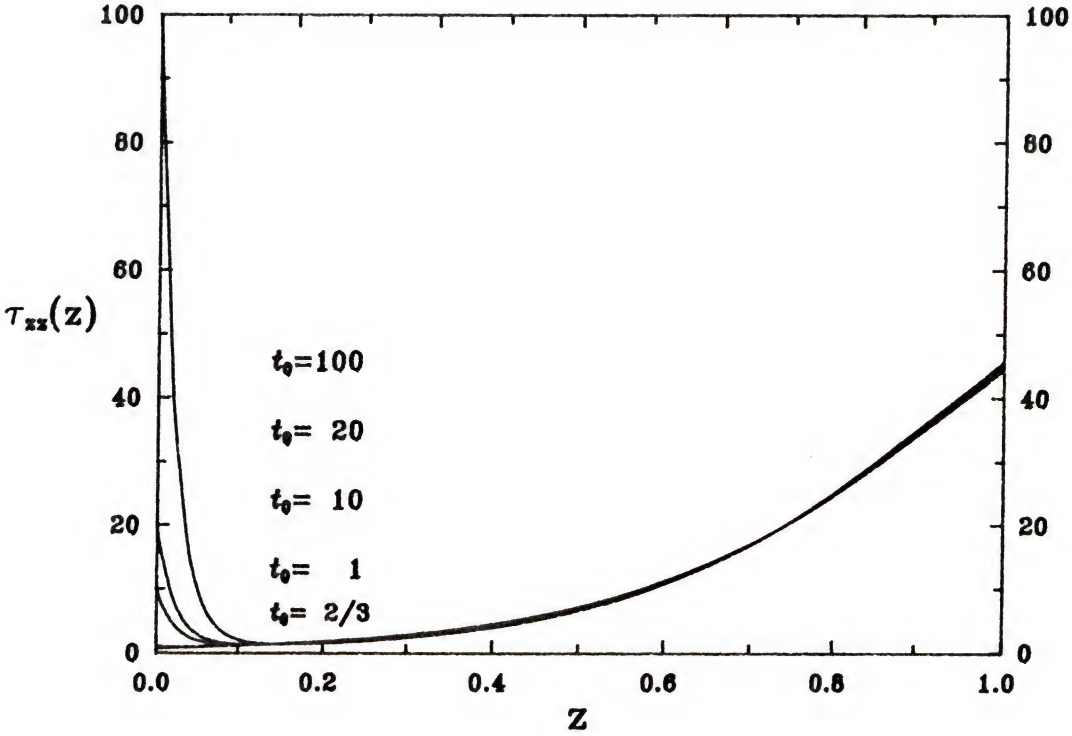

Figure 8. (continued).

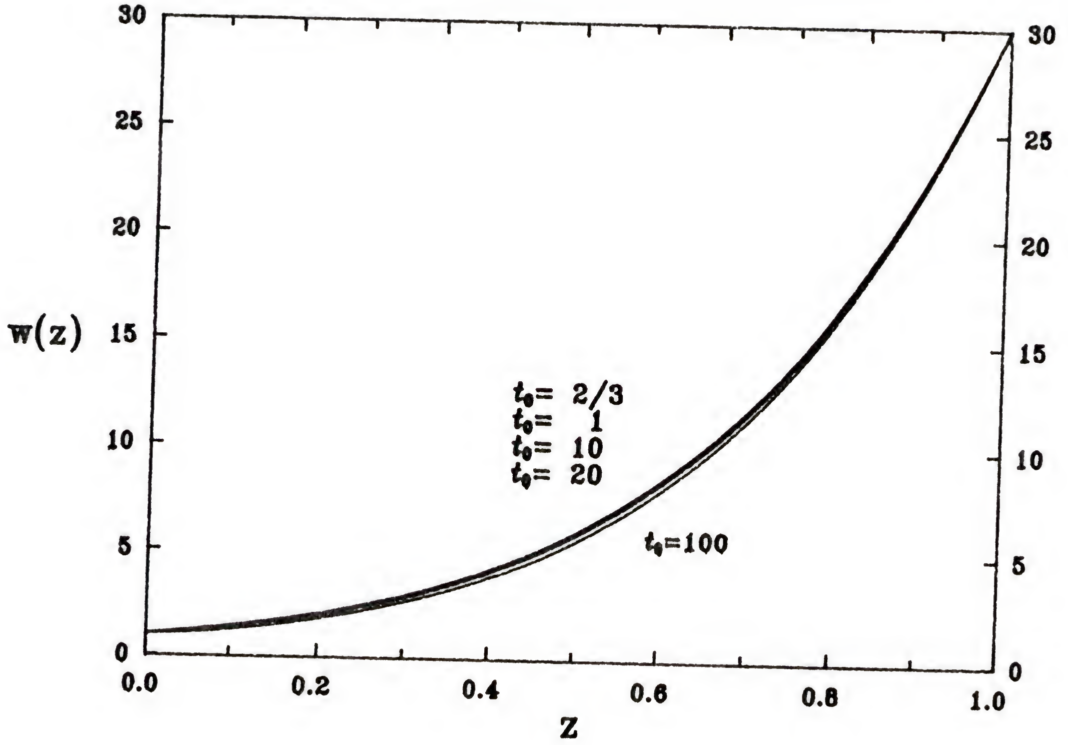

Figure 9. Steady state axial velocity profiles at different initial values of shear stress: (a) f=0.2, Dr=30, De=0.02, t_0=10, M=1; (b) f=0.5, Dr=30, De=0.02, t_0=10, M=1.

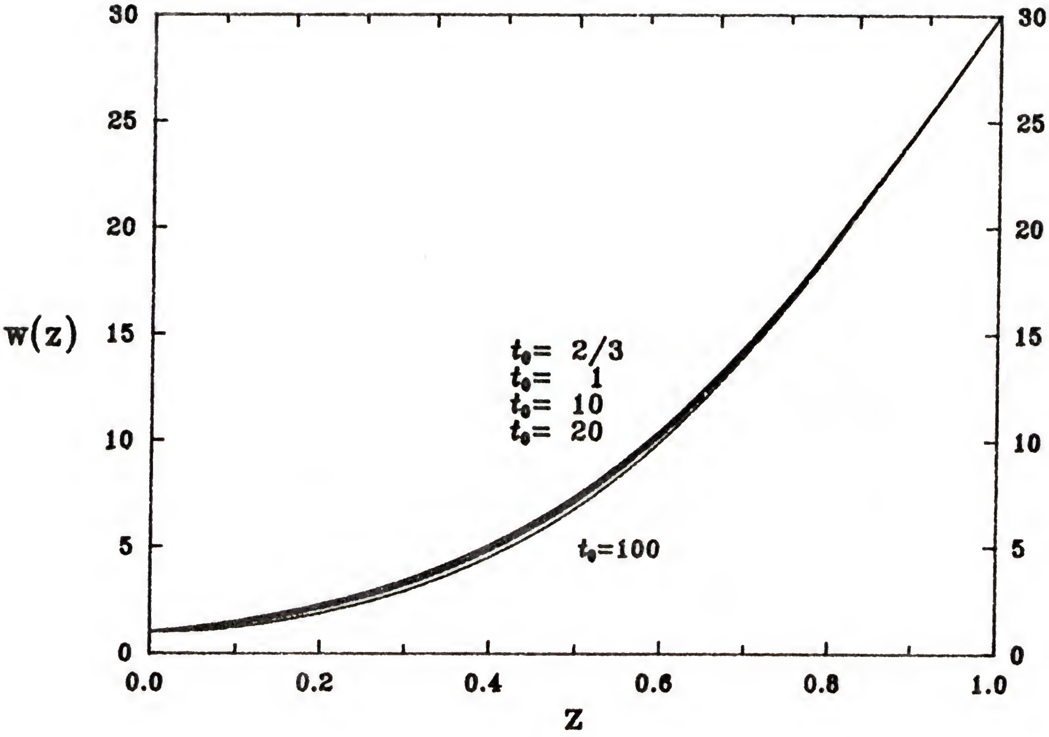

Figure 9. (continue).

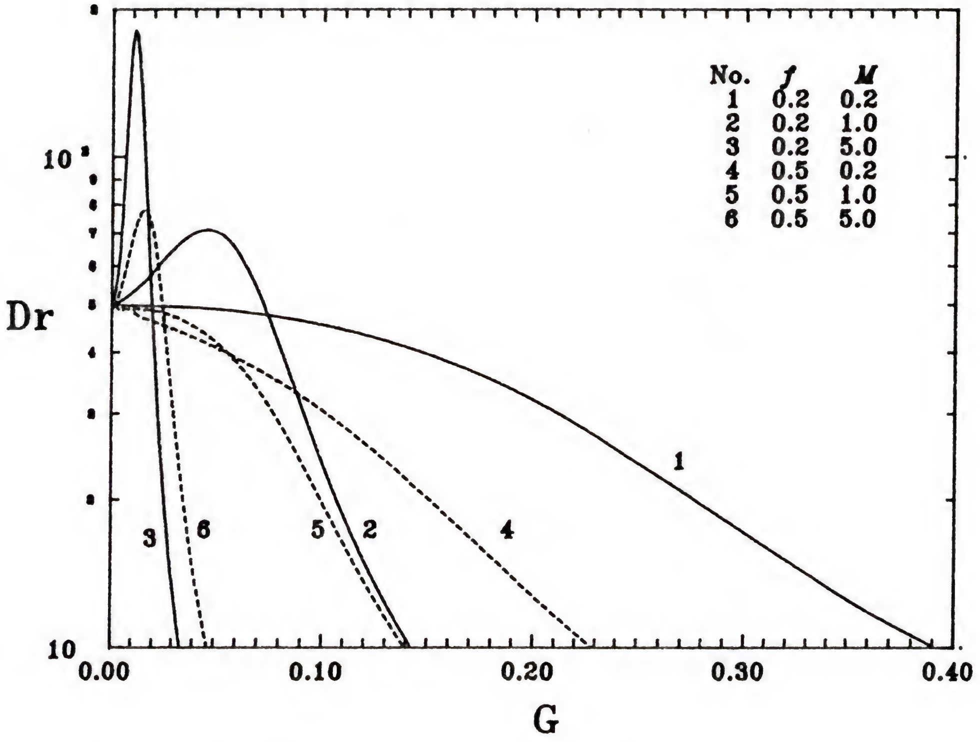

Figure 10. Draw ratio as a function of inverse axial force at different shear viscosity ratios; De=0.02, t_0=10.

When M is small (e.g. M=0.2, curve 1) the relative influence of the Newtonian fluid becomes weaker and the flow dynamics is dictated by the viscoelastic skin layer at a smaller value of Dr compared to larger M cases (i.e., curves 2 and 3). Consequenly, curve 1 for small M does not show the multiple steady state solutions that are observed with curve 2 or 3. The same behavior is also observed with a larger values of f (i.e., curves 4, 5 and 6). The stability behavior of these curves are discussed in Chapter 3.

2.8 Summary and Conclusion

The steady state flow characteristics of a two-phase fiber spinning flow has been investigated in this Chapter. It has been assumed that the core and the skin layers are a Newtonian and an upper-convected Maxwell fluid, respectively. These constitutive models are chosen since the major objective of the study is to investigate the competing influence of the viscous and viscoelastic forces of the core and skin layers. In order to avoid unnecessary complexity it has been further assumed that the flow is isothermal and that all external and surface forces are negligible other than the viscous and viscoelastic forces. Based on the results of the asymptotic analyses by previous investigators, the one-dimensional approximation has been applied at the outset in formulating the system equations. The one-dimensional approximation is equivalent to assuming that the velocity and the stress fields of the fiber spinning flow is independent of the radial coordinate.

Among many variables which may affect the two-phase flow, the effect of the flow rate ratio f and the Deborah number De has been extensively studied. It is rather obvious to anticipate that the characteristics of the two-phase flow may sit between those of the single-phase flows of each constituent fluid. An unexpected behavior has been also predicted by the current model in that the coextrusion flow may enable us to obtain a higher draw ratio than possible with the upper-convected Maxwell fluid only. As it is well established that the spinning of a Newtonian fluid is limited to a relatively low value of draw ratio due to the draw resonance instability, this new finding may have important implications if the high draw ratio flow is confirmed to be stable. In the following Chapter, the stability of the two-phase flow is investigated by the method of linear stability analysis.

Although the system under current consideration is very simple, the procedure and results presented here may serve as a basis for treating more complicated elaborate two-phase systems, with more sophisticated rheological equation.

CHAPTER 3
LINEAR STABILITY ANALYSIS

3.1 Introduction

The physical mechanism of the draw resonance instability is not yet clearly understood. It, however, appears to be a kinematic instability in the sense that it is observed and predicted with purely viscous fluids even in the absence of all external and surface forces.

In case of a Newtonian fluid, only one dimensionless parameter (draw ratio *Dr*) appears in the system equations and the predicted instability is independent of the shear viscosity, the flow rate or the draw span. In case of viscoelastic fluids, on the other hand, the draw resonance is influenced by the viscoelasticity which is represented by the Deborah number, *De*. Since the Deborah number is the ratio of the material time constant to the processing time, the change in either the flow rate or the draw span results in the variation of *De* thus affecting the onset of draw resonance. When a purely viscous fluid and a viscoelastic fluid are spun together as in the present system, a unique situation may arise since the relative influence of the viscoelasticity may change with the flow rate ratio of the two materials even for a fixed value of *De*. In this Chapter the stability of the two-phase spinning flow is investigated using the steady state solutions given in Chapter 2 as the base flow.

The method of linear stability analysis is applied to the present system for which the mathematical treatment is straightforward although complicated. Only a limited information may be obtained by the linear analysis as it is relevant to only infinitesimal disturbances. The sustained periodic nature of the draw resonance instability, however, may make the linear stability analysis meaningful. While the accurate prediction of the wavelength and the amplitude of the periodic instability may be obtained only through a nonlinear analysis, the mathematical method adopted in this work allows us to estimate the wavelength of the draw resonance. The estimated trend in the wavelength of the instability is apparently in qualitative agreement with the experimental observations which will be discussed in Chapter 4. In the following sections the existing studies on the stability of single-phase flows are briefly reviewed followed by the detailed formulation and analysis for the two-phase system.

3.2 Stability of Isothermal Newtonian Fiber Spinning Flow

The stability analysis for the single-phase flow of a viscous fluid was first performed by Kase and Matsuo (1967), Matovich and Pearson (1969). Their analyses were in principle a linear stability analysis although they involved some mathematical ambiguities. Later, Gelder (1971) treated the same problem in a more comprehensive manner by using the finite difference method. As another method for solving the stability problem, the orthogonal collocation method was applied by Gupta and Ballman (1982). The various mathematical approaches predicted that the critical draw ratio for the onset of draw resonance is 20.21 for Newtonian fluids. That is, the spinning flow of a Newtonian fluid is stable up to $Dr \cong 20.21$. Beyond that critical value, the spinning flow becomes unstable.

In this study, the finite difference method of Gelder was adopted for the two-phase flow (see Appendix A). This method involves the conversion of a differential eigenvalue problem into an algebraic eigenvalue problem by a finite differencing scheme, which is then solved by a well developed standard technique. While the conversion of the problem into a matrix form is rather complicated algebraically and very tedious, this method has an extra advantage of being able to investigate higher mode eigenvalues in addition to the most dangerous one.

As a measure of accuracy of the present calculation, the single-phase flow of a Newtonian fluid was treated and its results compared with the existing one. In Table 1, the present computational results are compared with those of Chang et al. (1981) for various spatial resolution. While the slight numerical difference may result from the difference in the differencing scheme (i.e., forward, central, backward differencing), this comparison confirms that present computational procedure is correct and accurate.

3.3 Stability of Isothermal UCM Fiber Spinning Flow

For viscoelastic fluids, the stability of fiber spinning flow was first studied by Fisher and Denn (1976). The generalized upper-convected Maxwell model (or White-Metzner model) was used for the analysis in which the shear viscosity and the elastic modulus are allowed to be dependent on the shear rate. The UCM model is a special case in which both the shear viscosity and the elastic modulus are fixed as constants. When $f=1$, the present two-phase system is reduced to the single-phase flow of a UCM fluid. Therefore, the present results can be also compared with those of Fisher and Denn (1976) for this extreme case. The stability analysis shows that the viscoelasticity generally has a stabilizing influence of the draw resonance especially when the Deborah number is large.

3.4 Stability of Two-Phase Fiber Spinning Flow

There exists no study on the stability of a two-phase fiber spinning flow to date. As mentioned in the preceding sections, existing analyses are only for the single-phase flows. The stability of the two-phase fiber spinning system is investigated in this section for the first time.

Table 1. Values of λ^1 for isothermal, Newtonian spinning at Dr=20.21

Discretisation points N	λ^1_{real}	λ^1_{imag}	λ^1_{real}	λ^1_{imag}
	(Chang et al., 1981)		(Present calculation)	
11	−1.0959	12.594	−1.1033	12.3898
21	−0.1489	13.561	−0.1811	13.5519
31	−0.0547	13.808	−0.0683	13.8061
41	−0.0294	13.895	−0.0367	13.8954
51	−0.0205	13.930	−0.0233	13.9365
N→∞	0.0	14.012	0.0012	14.0092

The present study is only a linear stability analysis and the results indicate that the onset of draw resonance of a Newtonian fluid is delayed to a higher draw ratio by the presence of the viscoelastic skin layer. It is also predicted that in a coextrusion flow under certain conditions, the highest draw ratio for a stable spinning can be much larger than that of the single-phase spinning of either fluid (Newtonian or UCM).

The stability of steady state solutions to infinitesimal disturbances is determined by the following standard procedure of the perturbation analysis in which solutions of the following form are sought:

$$A(z,t) = A^{ss}(z)\left[1 + a^{*}(z)e^{\lambda t}\right] \tag{3.1}$$

$$w(z,t) = w^{ss}(z)\left[1 + w^{*}(z)e^{\lambda t}\right] \tag{3.2}$$

$$\tau_{zz}(z,t) = \tau_{zz}^{ss}(z)\left[1 + \tau_{zz}^{*}(z)e^{\lambda t}\right] \tag{3.3}$$

$$T(z,t) = T^{ss}(z)\left[1 + T^{*}(z)e^{\lambda t}\right] \tag{3.4}$$

Here the superscripts *ss* denotes the steady state, and T is defined as $\tau_{zz} - \tau_{rr}$. The perturbation functions a^{*}, w^{*}, τ_{zz}^{*} and T^{*} are assumed to be very small, and the real part of λ, which is the eigenvalue of a normal mode, determines the stability of the steady solution.

By substitutiting (3.1)–(3.4) into the system partial differential equations (2.1), (2.13),(2.14) and (2.25) and by linearizing the resulting equations about the perturbation functions, the following homogeneous ordinary differential equations are derived

$$w^{ss}a^{*}{}' + w^{ss}w^{*}{}' = -\lambda a^{*} \tag{3.5}$$

$$
\begin{aligned}
&\left[3(1-f)GM(w^{ss})^2\right]w^{\bullet}{}''+\left[3(1-f)GMw^{ss}w^{ss}{}'\right]w^{\bullet}{}' \\
&+\left[3(1-f)GM\left\{w^{ss}w^{ss}{}''-(w^{ss}{}')^2\right\}\right]w^{\bullet}=\left[-fw^{ss}T^{\bullet}-3(1-f)GMw^{ss}w^{ss}{}'\right]a^{\bullet}{}' \\
&+\left[f(T^{\bullet}w^{ss}{}'-w^{ss}T^{\bullet}{}')+3(1-f)GM\left\{(w^{ss}{}')^2-w^{ss}w^{ss}{}''\right\}\right]a^{\bullet}+\left[-fw^{ss}T^{ss}\right]T^{\bullet}{}' \\
&+\left[f(T^{ss}w^{ss}{}'-w^{ss}T^{ss}{}')\right]T^{\bullet}
\end{aligned}
\tag{3.6}
$$

$$
\begin{aligned}
&\left[-2w^{ss}\left(1+\frac{G}{De\tau_{zz}^{ss}}\right)\right]w^{\bullet}{}'+\left[\frac{w^{ss}\tau_{zz}^{ss}{}'}{\tau_{zz}^{ss}}-2w^{ss}{}'-\frac{2Gw^{ss}{}'}{De\tau_{zz}^{ss}}\right]w^{\bullet} \\
&+\left[w^{ss}\right]\tau_{zz}^{\bullet}{}'+\left[\frac{1}{De}+\frac{w^{ss}\tau_{zz}^{ss}{}'}{\tau_{zz}^{ss}}-2w^{ss}{}'\right]\tau_{zz}^{\bullet}=-\lambda\tau_{zz}^{\bullet}
\end{aligned}
\tag{3.7}
$$

$$
\begin{aligned}
&\left[w^{ss}-\frac{3\tau_{zz}^{ss}w^{ss}}{T^{ss}}-\frac{3Gw^{ss}}{DeT^{ss}}\right]w^{\bullet}{}'+\left[\frac{w^{ss}T^{ss}{}'}{T^{ss}}+w^{ss}{}'-\frac{3\tau_{zz}^{ss}w^{ss}{}'}{T^{ss}}-\frac{3Gw^{ss}{}'}{DeT^{ss}}\right]w^{\bullet} \\
&+\left[-\frac{3\tau_{zz}^{ss}w^{ss}{}'}{T^{ss}}\right]\tau_{zz}^{\bullet}+\left[w^{ss}\right]T^{\bullet}{}'+\left[\frac{1}{De}+\frac{w^{ss}T^{ss}{}'}{T^{ss}}+w^{ss}{}'\right]T^{\bullet}=-\lambda T^{\bullet}
\end{aligned}
\tag{3.8}
$$

Here the prime denotes the differentiation with respect to the axial coordinate z. For the spinning process in which the take-up speed is held constant, the boundary conditions for the eigensystem (i.e., Equations (3.5)–(3.8)) follow from Equations (2.19)–(2.23):

$$
a^{\bullet}(0)=w^{\bullet}(0)=\tau_{zz}^{\bullet}(0)=T^{\bullet}(0)=w^{\bullet}(1)=0 \tag{3.9}
$$

Equations (3.5)–(3.9) constitute an eigenvalue problem for which nontrivial solutions exist only for certain values of λ. A steady state solution is stable to infinitesimal disturbances if all eigenvalues λ have negative real parts, since the perturbations defined by (3.1)–(3.4) then decay to zero.

To discretize the eigenvalue problem (Equations (3.5)–(3.9)), the finite difference method was used with the step size h. The grid points are either boundary or regular interior points. For all grid points in the interior, the central difference was applied. Either forward difference or backward difference was used at the two boundary points. Using this finite differencing scheme, the system equations are converted into a standard form of an algebraic eigenvalue problem. For the spatial resolution of n, the dimension of the eigenvector is $3n$. The detailed derivation of the algebraic eigenvalue problem is described in Appendix A. The eigenvalue equations are solved by using the subroutine called DEVLRG in IMSL mathematical package.

3.5 Results and Discussion

In principle, there exist infinite number of eigenvalues for the given eigenvalue problem indicating that the number of discretisation points should be infinite. Due to the computational limitation, the calculation can be done only with a finite number of discretisation points. Then, the numerical value of eigenvalues will depend on the spatial resolution N. In Table 2, the dependence of the first eigenvalue (i.e., the eigenvalue with largest real part) on the number of discretisation points N is given for f=0.2 and 0.5 when Dr=30 and De=0.02. The Richardson extrapolation (Fröberg, 1985) is applied to these data to obtain the limiting value of λ as the number of discretisation points tends to infinity. The positive real part for f=0.2 indicates that the steady state solution at Dr=30 is unstable whereas it is stable when f=0.5 since the most dangerous eigenvalue has the negative real part. Thus, in Figure 6a, the two velocity profiles for f=0.5 and 1.0 are stable to infinitesimal disturbances while the others are unstable.

In Figure 11 the real parts of the first eigenvalue is plotted as a function of draw ratio Dr for f=0.5 at three different values of Deborah number. This figure indicates that when De=0.016 the spinning flow is stable at all draw ratios smaller than the maximum

Table 2. Values of λ^1 for differential values of discretisation points (De=0.02, Dr=30, t_0=10.0, M=1.0)

Discretisation points	f=0.2		f=0.5	
N	λ^1_{real}	λ^1_{imag}	λ^1_{real}	λ^1_{imag}
11	−0.6521	12.8830	−0.9022	11.5929
21	0.2415	14.3838	−0.9969	14.0687
31	0.2959	14.7408	−1.2054	14.6858
41	0.2938	14.8688	−1.3359	14.8928
51	0.2977	14.9406	−1.3841	15.0186
61	0.2992	14.9879	−1.4117	15.1019
71	0.2994	15.0209	−1.4208	15.1591
N→∞	0.3211	15.1006	−1.4272	15.3224

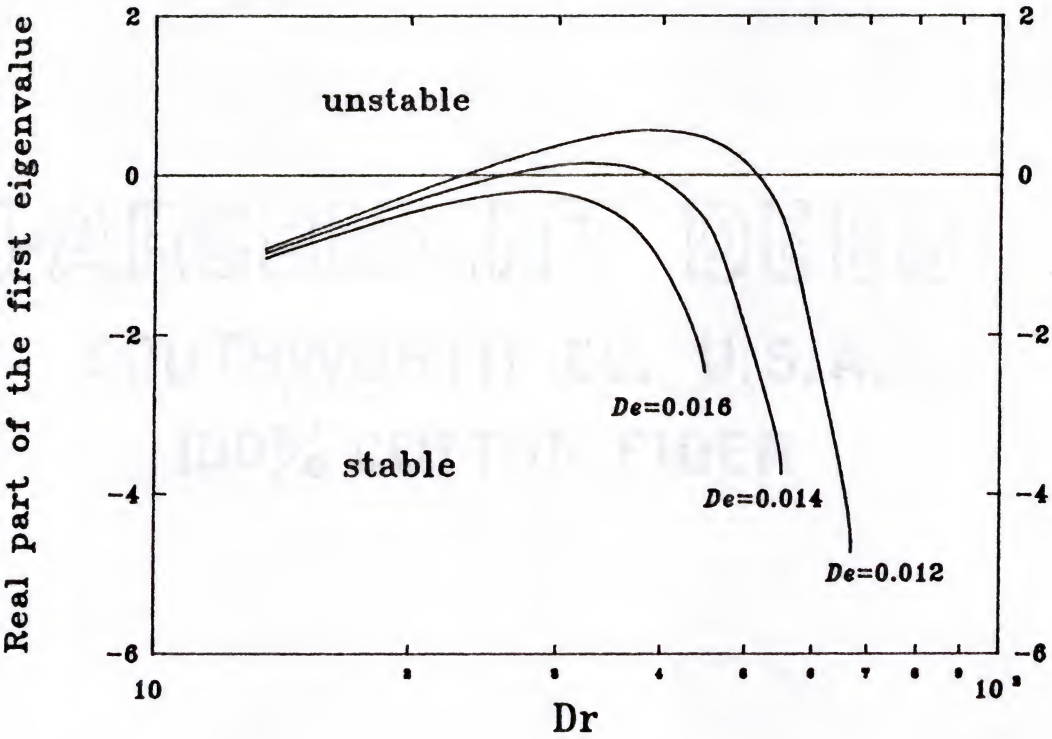

SOUTHWORTH CO., U.S.A.
100% COTTON FIBER

Figure 11. Variation of the real part of the first eigenvalue with draw ratio for various Deborah numbers at f=0.5, t_0=10, M=1

attainable value which corresponds to the infinite applied force. When *De*=0.012 or 0.014, on the other hand, there exist two stable regions: one at a low value of *Dr* and the other at a higher value of *Dr*. These behaviors are very similar to those of a single-phase flow of an UCM fluid for which the upper stable region at high draw ratio was first found by Fisher and Denn (1976). The general behavior given in Figure 11 is typical of all *f* in the range of between 0.1 to 0.8.

The critical draw ratio at which the real part of the first eigenvalue becomes zero is plotted as a function of Deborah number in Figure 12. In this plot of *Dr** vs. *De*, each pair of neutrally stable points described in Figure 11 appears as a continuous line dividing the whole domain into the stable and unstable regions. In typical fiber spinning operations, the spinning conditions (i.e., output, draw span, material, etc.) are predetermined and the take-up speed is gradually increased to achieve a desired draw ratio. In other word, *Dr* is gradually increased to the target value for a fixed *De*. Therefore, the upper stable region is generally unattainable unless special approach is taken to go around the nose (or tip) of the neutral-stability curve. While a few investigators alleges experimental observation of the upper stable region (Fisher and Denn, 1976), others contend that it is an artifact of the unrealistic constitutive model. In any case, the more important character of the neutral-stability curve is the sharp upward turn from a near horizontal shape with increasing *De* whether it turns further backward forming the upper stable region or not. This sharp upward turn occurs at about *De*=0.01 when *f*=1.0. When *Dr* reaches about 100, the fiber may snap instead. Thus, when *De*>0.1, the draw resonance is unobservable (or the critical draw ratio for its onset increases drastically). The dotted diagonal line (c) indicates the maximum obtainable draw ratio for *f*=1.0 at which the axial tension becomes infinity. This behavior is physically plausible since the viscoelasticity effect is influential only when the Deborah number is large.

As the skin-layer flow rate fraction *f* is decreased, the nose of the unstable

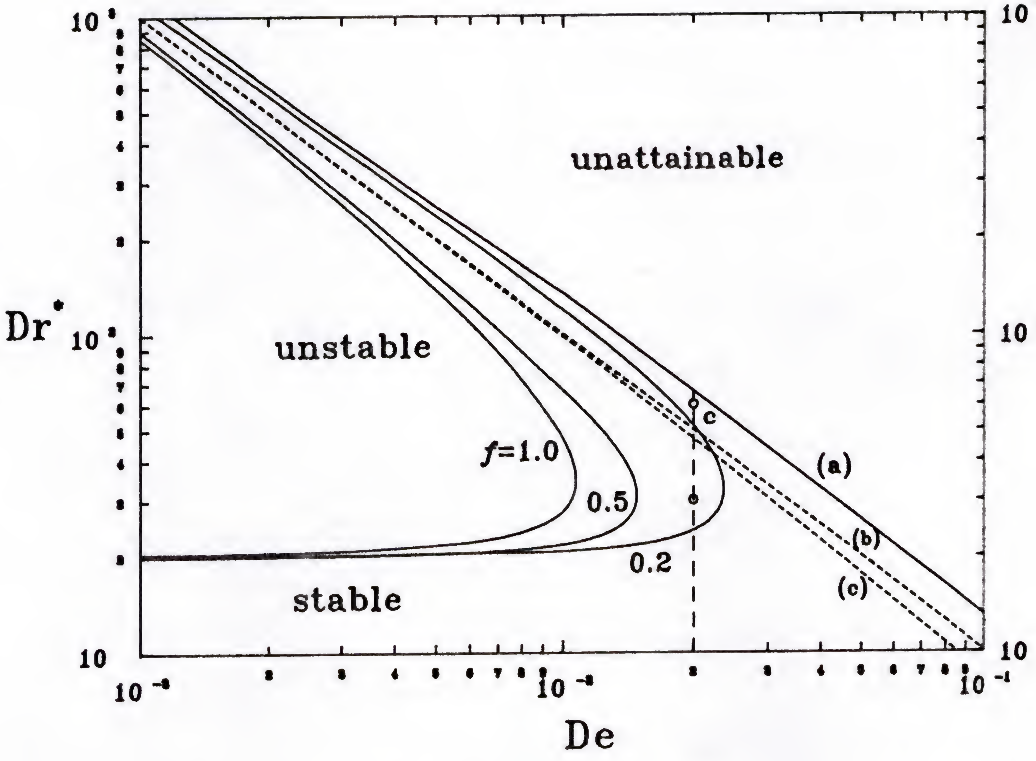

Figure 12. Critical draw ratio as a function of Deborah number for various *f* at t_0=10, *M*=1 (maximum attainable *Dr* for (a) *f*=0.2(Max); (b) *f*=0.2(Asymptote); (c) *f*=0.5 and 1.0)

envelope extends to a higher value of *De*. When *De* is small, the lower critical draw ratio does not vary significantly with *f* and it is close to the Newtonian value of 20.21. At a higher *De* (i.e., *De*>0.01), however, the lower critical draw ratio increases with *f* indicating the stabilizing effect of the viscoelastic skin layer. From this figure the stability of the velocity profiles given in Figure 6 can be determined. The steady state solution described in Figure 6a (*De*=0.02 and *Dr*=30) falls on the stable region if *f*=1.0 or 0.5 whereas it falls on the unstable region if *f*=0.2. When *Dr* is increased up to 60 at the same *De* (i.e., *De*=0.02), the spinning condition belongs to the upper stable region of *f*=0.2 curve. Thus, in Figure 6 the two curves for *f*=1.0 and 0.5 are stable whereas those for *f*=0.2 and 0.0 are not. It should be pointed out again that the upper stable region may be an artifact which may not exist in real systems.

The most interesting feature of the coextrusion fiber spinning may be the possibility of a substantial increase in the maximum attainable draw ratio when *f* is relatively small. As discussed previously, Figure 13 indicates that a draw ratio which is much greater than the asymptotic value for an infinite draw force (i.e., $G \rightarrow 0$) is attainable when *f*=0.2. The stability analysis shows that the low-*G* branch of the multiple steady solutions (i.e., the portion of the *f*=0.2 curve where *G*<0.045 including point **a**) is always unstable. The high-*G* branch of the solution, on the other hand, is either stable or goes through two transitions with increasing *Dr* depending upon the magnitude of *De*. These behaviors are clearly shown in Figure 12 and 13. When *De*=0.02 and *f*=0.2, a stable-to-unstable and an unstable-to-stable transitions occur at *Dr*=24.07 and 51.24, respectively as *Dr* is increased. When *De* is greater than 0.0236, on the other hand, the spinning condition is outside the nose of the unstable envelope and the "spinning stability is sustained up to 62." The solid line (a) in Figure 12 is the locus of the maximum points of *Dr* vs. *G* curve (e.g. point **c** in Figure 13) for *f*=0.2 which includes (*De*,*Dr*)=(0.0236,62) point. When *f*=1.0 or 0.5, the maximum attainable draw ratio at

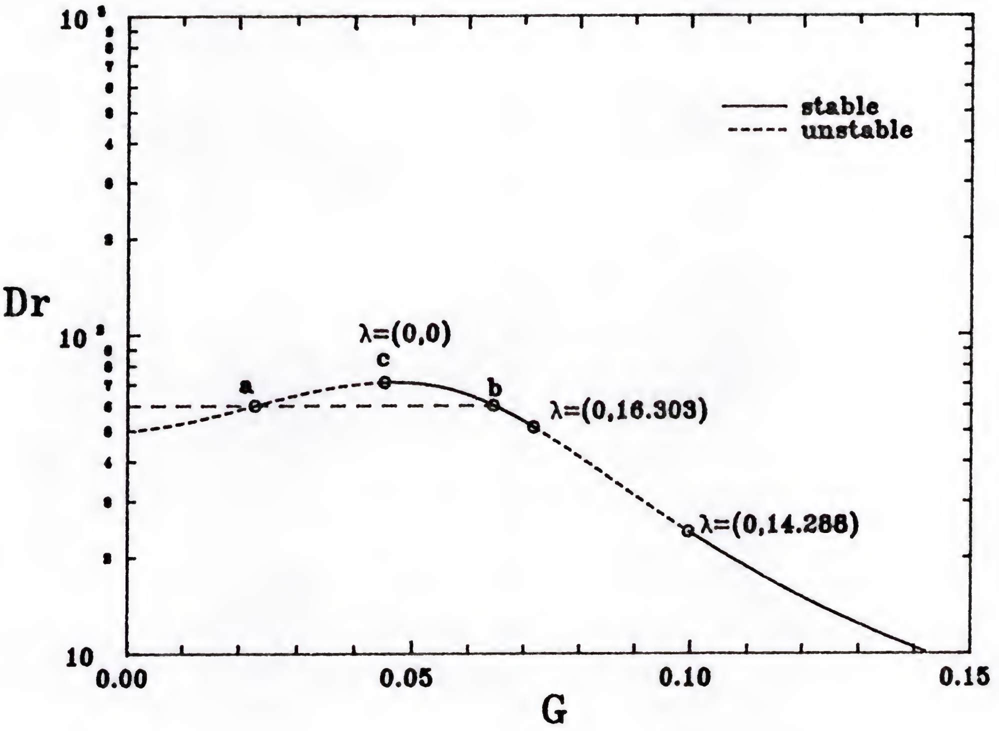

Figure 13. Draw ratio as a function of inverse axial force (f=0.2, De=0.02, t_0=10, M=1)

De=0.0236 is about 43. Therefore, much higher value of Dr is obtainable when f=0.2 than when f=0.5 or 1.0.

In Figure 14, Dr vs. G curves are given for various values of De when f=0.2. Also indicated in the figure are the neutral-stability curves dividing the stable and the unstable region. It may be noted that the neutral-stability curve on the left hand side coincides with the locus of the maximum points of Dr–G curves. It is interesting to point out that the imaginary part of the first eigenvalue is zero along this curve (see point **c** in Figure 13) indicating catastrophic failure (e.g., sudden snap or breakage) beyond this curve. The location of this curve depends on the value of f. As f increases, the maximum point of the Dr–G curve disappears and the neutral stability curve coincides with the vertical axia (i.e., Dr axis). On the other hand, the neutral stability curve on the right hand side is a universal curve whose location is fixed regardless of other parameters. This right hand side neutral stability curve cuts through the portion of Dr vs. G curves for De<0.0236. Since in a typical operation, the high Dr is approached along the Dr–G curve from the large-G side, the stable region between the two unstable regions is not attainable when De<0.0236. Therefore, only the shaded region is the stable region that is attainable.

One of the most important findings may now be reiterated as follows. For a given choice of material, the Deborah number is the same regardless of the skin-layer fraction f if the total flow rate is the same and the spinning occurs over the same draw span. Thus, it is possible to obtain a much higher draw ratio with coextrusion than obtainable with either the UCM fluid or the Newtonian fluid, if De is large enough so that the high–G branch solution is stable without cutting through the unstable region. For example, if a skin-layer material is chosen so that De is about 0.0236, a stable spinning is possible up to Dr≈62 when f=0.2. This draw ratio is much larger than the value which is attainable with either the core material ($Dr_{\max}$=20.21) or the skin material ($Dr_{\max}$=43.37) for the same value of De.

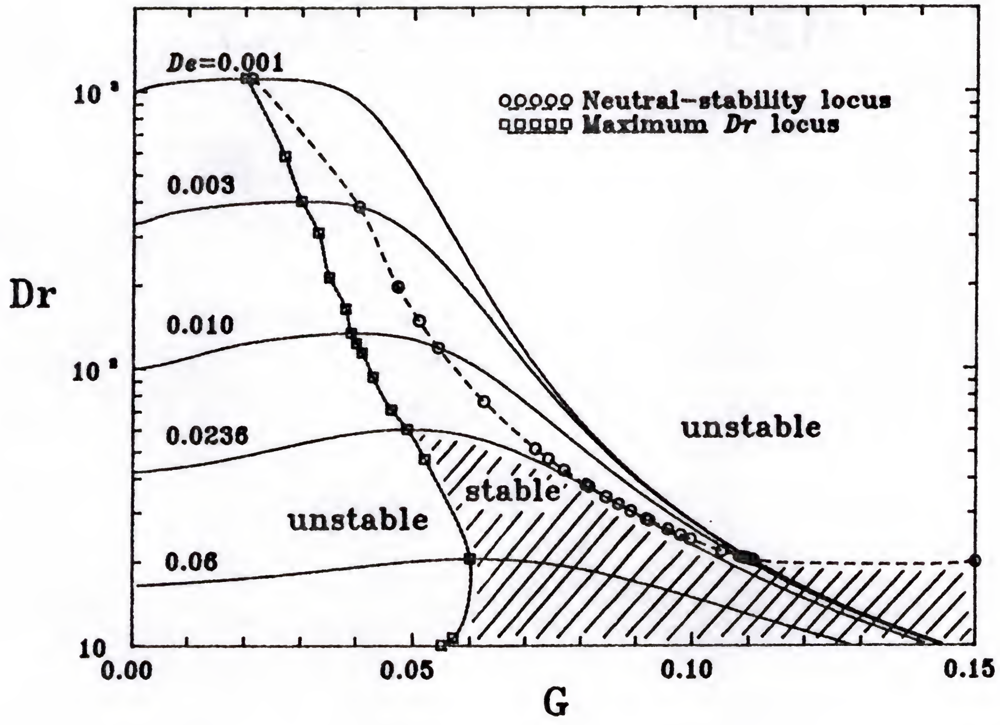

Figure 14. Draw ratio as a function of inverse axial force for various Deborah numbers (f=0.2, t_0=10, M=1)

These stability characteristics of the two-phase flow may be presented in another way using the $3G\ln Dr$ vs. *De* curves discussed in Chapter 2. These have been already indicated in Figures 4a and 4b. When f=1.0, 0.5 or 0.2, the system for Dr=20 is always stable for any *De* which is smaller than the maximum values. It is not surprising when considering the critical draw ratio of 20.21 for a Newtonian fluid. An interesting point though is the value of the maximum *De* which is 0.061 for f=0.2 that is much larger than those for f=0.5 or 1.0. When *Dr* is larger (i.e., Figure 4b for Dr=30), the system is unstable for small *De* and moves into a stable region as *De* is increased. Following the $3G\ln Dr$ vs. *De* curve from left to right is equivalent to following a horizontal line in Figure 12 (i.e., constant *Dr* line). Thus, the lower neutral-stability curve in Figure 15 which connects the maximum *De* points is equivalent to the diagonal line (a) in Figure 12. The unstable region in the upper left corner is then the draw resonance region and the lower unstable region is the catastrophic failure (i.e., breakage) region.

An important advantage of using the finite difference technique for the eigenvalue problem is the information regarding the higher modes of instability (Geyling and Homsy, 1980). In Table 3 the real parts of the first four eigenvalues are given at the two critical draw ratios. These data represent the general trend of eigenvalues at all critical conditions that have been examined. It may be noted that the higher modes for these cases have relatively large negative values (i.e., $\lambda_{\text{real}}<-2.6545$) indicating that they are strongly damped. Although the linear stability analysis provides only a limited information about the dynamical behavior of the process for small time, this trend in the real part of the eigenvalues suggests that the instability may quickly evolve to a nonlinear regime with the wavelength (or the period) defined by the imaginary part of the first eigenvalue (i.e., 14.05 for Dr=21.79 and 17.78 for Dr=75.96). Thus, a measured period of draw resonance instability may agree with this predicted value if the constitutive model properly represents the spinning material.

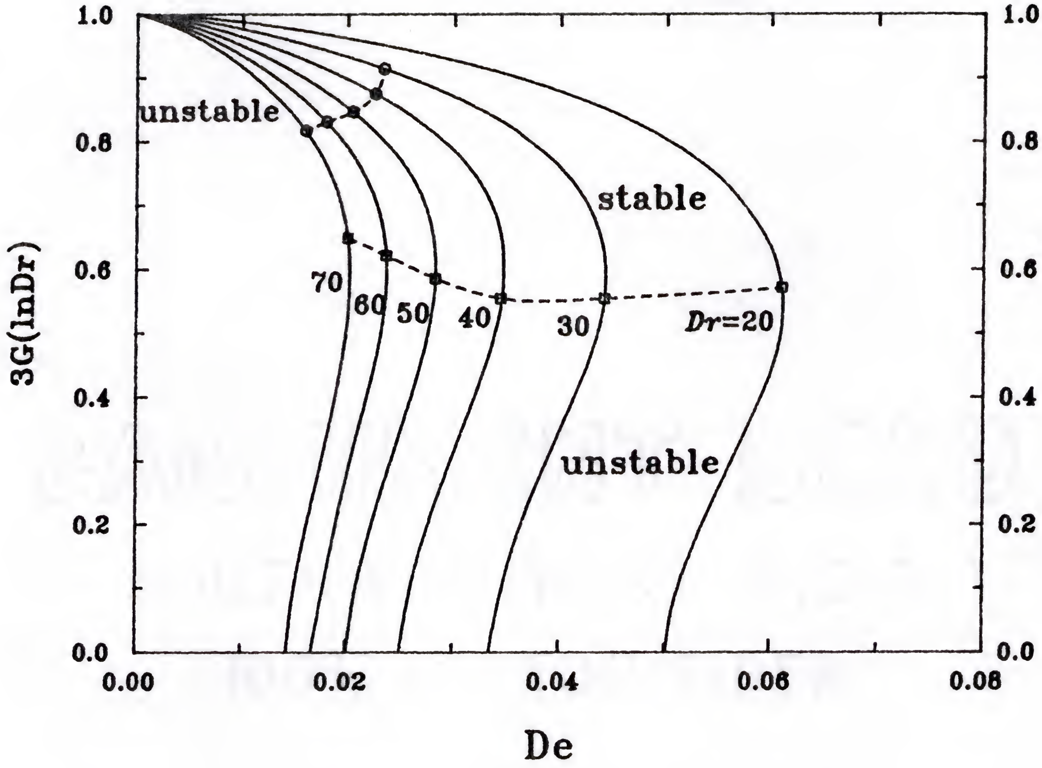

Figure 15. Inverse axial force as a function of Deborah number for various draw ratios (f=0.2, t_0=10, M=1)

Table 3. Real and imaginary parts of first four eigenvalues at the critical Dr^* (f=0.2, De=0.015, t_0=10.0, M=1.0)

	Dr^*=21.79		Dr^*=75.96	
	λ_{real}	λ_{imag}	λ_{real}	λ_{imag}
1st eigenvalue	0.0000	14.0517	0.000	17.7820
2nd eigenvalue	−2.6545	33.8660	−7.1597	47.2597
3rd eigenvalue	−4.5370	62.9363	−10.6844	67.6269
4th eigenvalue	−4.7455	49.9121	−14.2681	83.1421

In Figure 16 the neutral-stability curve for f=0.2 is given along which all the real parts of the first eigenvalues are zero. Also given on the curve are the imaginary parts of the first eigenvalues, λ^1_{imag}. A noticeable trend is that the imaginary part of the first eigenvalue increases with the critical draw ratio, Dr^*.

The dimensionless period $\bar{t}$ (scaled by L/w_0) which corresponds to λ^1_{imag} can be calculated by the following equation.

$$\bar{t} = \frac{2\pi}{\lambda^1_{\text{imag}}} \tag{3.10}$$

In Figure 17, the period thus calculated is given as a function of critical draw ratio for various values of f. This figure indicates that the period (thus the wavelength of the instability) decreases with increasing critical draw ratio. As pointed out earlier this predicted period (or wavelength) may agree with measured value if the constitutive model accurately describes the rheology of the material being spun. The UCM fluid model is too simple to be realistic. Thus, quantitative agreement between the measured and predicted period is not expected. The Newtonian limit (i.e., $\lambda^1_{\text{imag}}\cong 14$), however, should show the agreement if the current argument is correct. Unfortunately, no polymers are Newtonian. However, the relative insensitivity of the critical Dr^* over a broad range of De (see Figure 16 for $De<0.01$) suggests that if a polymer with a small relaxation time is spun the period of draw resonance instability may closely simulate the Newtonain value. As will be discussed in Chapter 4, the quantitative agreement is in fact obtained in the Newtonian limit. It will be also shown that the decreasing trend of period with increasing Dr^* is also in accordance with the experimental observations.

A characteristic time which may be closely related with the kinematics of the fiber spinning flow is the material residence time, T_{RST}. T_{RST} is the time needed for a

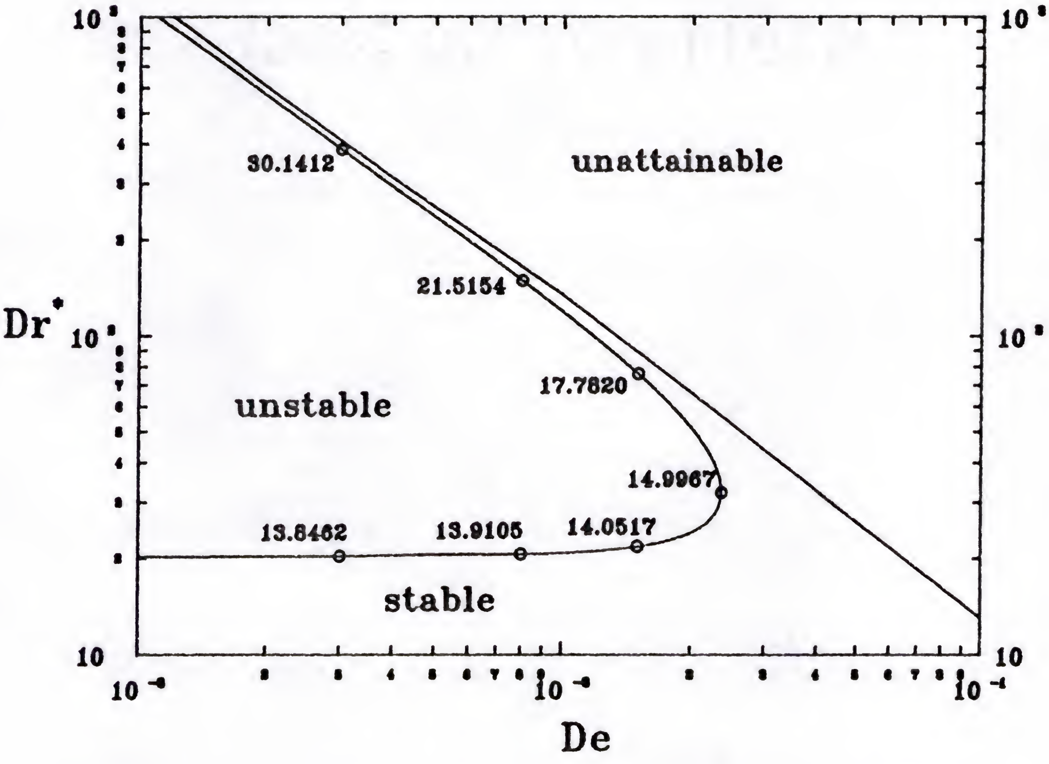

Figure 16. Neutral-stability curve for f=0.2, t_0=10, M=1. Values of λ^1_{imag} indicated on curve.

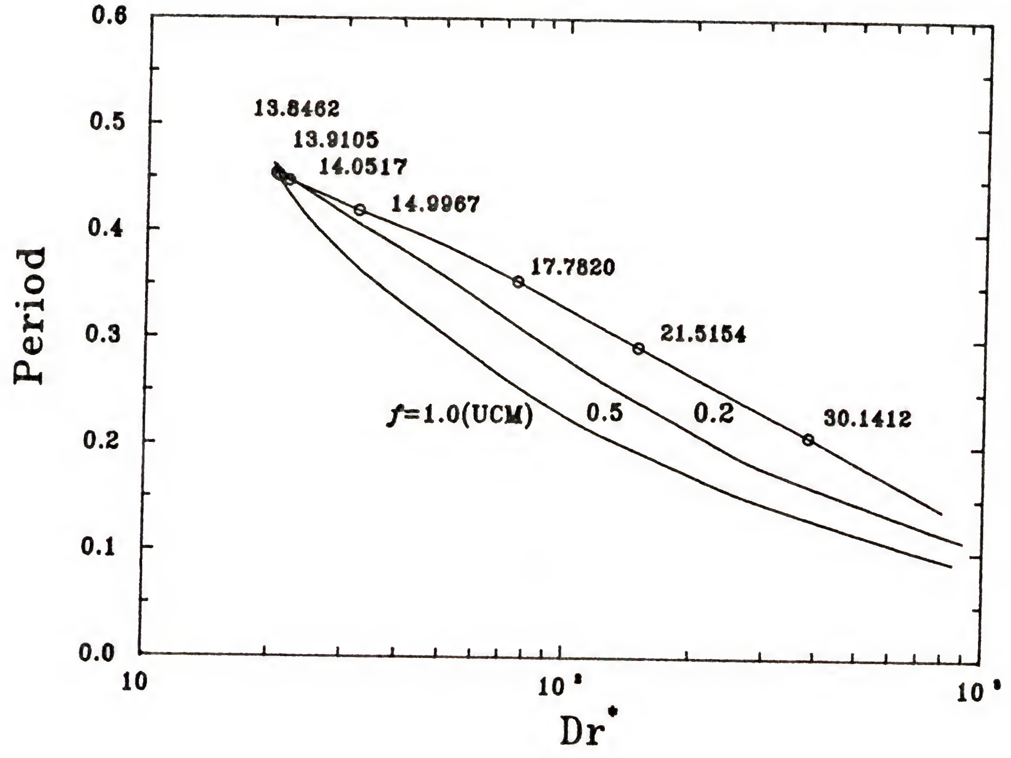

Figure 17. Period of the first normal mode at critical conditions. Values of λ^1_{imag} indicated on curve.

small fluid element to travel from the die exit to the take-up (i.e., Lagrangian time at the take-up). Once the axial velocity is determined, the material residence time can be calculated as follows:

$$T_{RST} = \int_0^1 \frac{dz}{w(z)} \tag{3.11}$$

As discussed in Chapter 2, the axial velocity profile is significantly affected by the viscoelasticity through the changes in the kinematics of the flow. If the draw resonance instability is to be closely related to the kinematics of the flow, so is the characteristic time of the instability (i.e., period) to the residence time which may represent the flow kinematics. In Figure 18, the dimensionless period $\bar{t}$ at the critical draw ratio is plotted against the residence time determined from the steady velocity profile at that draw ratio. The Simpson's 3/8 integration rule has been used to calculate the residence time. Although it is not clear at this point what the relationship between $\bar{t}$ and T_{RST} should be if there exists any, Figure 18 shows a rather strong correlation between the two characteristic times in that the period of the instability is small if the material residence time is short. All data are near the straight dashed line which is a linear regression from those data of f=1.0 (i.e., UCM single-phase fiber). The regression expression is written as follows:

$$\bar{t} = 0.062 + 1.226 \times T_{RST} \tag{3.12}$$

The influence of the shear viscosity ratio M on the steady spinning flow has been discussed in the previous Chapter. Here the influence of M on the flow stability has been investigated and the results are given in Figure 19. For a fixed value of f (i.e., f=0.2), the

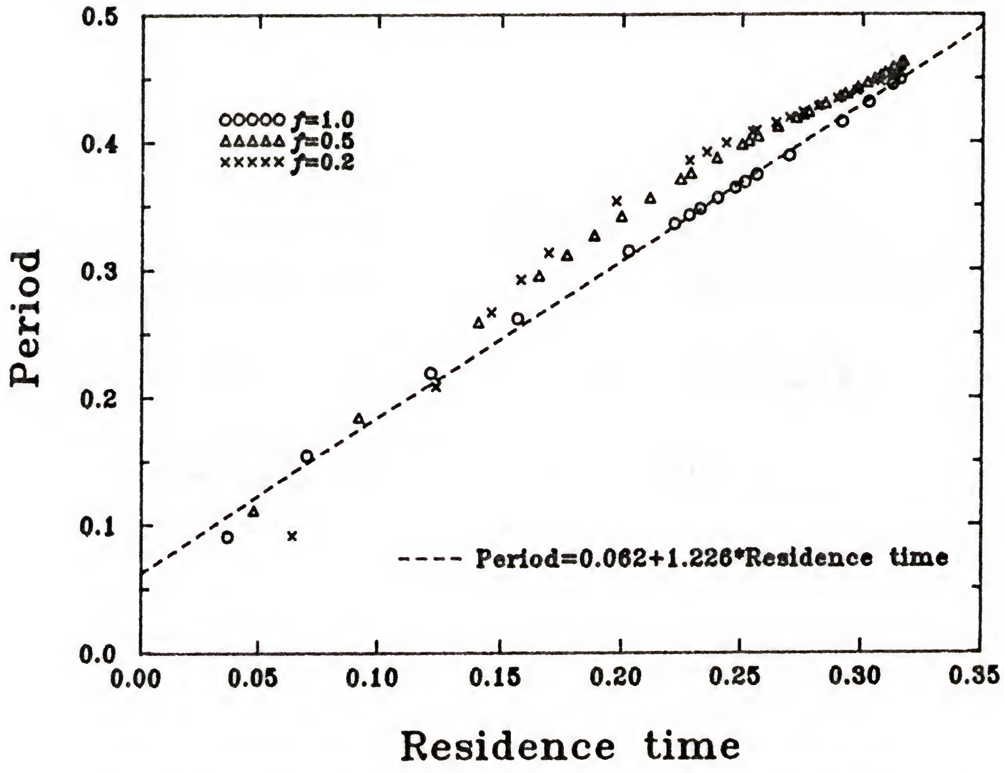

Figure 18. Dimensionless period as a function of residence time for various f at t_0=10 and M=1

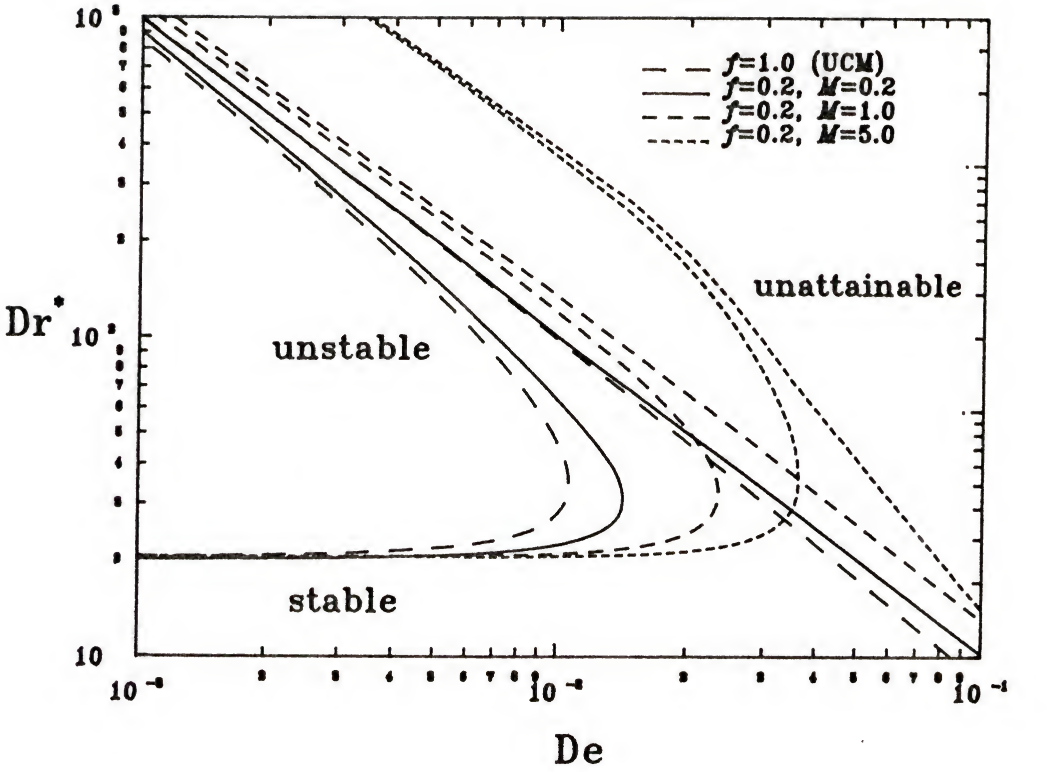

Figure 19. Critical draw ratio as a function of Deborah number for various M at f=0.2, t_0=10, compared with that for f=1.0(UCM), M=1 and t_0=10; curves: neutral-stability curves, straight lines: maximum draw ratio locus

shear viscosity of the Newtonian core was varies to get M=0.2, 1.0 and 5.0, respectively. The neutral-stability curves shown in Figure 19 with various M show that when the values of M decrease, the nose of the neutral-stability curve on the Dr^*–De plane is moved toward left. This trend is plausible since the influence of the Newtonian core weakens as M decreases resulting in the shift of the neutral-stability curve toward that for the UCM fluid. Decreasing M is equivalent to decreasing the shear viscosity of the Newtonian core. While the overall shape (or trend) of the neutral-stability curve remains the same, this figure bears an interesting implication. For a fixed total flow rate and f, if the same skin-layer material is used while changing the viscosity of the core material, the Deborah number remains the same. If De is 0.02, the coextrusion flow for M=0.2 is stable until it breaks at $Dr \cong 50$. Draw resonance, however, is encountered at a much smaller Dr for others (i.e., M=1.0 or 5.0). If the skin material has a large relaxation time so that $De \cong 0.4$, on the other hand, all three curves indicate stability. The maximum attainable Dr for M=5.0, however, is about 60 whereas those for others (i.e., M=0.2 or 1.0) are smaller than about 35. Thus, from a processing standpoint this plot suggests that a higher viscosity of the Newtonian core is favorable as long as the skin layer has a large enough relaxation time.

3.6 Summary and Conclusion

The stability of a two-phase fiber spinning flow to an infinitesimal disturbance has been investigated in this Chapter. By the method of linear stability analysis, the critical draw ratio for the onset of draw resonance has been determined as a function of Deborah number De and the skin-layer flow rate fraction f. The shape of the neutral-stability curve in a Dr vs. De plane for the two-phase flow is similar to that for the single-phase flow of a UCM fluid.

When *De* is small (i.e., when the viscoelasticity of the skin layer is small), the critical draw ratio remains in the vicinity of 20.21 which is the value for a Newtonian fluid. As *De* is increased, the neutral-stability curve make a sharp upward turn thus making the spinning flow free from the draw resonance instability. In this case, the spinning flow is limited by the large axial stress which can exceed the cohesive strength of the material resulting in a spinline breakage. This general trend is preserved for all values of *f* although the value of *De* where the sharp upturn occurs shifts to a larger value with decreasing *f*. On the other hand, the upper limit of draw ratio at which the spinline may break increases with decreasing *f*. Consequently, an interesting behavior can be observed with the coextrusion flow in that the highest draw ratio for a stable two-phase spinning can be larger than that for each constituent material under a certain condition. This prediction may have important practical implication if it can be proved experimentally. Although the present result is based on a simple constitutive model, the overall characteristics is physically plausible and other viscoelastic constitutive model may result in a similar prediction.

The linear stability analysis provides only a limited information for the short-time behavior of the instability. Nevertheless, the qualitative trend predicted by the theory regarding the critical draw ratio as well as the wavelength of the instability is apparently in reasonable agreement with the experimental observations which will be discussed in the following Chapter.

CHAPTER 4
DRAW RESONANCE EXPERIMENTS

4.1 Introduction

Coextrusion fiber spinning experiments have been conducted using a linear low-density polyethylene (LLDPE) and a low-density polyethylene (LDPE) for the core and the skin layers, respectively. These two materials are chemically identical, yet their rheological properties are very different from one another as they are manufactured by completely different processes. The LDPE has a high degree of long chain branching, and has a large relaxation time compared to the LLDPE. Consequently, the former tends to show a distinct strain hardening behavior when subjected to an extensional flow whereas the latter does not. Furthermore, the LLDPE is known to be very prone to draw resonance whereas the LDPE is not. The spinability of the LDPE is in fact observed to be limited by the breakage of the spinline rather than by the draw resonance.

The objective of the experimental study is to investigate the draw resonance characteristics of a bicomponent fiber spinning process and to compare them with the theoretical investigation described in the previous chapters.

The theory mentioned in previous chapters is for a simple constitutive model with many simplifying assumptions. Consequently, any quantitative agreement with experimental observations may not be expected. Nevertheless, the general trend predicted by the theory seems to be in reasonable agreement with the experimental results at least qualitatively.

In most of the experiments on the single-phase fiber spinning, the ratio of maximum-to-minimum diameter, critical draw ratio and period (and sometimes draw force) were measured while the extrusion output (or flow rate), take-up velocity, spinning length (or draw span) and melt temperature were varied. Although there are some contradicting reports depending upon the choice of the materials and extrusion conditions, many experiments have shown the following general characteristics of draw resonance:

(1) A longer draw span results in a decrease in the maximum-to-minimum diameter ratio and an increase in period, whereas it has negligible influence on the critical draw ratio.

(2) Increasing output typically has the opposite effect of increasing draw span.

(3) A higher melt temperature results in a larger critical draw ratio and a smaller maximum-to-minimum diameter ratio.

The proper time scale for the fiber spinning flow is the processing characteristic time L/w_0 which is the ratio of the draw span to the initial average velocity as discussed in the previous chapters. It seems that the observations (1) and (2) simply reflect the nature of the time scale for this process.

A similar experimental procedure was followed for the present study in which the critical draw ratio, the ratio of the maximum-to-minimum diameter, and the period were measured while the spinning length (or draw span) and the flow rate fraction of the skin layer were varied.

4.2 Experiment Materials

Four different polyethylenes were used for the experimental study. Two of them were linear low-density polyethylene (LLDPE) and the rest were low-density polyethylene (LDPE). The two LLDPEs were for the core while the LDPEs were for the skin layer. These materials are commercial products of Union Carbide Corporation and DuPont. As pointed out previously, LLDPEs are very prone to draw resonance whereas LDPEs are not due to their large relaxation time. The significant difference in their rheological properties results from their different molecular structures. None of these materials may be adequately described by either the Newtonian or the upper-convected Maxwell fluid model. Nevertheless, these materials were chosen with a Newtonian and a UCM fluid in mind. Despite the differences in their rheological properties, all of them are chemically compatible with each other and consequently, good adhesion at the core-skin interface is ensured.

In Table 4, the nominal information for the materials is given which has been provided by the Manufacturers. Also included are the zero-shear viscosities that have been measured in our Department. The important difference between the two LLDPEs is their shear viscosities represented by the melt index. The melt index, which is one of the standard parameters that characterize the material, represents the flow rate of the material through a capillary at a fixed temperature and a fixed pressure drop. Thus, a high value of melt index indicates a low viscosity. In case of LLDPEs, the shear viscosity is, very roughly, inversely proportional to the melt index, and the zero-shear viscosities seem to confirm the rough relationship.

The two LDPEs listed in Table 4 are known to have different level of long chain branching. DYNH-1 (Union Carbide) is produced by a tubular reator whereas Alathon-1540 (DuPont) is by an autoclave reactor. Autoclave resins are known to have much higher level of long chain branching than others, and consequently have larger relaxation time than others at a similar molecular weight. Thus, it is expected that Alathon-1540 will have a higher Deborah number than DYNH-1 under the same extrusion condition despite its larger melt index.

Table 4. The properties of experiment materials

Material type	Nomenclature (Manufacturer)	Melt Index	Density, ρ (kg/m^3)	Zero shear viscosity, η_0 (Pa-sec)	(at °C)
LLDPE	HS-7028 (Union Carbide)	1	918	9919	(200)
LLDPE	DMDA-8320 (Union Carbide)	20	922	2228	(200)
LDPE	DYNH-1 (Union Carbide)	1	918	22240	(145)
LDPE	Alathon-1540 (DuPont)	6.5	918	7899	(145)

The most desirable choice of materials for the current experiment may be two LLDPEs with different shear viscosity with all other proporties the same and two LDPEs with different elasticity while all other properties remain the same. In case of LLDPEs, such condition is met reasonable well with the current materials. In case of LDPEs, however, the shear viscosities are very different. It is an unfortunate situation, but limited availability of materials provided no other choice.

The rheological property information given above is rather qualitative. The most important rheological property relevant to the fiber spinning process is the elongational viscosity. The measurement of steady elongational viscosity, however, is very difficult if not impossible. Furthermore, the interpretation of the data provided by any existing "elongational viscometer" is controversial since what is measured may not be a steady behavior but the transient behavior of the strong flow.

In Figures 20~23, additional information is given for the rheological properties of the materials. These were measured using a rheogoniometer (Model # RMS-800). Parallel plates of 25 mm in diameter were run at a steady mode to measure the shear viscosity and the normal stress differences. The gap distance were varied at 0.4, 0.8, 1.0 1.1 and 1.5 mm. The temperature for the measurements was fixed at 145°C and 200°C for the LDPEs and the LLDPEs, respectively, to match with the operation temperatures for the fiber spinning experiment.

The results in Figure 20 show that the viscosities of all materials have no apparent change with shear rate at low shear rate range whereas DYNH-1 shows a little shear thinning behavior at a higher shear rate. The high viscosities of LDPEs which are apparently higher or equivalent to that of HS-7028 are due to the low mearsurement temperature. The DMDA-8320 has a much smaller viscosity than others as expected.

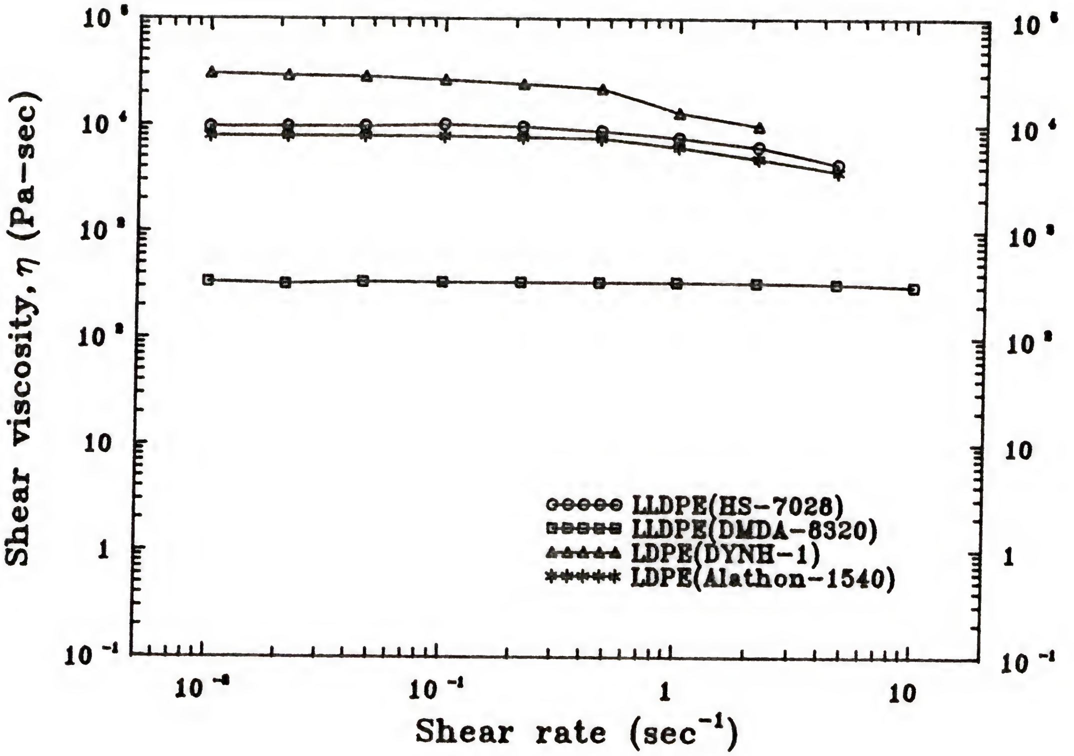

Figure 20. Shear viscosity function η versus shear rate $\dot{\gamma}$ of linear low-density polyethylene at 200°C: (○) HS-7028; (□) DMDA-8320, and low-density polyethylene at 145°C: (△) DYNH-1; (∗) Alathon-1540.

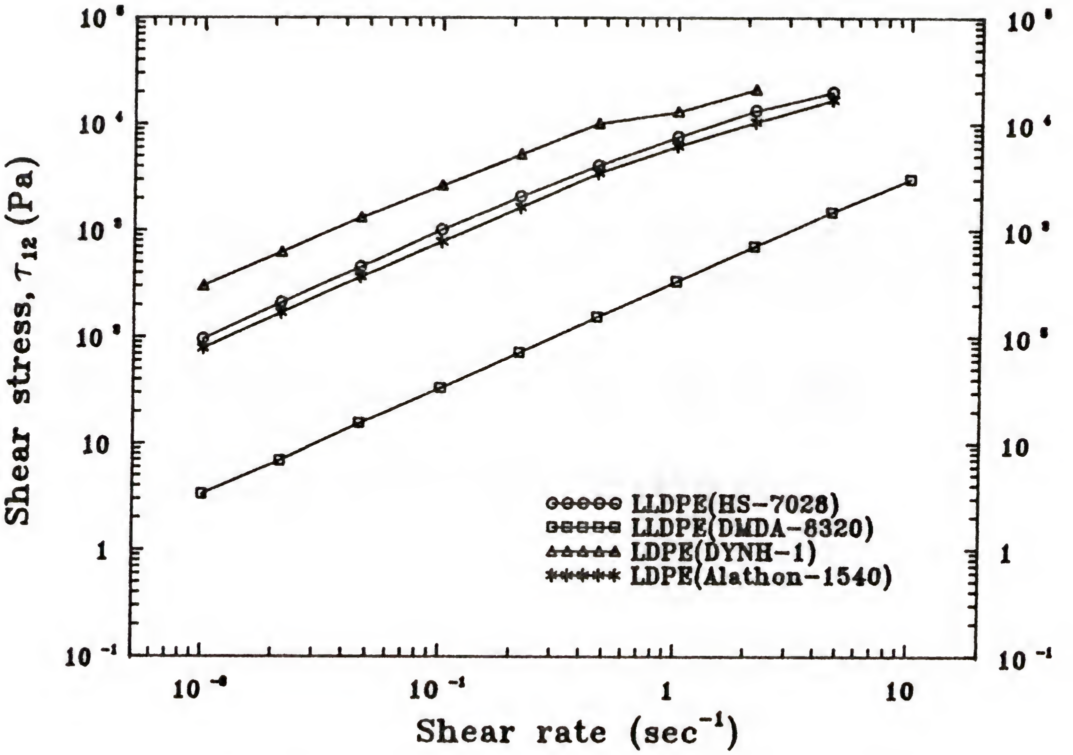

Figure 21. Shear stress τ_{12} versus shear rate $\dot{\gamma}$ of linear low-density polyethylene at 200°C: (○) HS-7028; (□) DMDA-8320, and low-density polyethylene at 145°C: (△) DYNH-1; (∗) Alathon-1540.

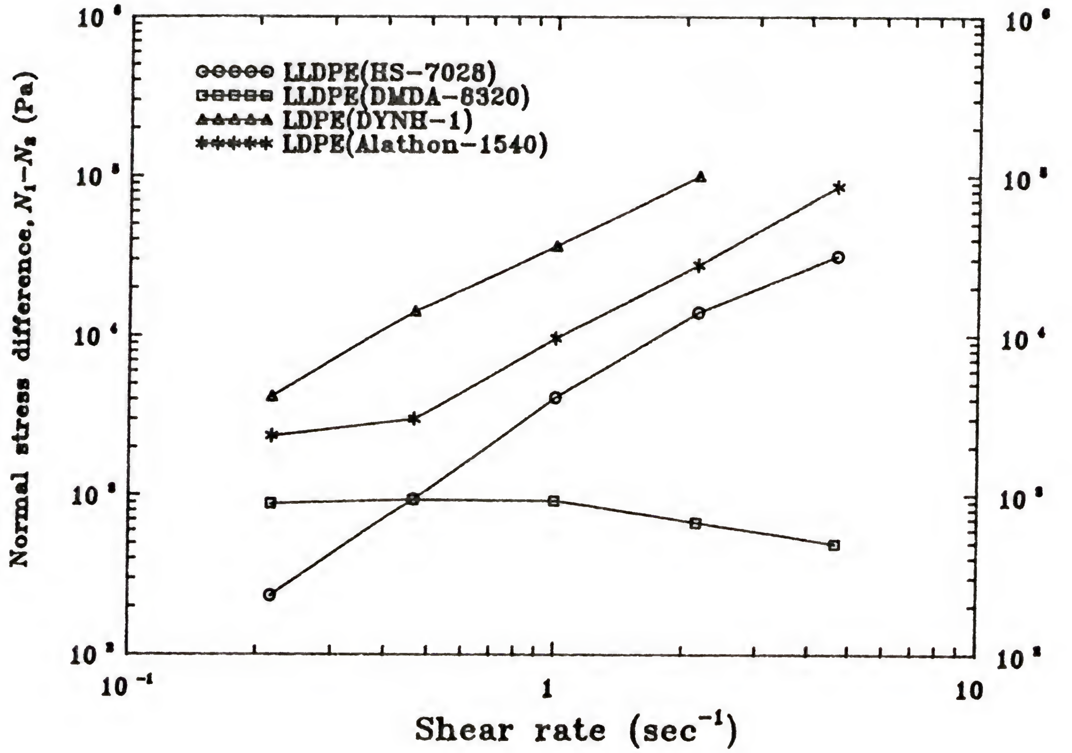

Figure 22. Normal stress difference N_1-N_2 versus shear rate $\dot{\gamma}$ of linear low-density polyethylene at 200°C: (○) HS-7028; (□) DMDA-8320, and low-density polyethylene at 145°C: (△) DYNH-1; (∗) Alathon-1540.

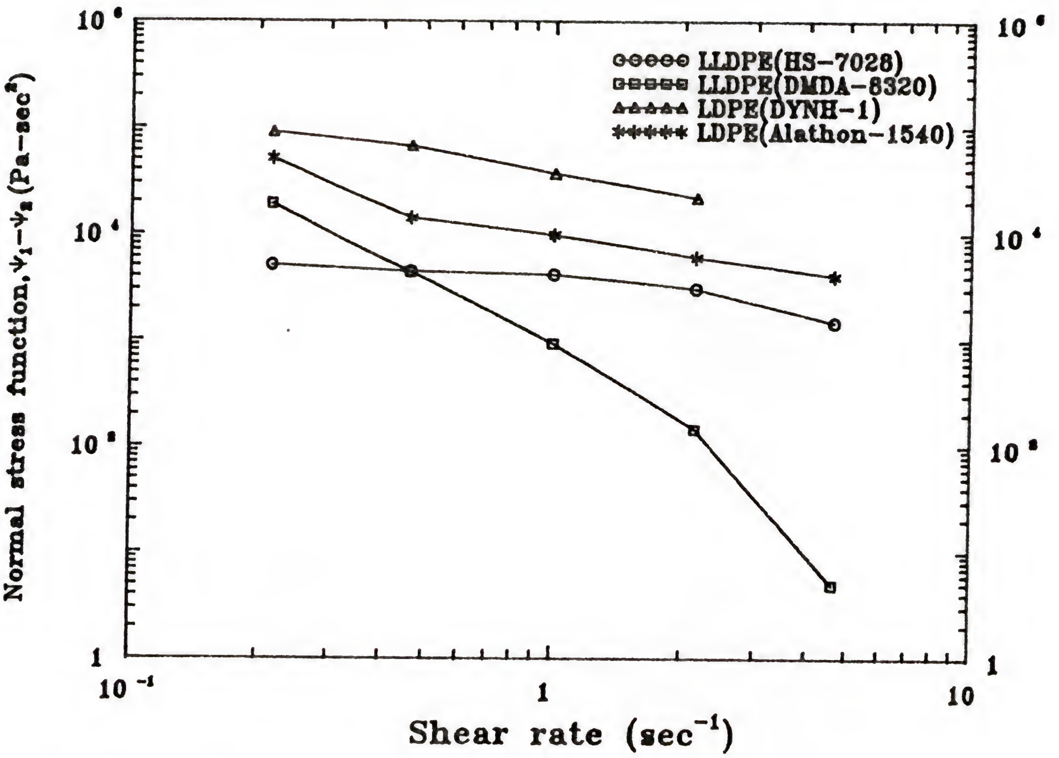

Figure 23. Normal stress function $\Psi_1-\Psi_2=(N_1-N_2)/\dot{\gamma}^2$ versus shear rate $\dot{\gamma}$ of linear low-density polyethylene at 200°C: (○) HS-7028; (□) DMDA-8320, and low-density polyethylene at 145°C: (△) DYNH-1; (∗) Alathon-1540.

The difference between the first and the second normal stress difference is plotted as a function of shear rate in Figure 22 and Figure 23 represents the difference between the normal stress functions, $\Psi_1 - \Psi_2$. The normal stress function Ψ_i is defined as $\Psi_i = N_i / \dot{\gamma}^2$ (i=1,2). The normal pressure on the plate at the center or at the rim cannot be measured with the current instrument. Thus, the first and the second normal stresses could not be decoupled. The second normal stress difference N_2, however, is typically much smaller than the first normal stress difference, and $(N_1 - N_2)$ may well represent N_1. It was pointed out that Alathon-1540 might have higher viscoelasticity than DYNH-1 due to its higher degree of long chain branching. Contrary to the speculation, $(N_1 - N_2)$ of DYNH-1 is larger than that of Alathon-1540. It may be due to the high shear viscosity of DYNH-1. The first normal stress function $\Psi_1 (= N_1 / \dot{\gamma}^2)$ of a UCM fluid is proportional to its shear viscosity; that is

$$\Psi_1 = 2\eta\lambda \tag{4.1}$$

Although none of the LDPEs may be well represented by the UCM model, this equation indicates the strong influence of shear viscosity on Ψ_1.

All these properties are for a shear flow situation and the direct correlation between the shear flow properties and those for an elongational flow is unknown. However, if it is assumed that the first normal stress difference may represent the magnitude of the material time constant (or relaxation time) λ, DYNH-1 may have a larger relaxation time than Alathon-1540.

Even though the shear viscosity of HS-7028 is much larger than Alathon-1540, its $(N_1 - N_2)$ is much smaller indicating the low viscoelasticity of HS-7028. As expected, the value of $(N_1 - N_2)$ for DMDA-8320 is much smaller than others. Its value, however, is apparently decreasing with the shear rate unlike all others. Consequently, $(\Psi_1 - \Psi_2)$ of

DMDA-8320 show stronger shear thinning behavior than others. The reason for the crossover between HS-7028 and DMDA-8320 is unknown. It may be possible, though, that the first data point for HS-7028 may not be reliable since its low value may be close to the low limit of the transducer of the instrument.

4.3 Coextrusion Fiber Spinning

The experimental set-up for the two-phase fiber is shown schematically in Figure 24. The core and the skin materials were fed by two 19 mm single screw extruders into a coextrusion die with a 5.21 mm diameter hole. The schematic of the coextrusion die is shown in Figure 25. To prevent interfacial instability which may result from the shear viscosity mismatch between the core and the skin materials, the feed port for the core material was made to extend all the way to the exit of the coextrusion die. Consequently, the core and the skin material meet right at the exit of the die where both materials are exposed to an extensional flow. The concentric extrudate was then pulled under tension and quenched as it passed through a water bath which was located directly below the die. The melt temperatures of the core and skin materials were maintained at 200°C and 145°C, respectively. The total extrusion output was held constant at 250 g/hr throughout the experiment while the skin-layer flow rate fraction f was varied at 0.0, 0.2, 0.5, 0.8, and 1.0. For the single-component spinning (i.e., f=0.0 and 1.0), the same material (either LLDPE or LDPE) was fed to both extruders rather than using only one extruder. For each experiment, the draw span was also varied between 3 cm and 10 cm. In the draw span the polymer melt was exposed to the ambient air without any special care to maintain the melt temperature. The spinning process, however, was presumably at a near isothermal condition since the radii of both extrusion die and the fiber were very large compared to those of existing studies.

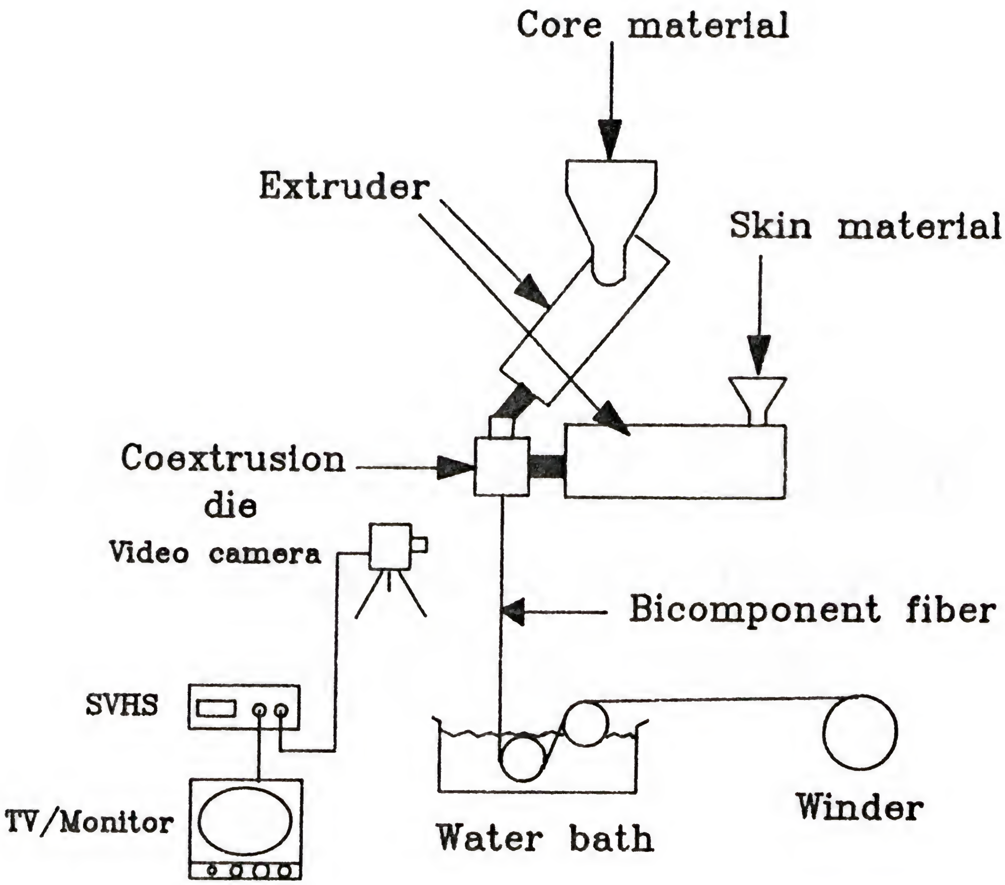

Figure 24. Schematic of coextrusion fiber spinning system.

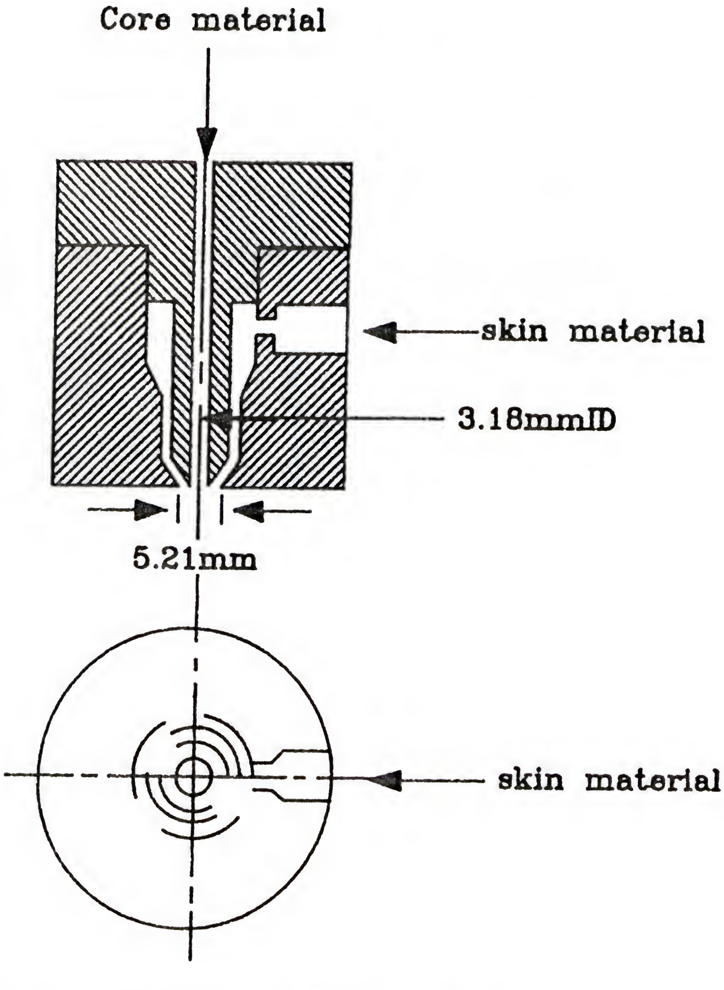

Figure 25. Schematic of coextrusion die.

The experiment was started at a low take-up speed at which fibers with a uniform diameter were made. The take-up speed was then increased gradually in a stepwise manner while taking samples at each speed. A video camera which was connected to a TV monitor was used to observe the variation of threadline diameter. In all cases except the single-component LDPE spinning, the draw resonance instability became visible beyond a certain critical take-up speed. Most experiments were continued to a much higher take-up speed than the critical value as long as fiber breakage did not occur. The fiber diameter of each sample was then measured at a 2.5 cm interval over a 5 m distance to determine the critical draw ratio, the maximum-to-minimum diameter ratio as well as the wave length of the instability. Whenever the draw resonance was visible, its period was also measured using a stop watch as a supplementary measurement.

4.4 Results and Discussion

The variation of the fiber diameter with its axial distance is given for increasing values of draw ratio in Figure 26. This figure, which is for f=0.23 (23%LDPE(Alathon-1540)/77%LLDPE(HS-7028)) at a draw span of 3 cm and at a flow rate of 250 g/hr, represents the general trend of all fiber samples excluding the one for f=1.0 which did not show draw resonance. It is apparent from the figure that the critical draw ratio for this experiment is between 51 and 57. This figure also indicates that the draw resonance is sustained beyond the critical draw ratio. With increasing Dr, both amplitude and wave length are observed to be increasing. However, the period of the instability that is determined by dividing the wavelength by the take-up speed appears to remain constant within the measurement error. A similar behavior was observed with a polystyrene by Matsumoto and Bogue (1978). In the experiment of Demay and Agassant (1985) which used a linear polyester, however, the period increased slightly with draw ratio.

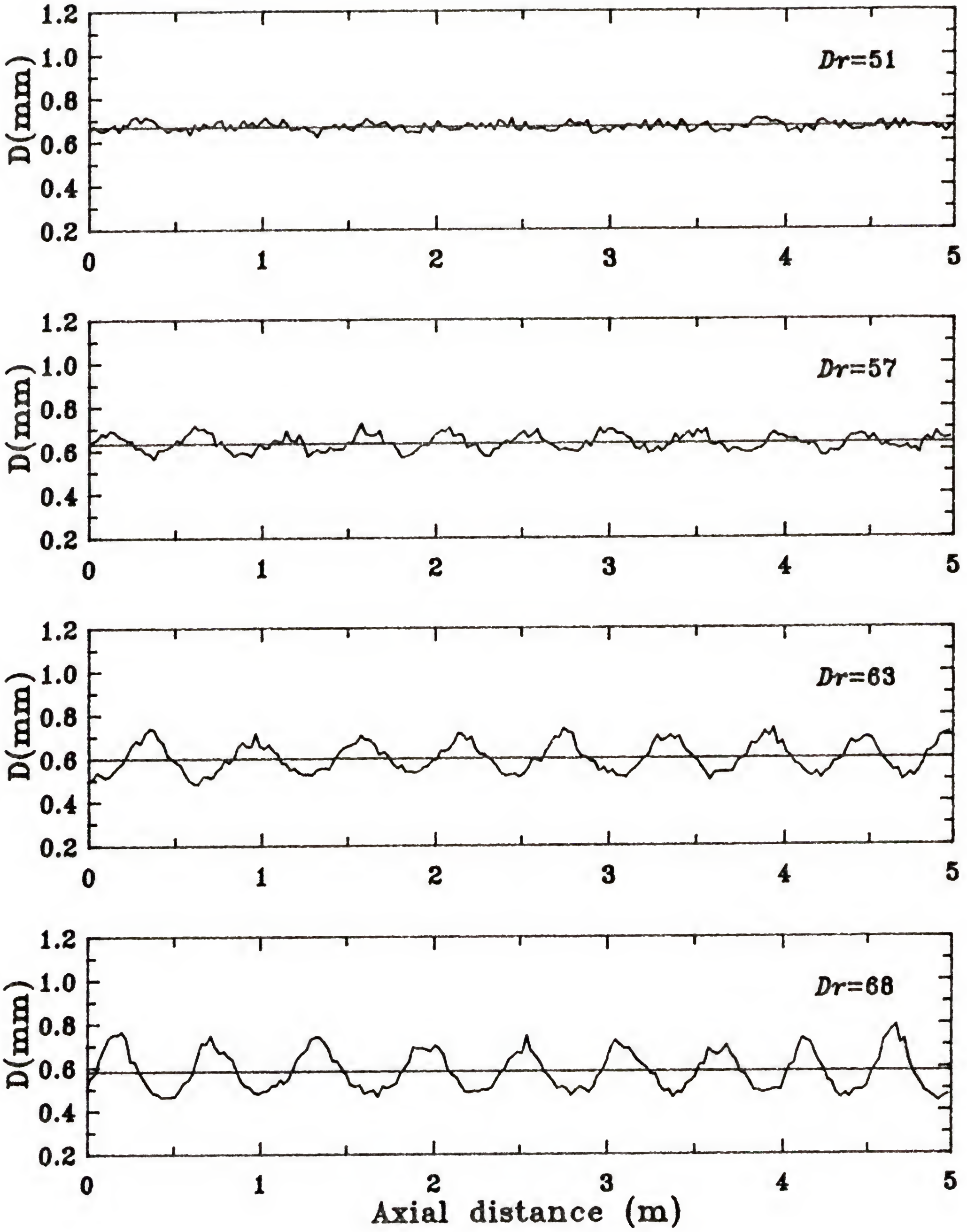

Figure 26. Variation of fiber diameter with increasing draw ratio; (f=0.23, draw span L=3 cm).

In Figure 27, the period of draw resonance instability (t^*) is plotted as a function of L/w_0 for various values of f. L and w_0 are the draw span and the average extrusion velocity, respectively. It seems that the period increases linearly with L/w_0 while it decreases as the thickness of the more viscoelastic cladding is increased. Also included in the figure is the prediction of the linear stability theory for an isothermal Newtonian fluid (solid line in Figure 27) in which the imaginary part of the first eigenvalue is 14.02. From Equation (3.10), $\bar{t}$ =0.448; that is

$$t^* = 0.448\frac{L}{w_0} \tag{4.2}$$

It appears that this theoretical prediction is in good agreement with the single-phase LLDPE data for which the linear regression yields

$$t^* = 0.445\frac{L}{w_0} + 1.5 \tag{4.3}$$

This linear relation between t^* and L/w_0 is presented by the dashed line in Figure 27. The coefficient of correlation for the regression is 0.97. In calculating the average extrusion velocity w_0, we have used the cross-sectional area of the die hole as the basis. If the maximum cross-sectional area of the fiber at the die swell region is used as the basis, the corrected w_0 will become smaller and all data points in Figure 27 will shift to the right resulting in an improved agreement between the LLDPE data and the Newtonian theory. The LLDPE, which shows a shear thinning behavior, is by no means a Newtonian fluid. Nevertheless, considering the fact that it does not exhibit a strain hardening behavior. The agreement between the experimental data and the Newtonian theory appears to be

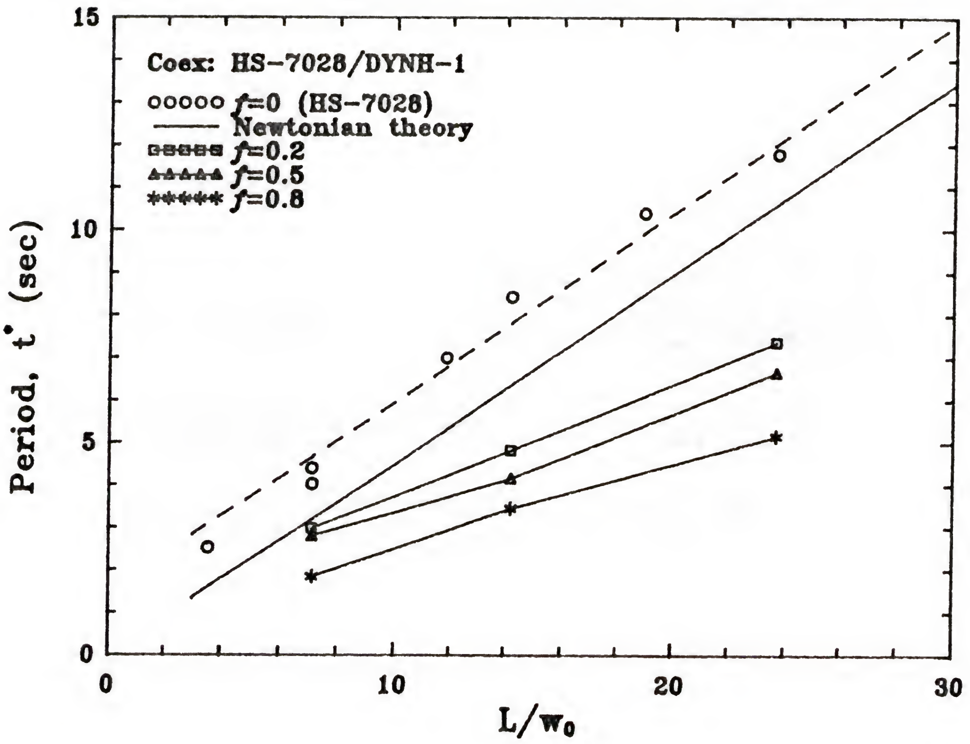

Figure 27. Period t^* of draw resonance versus L/w_0 for the coextrusion of (a) LLDPE(HS-7028)/LDPE(DYNH-1): (o) 100% HS-7028, (—) Newtonian theory, (□) 20% DYNH-1, (△) 50% DYNH-1, (*) 80%DYNH-1; (b) LLDPE(HS-7028)/LDPE (Alathon-1540): (o)100%HS-7028, (—)Newtonian theory, (□) 20% Alathon-1540, (△) 50% Alathon-1540, (*) 80% Alathon-1540; (c) LLDPE(HS-7028)/LDPE: (o) 100% HS-7028, (—) Newtonian theory, (□) 50% DYNH-1, (△) 50% Alathon-1540.

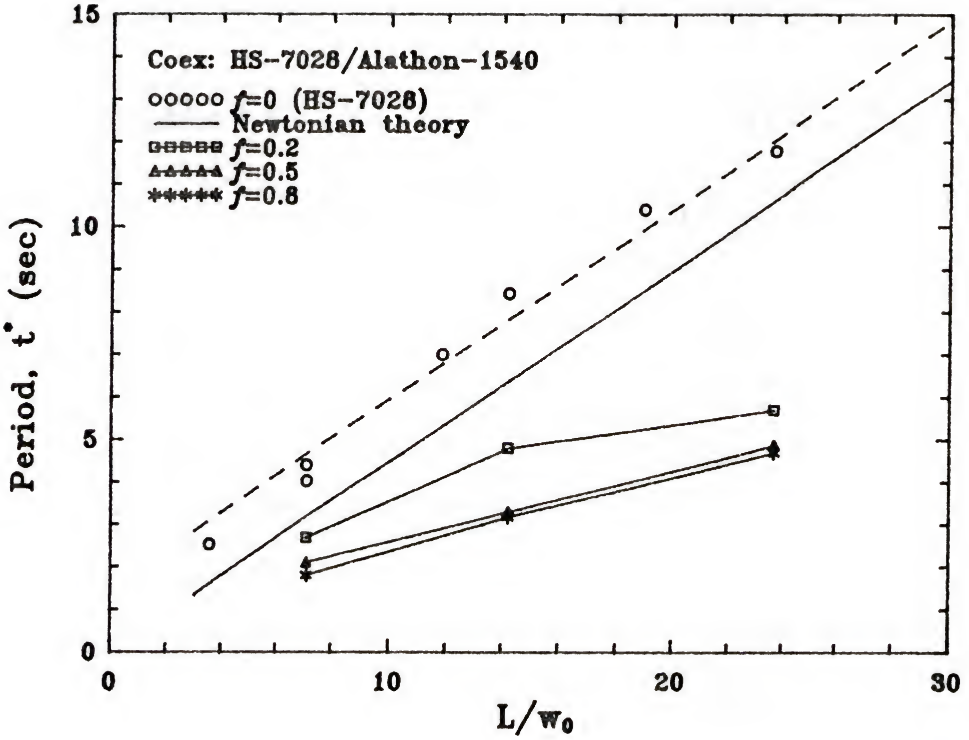

Figure 27. (continued)

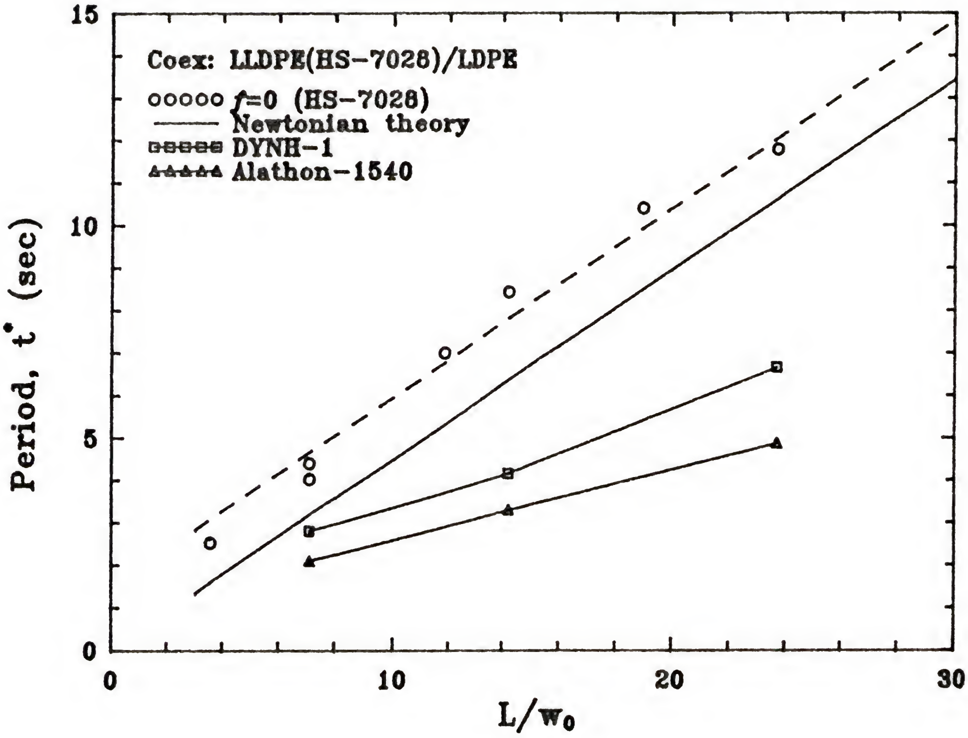

Figure 27. (continued)

too good to be a simple coincidence. In addition, the measured critical draw ratio was 18 which is not much different from the Newtonian value of 20.21. The critical draw ratio will be even closer to 20.21 if the maximum cross-sectional area at the die swell region is used to calculate w_0. Furthermore, in our experiment, the diameter of the die hole (thus, the diameter of the fiber) was very large compared with those of other experimental studies. Consequently, cooling of the fiber by ambient air during spinning could be relatively small creating a near-isothermal spinning condition.

The decreasing trend of period with increasing skin-layer flow rate fraction f depicted in Figure 27 also appears to agree with the theoretical prediction described in Figure 17. In the present experiment the critical draw ratio increased as the thickness of the skin-layer material was increased (Figure 30 and 31). Therefore, a large value of f corresponds to a large critical draw ratio. According to Figure 17, the draw resonance occurring at a higher draw ratio may have a smaller period.

Alathon-1540 among the two different skin materials is expected to have a larger relaxation time than the other. According to the theoretical prediction, then, the HS-7028/Alathon-1540 combination should have a larger critical draw ratio and a smaller period when the instability is encountered than the HS-7028/DYNH-1 combination. The current observations seem to be in fact in accordance with the predictions. In Figure 27c, the periods of the draw resonance instability of the two combinations are compared when f=0.5. The HS-7028/Alathon-1540 combination always showed smaller period than the other. Furthermore, the slope of the apparently straight line connecting the three data points is also smaller than the other, indicating that the dimensionless period for the HS-7028/Alathon-1540 combination is smaller than the other.

In Figure 26, it was described that the periodic instability was sustained beyond the critical draw ratio although the amplitude (or the maximum-to-minimum diameter ratio) apparently increased with the draw ratio. The maximum-to-minimum diameter ratio of the unstable fiber is plotted as a function of draw ratio for 20%–LDPE(DYNH-1) coextrusion fiber in Figure 28. It is apparent from the figure that the critical draw ratio for this experiment is in the vicinity of about 30. Furthermore, the amplitude of the instability (or the maximum-to-minimum diameter ratio) appears to be decreasing with increasing draw span although the critical draw ratio remains unchanged. A similar trend was observed with a Newtonian silicone oil by Donnelly and Weinberger (1975). In the experiment of Demay and Agassant (1985), however, somewhat different trend was observed with a linear polyester in that the critical draw ratio increased as the draw span increased from 2 to 6 cm.

The variation of the maximum-to-minimum diameter ratio is plotted in Figure 29a and 29b for three different values of f for the two different combinations, respectively. The changes in the amplitude of the instability with the draw span for all three combinations (f=0.2, 0.5 and 0.8) also show the same trend as in Figure 28. When comparing the data for the three different values of f at the same draw span, the rate of increase of the maximum-to-minimum diameter ratio with the draw ratio is apparently slower when the skin flow rate ratio f is increased. This may be another manifestation of the stabilizing effect of the skin layer. These figures also imply that the critical draw ratio increases with the skin flow rate fraction f. This behavior is summarized in Figure 30.

In Figure 30, the critical draw ratio is plotted as a function of the skin-layer flow rate fraction f for the two different material combinations. The mode of instability for all data was draw resonance except for the single-phase spinning of LDPE (i.e., f=1.0). When f=1.0, draw resonance was never observed. Instead, the fiber snapped at a relatively large draw ratio. It should be noted that the "maximum" draw ratio before the fiber breakage increased with increasing draw span whereas the "critical" draw ratio for all other fiber compositions was insensitive to the draw span. A similar behavior was also observed in the single-phase experiment of Chang and Denn (1979).

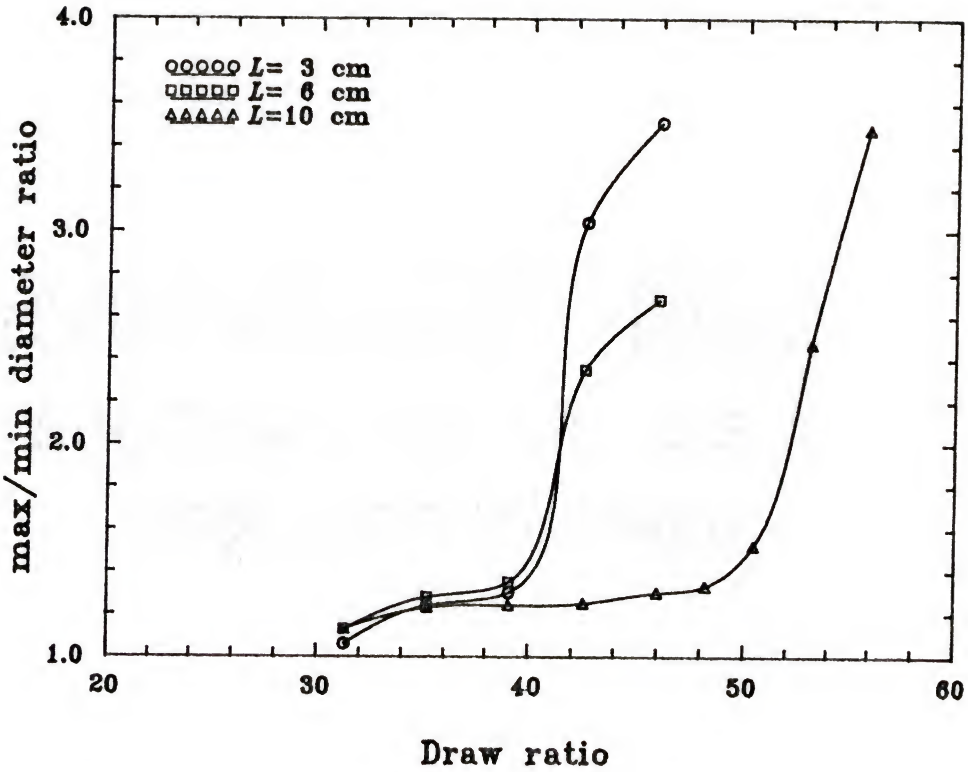

Figure 28. The maximum-to-minimum diameter ratio as a function of draw ratio for the combination of 20%–LDPE(DYNH-1)/80%–LLDPE(HS-7028) at three different draw spans: (o) *L*=3 cm; (□) *L*=6 cm; (Δ) *L*=10 cm.

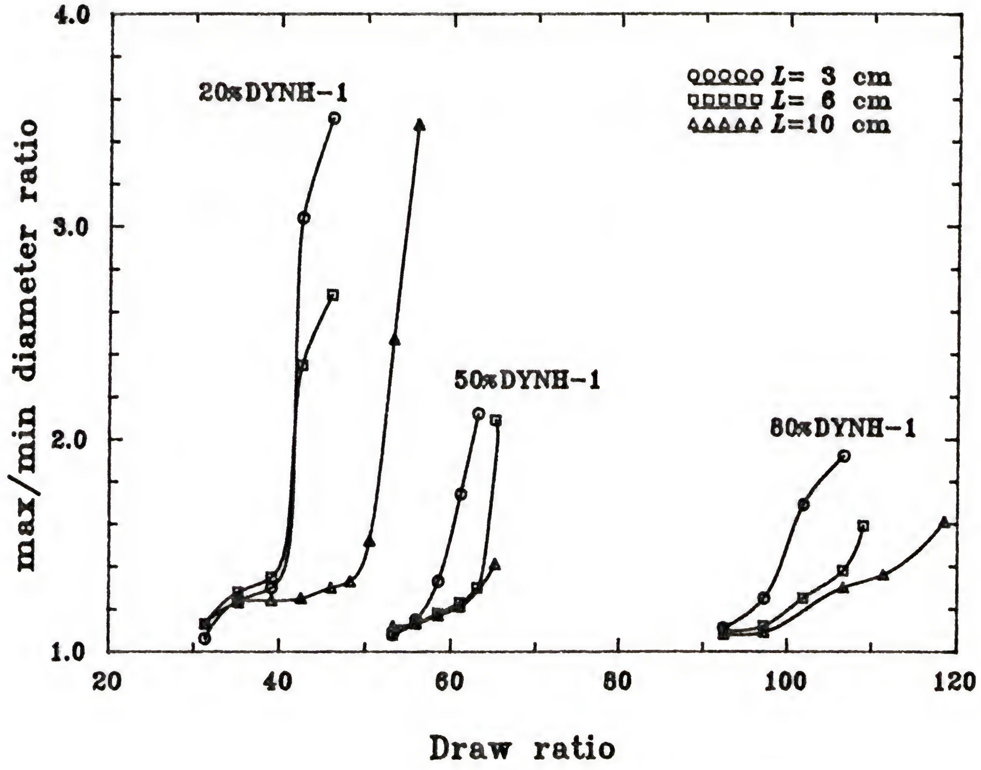

Figure 29. Variation of the maximum-to-minimum diameter ratio for three combinations of (a) LDPE(DYNH-1)/LLDPE(HS-7028); (b) LDPE(Alathon-1540)/LLDPE(HS-7028) at different draw spans: (○) L=3 cm; (□) L=6 cm; (△) L=10 cm.

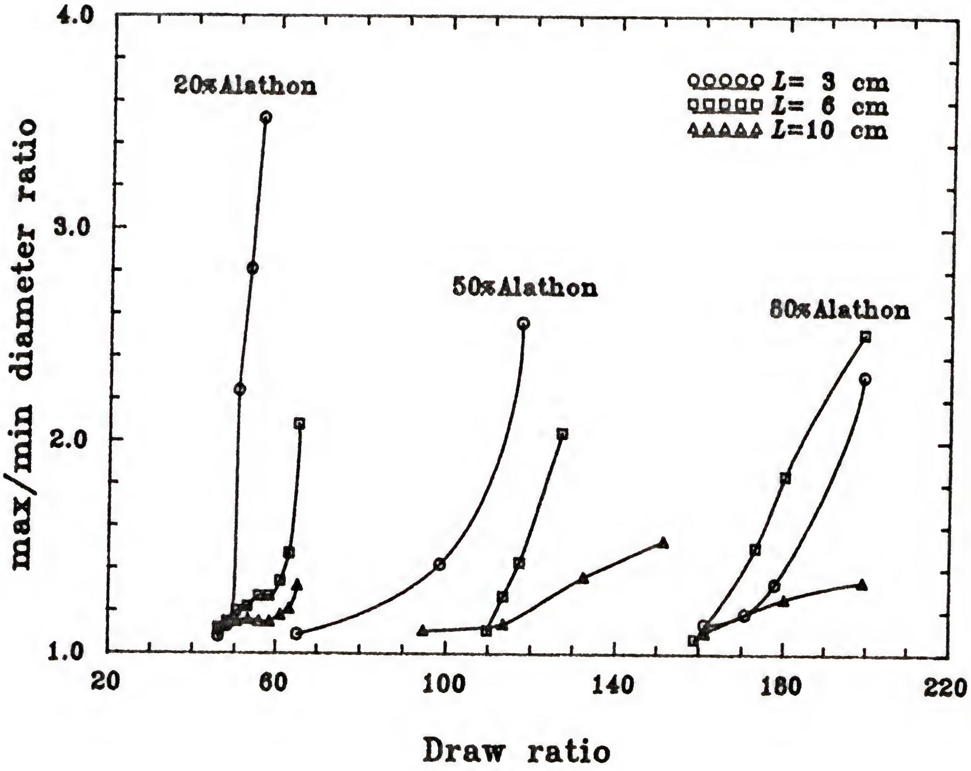

Figure 29. (continued)

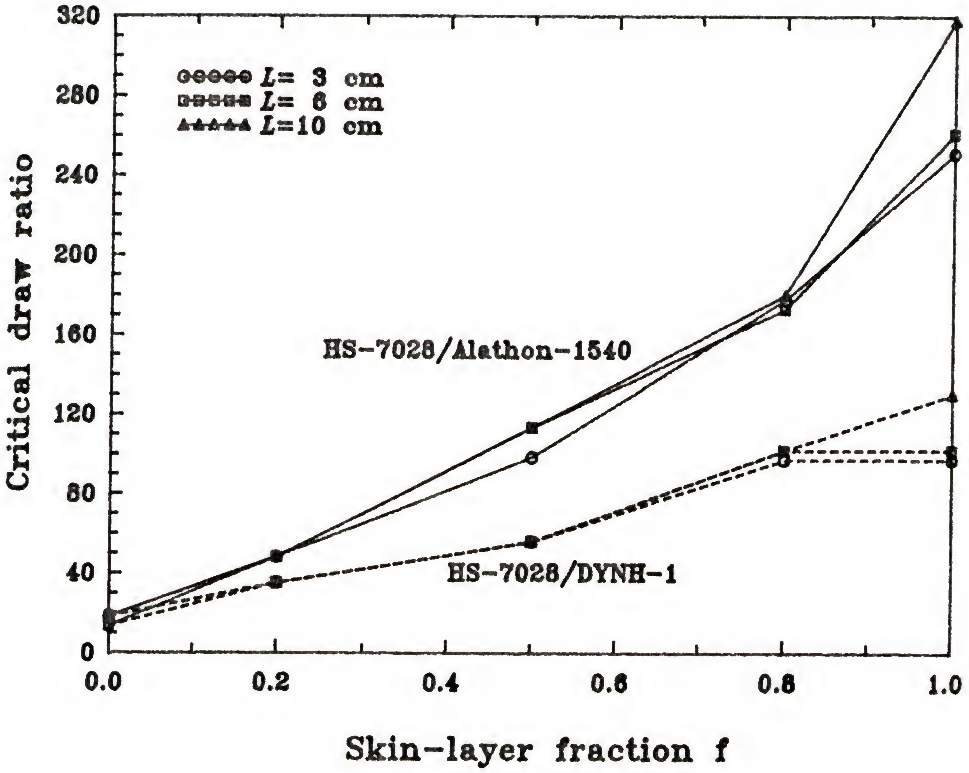

Figure 30. Critical draw ratio as a function of skin-layer flow rate fraction for different combinations at different draw spans: (○) *L*=3 cm; (□) *L*=6 cm; (△) *L*=10 cm. Core: LLDPE(HS-7028); Skin: LDPE (—: Alathon-1540, ------ : DYNH-1).

To this point, the draw resonance characteristics of only two different material combinations have been discussed in which the core material was fixed with HS-7028. Similar experiments have been also conducted with the DMDA-8320 as the core whose shear viscosity is much smaller than that of HS-7028. Thus, the following four different combinations were investigated in this experimental study:

(1) LLDPE(HS-7028)/LDPE(Alathon-1540)
(2) LLDPE(DMDA-8320)/LDPE(Alathon-1540)
(3) LLDPE(HS-7028)/LDPE(DYNH-1)
(4) LLDPE(DMDA-8320)/LDPE(DYNH-1)

The results for (1) and (2) have been already discussed extensively. The difference between (1) and (2) (or between (3) and (4)) are the shear viscosity of the core material. When compared with the theoretical analysis, the combination (1) has a higher value of M ($\equiv \mu^c / \mu^s$) than combiantion (2). Equivalently, (3) has a higher M than (4).

According to the theoretical predicition described in Figure 19, when M is decreased, the relative influence of the viscoelastic skin layer increases resulting in a slight increase in critical draw ratio *Dr** if draw resonance is still encountered or a large increase in *Dr** if the Deborah number happens to be on the right hand side of the unstable nose-shaped envelope. Unfortunately neither of these were observed in the present experiment. The measured dependence of the critical draw ratio on the skin-layer flow rate fraction f is given in Figure 31 for all four combinations. In all coextrusion experiments, the mode of instability was draw resonance. When (1) and (3) are compared, stronger influence of Alathon-1540 than DYNH-1 is apparent. When (2) and (4) are compared, however, no apparent difference between Alathon-1540 and DYNH-1 is observed. This result is rather perplexing since the viscoelasticity effect of the skin layer should be more pronounced when the shear viscosity of the core is smaller.

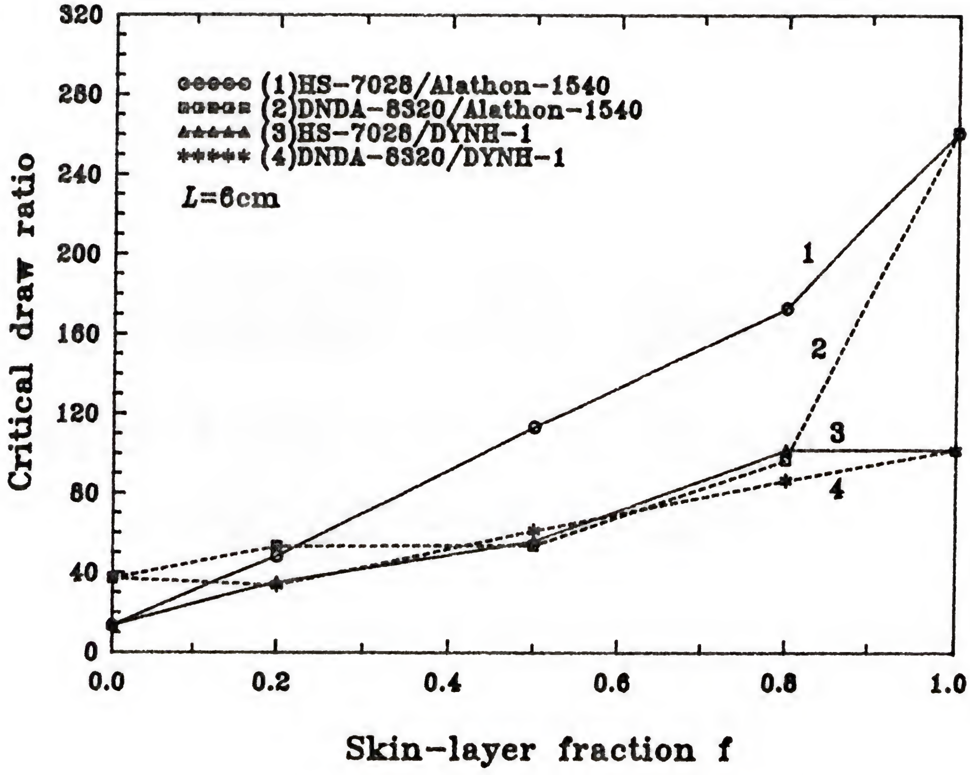

Figure 31. Critical draw ratio as a function of skin-layer flow rate fraction for different combinations at *L*=6 cm:

(1) Core:LLDPE(HS-7028); Skin:LDPE(Alathon-1540)
(2) Core:LLDPE(DMDA-8320);Skin:LDPE(Alathon-1540)
(3) Core:LLDPE(HS-7028); Skin:LDPE(DYNH-1)
(4) Core:LLDPE(DMDA-8320);Skin:LDPE(DYNH-1)

The theoretical prediction that the highest draw ratio for a stable coextrusion spinning can be larger than that for the single-phase spinning of either fluid was not also observed in the present experiments. However, it does not necessarily mean that the theory is incorrect. In all coextrusion experiments with the four different combination of materials, the mode of instability was draw resonance. This may indicate that the viscoelasticity of the skin materials are not large enough to exhibit the theoretical prediction.

4.5 Summary and Conclusion

Draw resonance instability in bicomponent fiber spinning has been studied experimentally using four polymers with different rheological properties; two linear low-density polyethylenes (LLDPE) and two branched low-density polyethylenes (LDPE). The LLDPEs which are very prone to draw resonance were used as the core material, whereas the LDPEs which do not show draw resonance instability were used as the cladding material. The results indicate that

1) In all coextrusion experiments with the given materials, the draw resonance was always the dominant mode of instability even when the LDPE fraction was as high as 0.8. The critical draw ratio, however, increased substantially with increasing LDPE fraction.
2) Draw resonance instability was sustained beyond the critical draw ratio. The amplitude of the instability was observed to be increasing with the draw ratio although its period remained unchanged.
3) The critical draw ratio appeared to be independent of draw span although the maximum-to-minimum diameter ratio decreased with increasing draw span.
4) The period of the instability increased linearly with L/w_0 while it decreased with increasing LDPE content.

Many of the experimental results are in reasonable agreement with theoretical predictions. However, one of the most interesting predictions regarding a kind of synergism in terms of maximum draw ratio was not observed with the given choice of materials. Although the present results are specifically for a fiber spinning process, the general trend should be also relevant to other fast-drawing processes such as extrusion coating or film casting.

CHAPTER 5
FABRICATION OF PLASTIC OPTICAL FIBERS

5.1 Introduction

A direct application of the two-phase fiber spinning process may be in the manufacture of plastic optical fibers. In this Chapter, a new processing method for the fabrication of plastic optical fibers is investigated which is a modified coextrusion process. The new method has been developed based on the fundamental understanding of the two-phase fiber spinning process which has been investigated in the previous Chapters.

Plastic optical fibers offer a number of advantages compared to silica glass optical fibers. Besides sizable cost savings in materials, toughness and durability of plastics allow plastic optical fibers to be handled without special care. In addition, the mechanical flexibility of plastic allows these fibers to have large size cores that may range from 0.5 to 1.0 mm in diameter. Consequently, a low-cost, large-area light source can be used and the connection between the fibers becomes easier and less costly. Furthermore, a high refractive-index difference can be achieved between core and cladding materials yielding a higher numerical aperture than glass optical fibers.

Plastic optical fibers, however, have much larger attenuation of light signals than glass fibers due to their large intrinsic absorption loss. In case of PMMA (poly(methylmethacrylate)) optical fibers, the theoretical lower loss limit is about 105 dB/km at 650 nm and the commercial PMMA fibers have a typical attenuation of about 200~400 dB/km at the same wave length. Silica glass optical fibers, on the other hand, are readily manufactured these days that have an attenuation as small as 0.5 dB/km at 1.30μm. Despite the high attenuation, plastic optical fibers are economically very attractive and are better suited than glass fibers to many applications such as fiber optic sensors, local area network, automotive and medical applications.

Commercial plastic optical fibers are typically made of a polystyrene(PS) core and a PMMA cladding or a PMMA core and a fluoropolymer cladding. These materials are amorphous thermoplastics that are optically transparent and drawable to fibers. In the fabrication of these plastic optical fibers, a cylindrical rod (or a preform) is made first using highly purified monomers. The preform is then heated and drawn to optical fibers. This two-step process which may be called as "thermal-drawing" process is similar to the vapor phase oxidation process for glass optical fibers as they both make preforms and then heat-draw fibers.

Since PS, PMMA, and fluoropolymer cladding are thermoplastic, a coextrusion process may be also applicable as an alternative method to fabricate optical fibers. In a coextrusion process the core and the cladding materials are extruded simultaneously into a coextrusion die using two separate extruders, and a clad fiber (i.e., optical fiber) is drawn out of the coextrusion die to a desired diameter. This process is, in a sense, similar to the direct-melt method (or double-crucible method) for glass fibers in which optical fibers are made directly from the molten state of silicate glasses following a traditional glass-making procedure.

The coextrusion method is a single-step process that may appear to be less complicated than the heat-drawing two-step process. This method, however, is commercially less prevalent due to its susceptibility to contamination by impurities. In the coextrusion process, polymers in a pellet form are used for both core and cladding. Although extra care may be taken to maintain the high purity of the materials, the pellets are highly susceptible to contamination by foreign materials such as dust particles during the materials handling (e.g., transportation and feeding for extrusion). In the two-step thermal-drawing process, on the other hand, a purified core material may never be exposed to foreign substances throughout the process from polymerization to heat-drawing resulting in superior quality optical fibers.

In these conventional methods (thermal-drawing or coextrusion), the materials that can be used to make optical fibers are limited to thermoplastics. Non-thermoplastic materials cannot be fabricated into optical fibers despite their excellent optical properties. To fabricate optical fibers using various classes of materials, a new processing method has been developed. The new method is a modified coextrusion process. Unlike the conventional coextrusion, however, only the cladding material has to be thermoplastic in this process and the core material can be any class of materials; liquids (monomers or prepolymers), elastomeric gels, thermoplastic or thermosetting materials.

The process modeling study described in the previous Chapters suggests that the mechanics of the two-phase flow is dictated by the more viscoelastic fluid of the two components under typical processing conditions. Thus, in the new method, several different types of materials can be used as the core as long as the skin material has high enough viscoelasticity to control the overall flow dynamics. In the following sections, a brief description of the new method and the experimental results on the feasibility of the new method are discussed including the advantages and limitations of the new method.

5.2 New Processing

In Figure 32, a schematic of the new processing method is given in which a thermoplastic cladding material is spun into a hollow fiber while a core material is fed by a piston-cylinder unit into the core of the hollow fiber at the same time. In this process, the cladding material has to be a thermoplastic as it is processed by an extruder. The core material, however, can be any type of materials which may be fed by an extruder, a

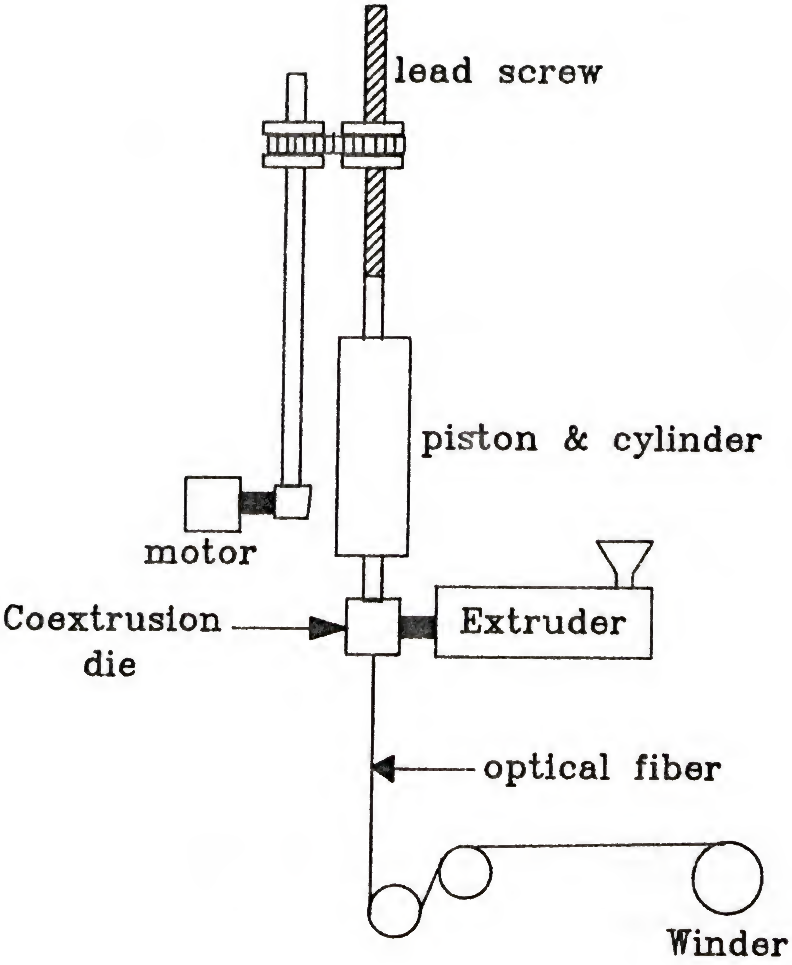

Figure 32. Experimental set-up for the spinning of plastic optical fibers

piston-cylinder assembly, or a gear pump depending upon its rheological properties. After fibers are made by this process, the core material may be either cross-linked or further polymerized (if the core is a low molecular weight prepolymer) to enhance the mechanical strength of the fiber if such post processing is necessary. In this way, the process of making preforms can be eliminated and both thermosetting and thermoplastic materials can be used for optical fibers. In addition, contamination by impurities (including dust) can be minimized since purified liquids (monomers or prepolymers) are fed directly into the core without contacting any foreign substances or without being exposed to ambient air.

While the most important feature of the new method is its applicability to various materials including those which cannot be made into optical fibers by the conventional methods, the new method also has some limitations. First, the liquid phase core should be a non-solvent of the thermoplastic cladding. Otherwise, the cladding will be seriously damaged before the core material is completely reacted. Furthermore, the polymerization or cross-linking reaction should take place at a temperature below the glass transition temperature of the cladding material (or below the melt temperature if the cladding is a semi-crystalline polymer). Finally, the density variation involved in the phase change of the core material should be minimal. Otherwise, the fibers may deform or bubbles may be formed during the post-reaction. Thus, prepolymers with a certain level of reaction are preferable to monomers as a core material. These appear to be rather severe restriction. Nevertheless, many different combinations of materials are possible with which the restrictive conditions can be met.

5.3 Optical Fiber Spinning

5.3.1 Experiments

A schematic of the equipmental set-up is given in Figure 32. A thermoplastic cladding material is fed into a coextrusion die by a 3/4" extruder while a core material is fed by a piston-cylinder assembly which has been custom-made. The volume of the cylinder is about 100 cm^3 which can effectively handle small quantity of materials to perform pilot scale experiments. The lead screw which drives the piston is driven by a motor which provides an accurate feed volume control of core materials from 4 cm^3/min to 40 cm^3/min.

The design of the coextrusion die is given schematically in Figure 25. The most important features of this design are (1) the protrusion of the core capillary to the end of the die and (2) a short thermal contact time between core and cladding materials. To handle a large viscosity difference between the core and cladding materials, the capillary that feeds the core material needs to be stretched to the end of the die exit. When a crosslinkable core material is used, excessive heating should be avoided to repress the reaction in the coextrusion die. In the current die design, the capillary diameter is small (3.21 mm) and its length short (7.5 cm). Thus, the residence time of the core material is relatively small minimizing its thermal contact with the hot environment which may be kept at 150 to 170°C depending upon the choice of the cladding material.

Using the prescribed experimental set-up, spinning experiments have been conducted with two different types of core materials; (1) styrene-hexyl methacrylate copolymer and (2) polysiloxanes. The most important properties of the optical polymers are their transparency and refractive indices to achieve a minimum level of light signal loss. Since optical polymers are highly proprietary, the raw materials are very difficult to obtain. Consequently, the choice of materials was limited in the present experiment. In any case, the major emphasis of the experiments was on the processing aspect of the new method to evaluate its feasibility to fabricate physically sound optical fibers that are free from critical defects (e.g., bubbles or diameter variation), and relatively little attention has been given to measure the attenuation length of the fiber. To achieve a high attenuation length, extensive purification of the core materials should be preceded which is not necessary for the present objective.

5.3.2 Styrene Core Fibers

Styrene is one of the most common materials that are used as the core of plastic optical fibers, and it has been chosen as the first material for the feasibility study of the new processing method. Purified styrene monomer was prepolymerized in a flask at 120°C for three hours. The prepolymer was then poured into the heated cylinder at 120°C where it was then kept for two more hours for further reaction (Figure 32). Since the density increase during the polymerization is rather substantial (about 16%), a high conversion of polymerization reaction was necessary before the coextrusion spinning to avoid bubble formation during the post-polymerization. The core material was then fed into the coextrusion die by a piston to fabricate 1 mm optical fibers. For this experiment an ethylene-vinyl acetate copolymer was used as a cladding material. The conventional PMMA was not used since the core material which might still contain styrene monomer could seriously damage the PMMA cladding. After the spinning, the fiber was kept in an oven at 100°C for 24 hours to complete the polymerization of the core material. Due to the high refractive index of the cladding material (n=1.50), the fiber was not expected to have a high attenuation length. Nevertheless, this experiment demonstrated the feasibility of the new processing method in which a polymerization reaction can be involved.

5.3.3 Modification of the Spinning Equipment

The piston-cylinder unit in Figure 32 served both as a reactor and as a feeder. One limitation of this unit as a reactor was its inability to provide good mixing during polymerization reaction resulting in a poor molecular weight control. Consequently, the polystyrene core of the fiber was very brittle. Good mixing is especially important for the copolymerization which is intended to fabricate flexible optical fibers by incorporating n-hexyl methacrylate into styrene. Thus, the experimental set-up has been modified as described in Figure 33. With this modification, not only the control of the polymerization reaction was more efficient with uniform mixing, but also the spinning experiment could be conducted for a longer period time due to the increase in reactor volume (1000 vs. 100 ml).

5.3.4 Styrene-Hexyl Methacrylate Copolymer

Spinning experiments were conducted using the modified experimental set-up with styrene and n-hexyl methacrylate copolymer as the core material. Copolymerization of styrene and n-hexyl methacrylate is to obtain a flexible material whose glass transition temperature is below the room temperature so that a large diameter (greater than 1mm) plastic optical fibers can be manufactured. The molar ratio of styrene and n-hexyl methacrylate was varied at 80/20 and 50/50, respectively. The refractive indices of polystyrene and poly(n-hexyl methacrylate) are 1.59 and 1.48, respectively and the refractive index of the copolymer is expected to be linearly dependent on the mole fraction of n-hexyl methacrylate between the two values. Therefore, as the molar content of n-hexyl methacrylate is increased, the refractive index of the core decreases whereas the fiber becomes more flexible.

In these experiments n-butyl mercaptan was added at 20 mmol/*l* as a chain transfer agent and the polymerization temperature was maintained at 120°C. Fiber

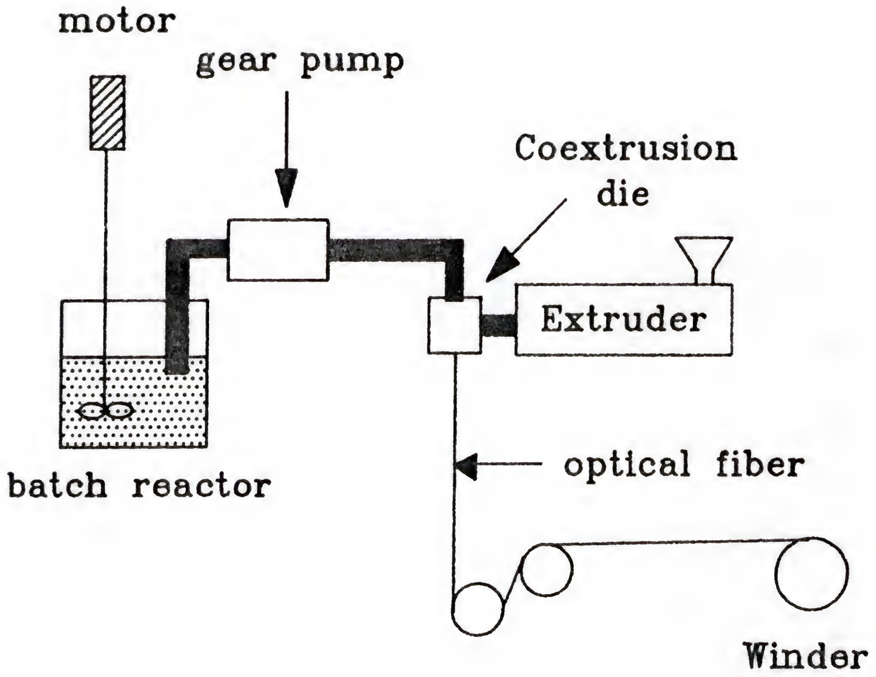

Figure 33. Batch reactor attachment for the plastic optical fiber spinning

spinning was initiated after four hours of reaction using the same ethylene-vinyl acetate copolymer as the cladding material. Fibers with 1.5~2.0 mm diameter were fabricated and aged in an oven at 100°C for post-polymerization. After the aging in the oven, it was found that the cross-section of the fiber was rather elliptic than circular. This deformation is presumably due to the volume change resulting from the loss of monomers by diffusion during the aging. This result suggests that further polymerization is necessary before the spinning experiment. Further polymerization, however, is not desirable with the current reactor set-up since the viscosity of the prepolymer will be increased substantially causing cavitation problem during pumping. This problem, however, can be resolve if the current reactor is replaced by a pressurizable one so that the pressure can be raised at the feeding port of the gear pump.

5.3.5 Polysiloxanes

Polysiloxanes based on the monomers of dimethyl, methyl-phenyl, and diphenyl siloxane are optically transparent. It is known that the refractive index (n) of polysiloxane increases linearly with its phenyl content. Among various polysiloxanes, poly(dimethyl diphenylsiloxane) and poly(methylphenylsiloxane) were initially used as the core along with a PMMA cladding. The poly(dimethyl diphenylsiloxane) was an elastomeric gel, whereas the poly(methylphenylsiloxane) was a viscous liquid. Since the viscosity of the latter was so low, it was fed by a liquid gear pump instead of the piston-cylinder unit. For both cases physically intact optical fibers could be made. Since both of these materials were chemically stable, crosslinking reaction could not be induced and the core materials remained as a gel and as a liquid phase, respectively.

Among many different commercial polysiloxanes, poly(dimethyl siloxane) with vinyl-phenyl-methyl termination was the only crosslinkable one we could find. Although its refractive index is as low as 1.39 due to its low phenyl content, this material was used to conduct a spinning experiment which involved a crosslinking reaction. The reaction study in a test tube has indicated that the volume change (or density change) is negligible during the crosslinking reaction. Thus, unlike the styrene-based material, polysiloxane could be coextruded as a liquid phase core followed by post polymerization after spinning. For the spinning experiment with this core material, benzoyl peroxide was added at 0.2% as an initiator of the crosslinking reaction and an ethylene-vinyl acetate copolymer was used as the cladding. After the spinning process the fibers were put in an oven at 100°C to induce the crosslinking reaction. Unlike the reaction study in test tubes, the crosslinking reaction was found to be rather irregular in that the reaction was complete with some samples while it was not with others. It is possible that the irregularity may result from a low reaction temperature, low initiator content, or some unknown interference of the cladding material. Further study should follow to resolve this problem.

The polysiloxanes were specifically studied in conjunction with the US Department of Energy Project to develop "radiation hard scintillating plastic optical fibers" for the Superconducting Super Collider (SSC). In the harsh environment of the SSC, the commercial optical fibers based on PS-PMMA materials are inadequate due to severe radiation damage. Siloxane based materials were identified as one of the possible choices for the radiation hard optical fibers, and attempts were made in the present study to convert the polysiloxane into optical optical fibers. The materials those have been evaluated are either in liquid or gel phase and consequently, the conventional thermal-drawing method is not applicable. In this study, it has been demonstrated that such materials can in fact be fabricated into optical fibers by the new processing method.

5.3.6 Uniformity of Fiber Radius

Uniformity of fiber radius is one of the most important physical aspects which has significant influence on the optical property of the optical fibers. Throughout the experiments, the fiber radius was not only monitored visually but also inspected physically using a micrometer within an accuracy of 0.01mm. For at least one-meter long fibers the outermost diameter was measured at a 10 cm interval. For an average diameter of 1 mm, the standard deviation was within 3%. This level of uniformity may be tolerable for the purpose of optical fibers.

5.4 Summary and Conclusion

A new processing method has been developed for the fabrication of plastic optical fibers in which a thermoplastic cladding material is spun into a hollow fiber while a core material is fed into the core of the hollow fiber at the same time. In conventional methods both core and cladding materials should be thermoplastics. In the new method, however, only the cladding material has to be a thermoplastic and the core material can be any class of materials including thermosetting polymers. The experimental study has focused on assessing the feasibility of the new fabrication method to fabricate physically sound plastic optical fibers. Lab scale experiments have demonstrated that the new method is capable of fabricating defect-free clad fibers using several different types of materials. The new method is possible because the mechanics of the bicomponent spinning flow is controlled by the viscoelastic cladding material under typical spinning conditions as predicted by the process modeling study.

CHAPTER 6
SUMMARY AND CONCLUSION

The two-phase flow of a bicomponent coextrusion fiber spinning has been studied theoretically and experimentally. A simple model has been adopted for the theoretical analysis in which a Newtonian and an upper-convected Maxwell fluid are the core and the skin layers, respectively. This model was chosen to investigate a flow situation in which the two fluids have quite different extensional rheology. The results indicate that the viscoelasticity of the skin layer plays a significant role in determining the overall mechanics of the two-phase flow. Thus, the stability of the flow is also significantly influenced by the viscoelastic skin layer and thereby the onset of draw resonance of a Newtonian fluid is delayed to a higher value of draw ratio in the two-phase coextrusion flow. This stabilizing effect becomes more prominent as the viscoelasticity represented by the Deborah number is increased. As a consequence of the competing influence of the purely viscous and viscoelastic fluid, an interesting behavior has been also predicted in that the highest draw ratio for a stable coextrusion spinning can be larger than that of the single-phase spinning of either fluid (Newtonian or UCM) under a certain condition.

In the experimental study linear low-density polyethylenes (LLDPE) and low-density polyethylenes (LDPE) were used as the core- and the skin-layer materials, respectively. This choice of materials has been made to simulate the flow situation considered in the theoretical investigation as closely as possible. The two materials are chemically identical although their molecular structures are different. Thus, they have good chemical compatibility ensuring the continuity of velocity at the interface.

However, they are known to have distinctly different extensional rheology resulting from the differences in their molecular structure. While the LLDPEs are very prone to draw resonance instability, the LDPEs are not. It is due to the larger relaxation time of the LDPEs compared to the LLDPEs. The experimental results may be summarized as follows:

1) The critical draw ratio for the onset of draw resonance increases as the flow rate fraction of the viscoelastic skin layer is increased.
2) Draw resonance instability appears to be sustained beyond the critical draw ratio. With increasing draw ratio, the amplitude of the instability increases whereas its period remains unchanged.
3) The critical draw ratio is apparently independent of the draw span although the maximum-to-minimum diameter ratio is observed to be decreasing with increasing draw span.
4) The period of the instability increases linearly with L/w_0, the ratio of the draw span to the average velocity at the die exit.

The linear stability theory provides only a limited information about the dynamical behavior of the instability for small time. Nevertheless, many aspects of the experimental observations seem to be in accordance with the predictions of the linear stability analysis at least qualitatively. The prediction that the highest draw ratio for a stable coextrusion spinning can be larger than that of the single-phase spinning of either fluid, however, has not been observed with the current choice of materials.

As a practical application of the two-phase fiber spinning process, a new processing method has been developed to fabricate plastic optical fibers using various type of materials. The new process method is possible since the more viscoelastic material of the two components, which is typically the skin-layer material, dictates the overall mechanics of the flow as predicted by the theoretical model. While the conventional coextrusion process is for extruding only thermoplastic materials, current study suggests a way to explore a variety of core material options for plastic optical fibers.

The study presented in this thesis is specifically for a fiber spinning process. The mathematical similarities in the governing equations, however, suggest that the mathematical approaches and the results regarding the characteristics of the two-phase flow are also relevant to other fast-drawing process such as extrusion coating or film casting. The present model is very simple in that simplest constitutive models have been used for an isothermal flow situation in the absence of the gravitational force or the surface forces. Nevertheless, it is believed that the present model represents the fundamental and the essential features of the two-phase flow system at least qualitatively, so that it may serve as a basis for more rigorous analyses using more complicated but more realistic constitutive models.

APPENDIX A
THE FINITE DIFFERENCE APPROACH OF EIGENVALUE PROBLEMS

Several mathematical approaches can be taken to solve the eigenvalue problem. In the present analysis, the eigenvalue λs are determined by reducing the eigenvalue problem to an algebraic eigenvalue problem by the use of finite differences.

The draw-down region was discretized into n equal spaces and the three point central finite difference was used as follows for the first and the second order derivatives:

$$\frac{dy_i^*}{dz} = \frac{y_{i+1}^* - y_{i-1}^*}{2h} \tag{A.1}$$

$$\frac{d^2y_i^*}{dz^2} = \frac{y_{i+1}^* - 2y_i^* + y_{i-1}^*}{h^2} \tag{A.2}$$

Here y^* represents all the variables involved in the fiber spinning flow problem; w^*, a^*, τ_{zz}^* and T^*. h is the equal-step size which is 1/n. Using equation (A.1) for the continuity equation (3.5) is given as

$$w_i^{ss}\left(\frac{w_{i+1}^* - w_{i-1}^*}{2h}\right) + w_i^{ss}\left(\frac{a_{i+1}^* - a_{i-1}^*}{2h}\right) = -\lambda a_i^*; \qquad \text{i=2,...,n} \tag{A.3}$$

Here i=1 and n+1 correspond to the two boundary points at z=0 and 1, respectively. At the initial point z=0 (i.e., i=1), all variables are specified as

$$a_1^{\bullet} = w_1^{\bullet} = \tau_{zz,1}^{\bullet} = T_1^{\bullet} = w_{n+1}^{\bullet} = 0 \tag{A.4}$$

when i=n+1, since the central differencing cannot be used, the backward differencing was used as follows:

$$w_{n+1}^{ss}(\frac{w_{n+1}^{\bullet} - w_n^{\bullet}}{h}) + w_{n+1}^{ss}(\frac{a_{n+1}^{\bullet} - a_n^{\bullet}}{h}) = -\lambda a_{n+1}^{\bullet}; \quad \text{i=n+1} \tag{A.5}$$

Using these finite difference equations for all nodal points within the boundary, the continuity equation is formulated in a matrix form as

$$\underline{\underline{A}}_{n\times(n-1)} \underline{w}_{(n-1)\times 1}^{\bullet} + \underline{\underline{B}}_{n\times n} \underline{a}_{n\times 1}^{\bullet} = \lambda h \underline{a}_{n\times 1}^{\bullet} \tag{A.6}$$

where

$$\underline{\underline{A}}_{n\times(n-1)} = \begin{bmatrix} 0 & -\frac{w_2^{ss}}{2} & 0 & 0 & \cdots & 0 \\ \frac{w_3^{ss}}{2} & 0 & -\frac{w_3^{ss}}{2} & 0 & \cdots & 0 \\ 0 & \frac{w_4^{ss}}{2} & 0 & -\frac{w_4^{ss}}{2} & 0 & 0 \\ & & \ddots & \ddots & \ddots & \\ 0 & \cdots & 0 & \frac{w_{n-1}^{ss}}{2} & 0 & -\frac{w_{n-1}^{ss}}{2} \\ 0 & \cdots & 0 & 0 & \frac{w_n^{ss}}{2} & 0 \\ 0 & \cdots & 0 & 0 & 0 & w_{n+1}^{ss} \end{bmatrix}; \quad \underline{w}_{(n-1)\times 1}^{\bullet} = \begin{Bmatrix} w_2^{\bullet} \\ w_3^{\bullet} \\ w_4^{\bullet} \\ \vdots \\ w_{n-2}^{\bullet} \\ w_{n-1}^{\bullet} \\ w_n^{\bullet} \end{Bmatrix}$$

$$\underline{\underline{B}}_{n\times n}=\begin{bmatrix} 0 & -\frac{w_2^{ss}}{2} & 0 & 0 & 0 & \cdots & 0 \\ \frac{w_3^{ss}}{2} & 0 & -\frac{w_3^{ss}}{2} & 0 & 0 & \cdots & 0 \\ 0 & \frac{w_4^{ss}}{2} & 0 & -\frac{w_4^{ss}}{2} & 0 & \cdots & 0 \\ & & \ddots & \ddots & \ddots & & \\ 0 & \cdots & 0 & \frac{w_{n-1}^{ss}}{2} & 0 & -\frac{w_{n-1}^{ss}}{2} & 0 \\ 0 & \cdots & 0 & 0 & \frac{w_n^{ss}}{2} & 0 & -\frac{w_n^{ss}}{2} \\ 0 & \cdots & 0 & 0 & 0 & w_{n+1}^{ss} & -w_{n+1}^{ss} \end{bmatrix};\quad \underline{a}^{\bullet}_{n\times 1}=\begin{Bmatrix} a_2^{\bullet} \\ a_3^{\bullet} \\ a_4^{\bullet} \\ \vdots \\ a_{n-2}^{\bullet} \\ a_{n-1}^{\bullet} \\ a_n^{\bullet} \\ a_{n+1}^{\bullet} \end{Bmatrix}$$

The velocity at z=1 is fixed. Thus, $w^{\bullet}_{n+1}$=0 and consequently, the dimension of the unknow vector $\underline{w}^{\bullet}$ is (n-1) whereas that of $\underline{a}^{\bullet}$ is n.

Similary, the axial force balance (3.6) can be expressed as follows at each nodal points:

$$\begin{aligned} &\left[3(1-f)GM(w_i^{ss})^2\right]\left(\frac{w^{\bullet}_{i+1}-2w^{\bullet}_i+w^{\bullet}_{i-1}}{h^2}\right)+\left[3(1-f)GMw_i^{ss}w_i^{ss}{}'\right]\left(\frac{w^{\bullet}_{i+1}-w^{\bullet}_{i-1}}{2h}\right) \\ &\left[3(1-f)GM\left\{w_i^{ss}w_i^{ss}{}''-(w_i^{ss}{}')^2\right\}\right]w^{\bullet}_i=\left[-3(1-f)GMw_i^{ss}w_i^{ss}{}'-fw_i^{ss}T_i^{ss}\right]\left(\frac{a^{\bullet}_{i+1}-a^{\bullet}_{i-1}}{2h}\right) \\ &+\left[f(T_i^{ss}w_i^{ss}{}'-T_i^{ss}{}'w_i^{ss})+3(1-f)GM\left\{(w_i^{ss}{}')^2-w_i^{ss}w_i^{ss}{}''\right\}\right]a^{\bullet}_i+\left[f(T_i^{ss}w_i^{ss}{}'\right. \\ &\left.-T_i^{ss}{}'w_i^{ss})\right]T^{\bullet}_i+\left[-fw_i^{ss}T_i^{ss}\right]\left(\frac{T^{\bullet}_{i+1}-T^{\bullet}_{i-1}}{2h}\right);\quad \mathrm{i}=2,\cdots,\mathrm{n} \end{aligned} \tag{A.7}$$

Here the prime and the double prime denote the first and the second order derivative with respect to the spatial variable z, and the superscript ss indicates the steady state solution which is known as the base flow for the stability analysis. The collection of equation (A.7) at all nodal points along with boundary conditions, $w^{\bullet}_1=w^{\bullet}_{n+1}=a^{\bullet}_1=T^{\bullet}_1=0$, gives the following axial force balance in a matrix form:

$$\underline{\underline{H}}_{(n-1)\times(n-1)}\,\underline{w}^{*}_{(n-1)\times 1} = h\,\underline{\underline{P}}_{(n-1)\times n}\,\underline{a}^{*}_{n\times 1} + h\,\underline{\underline{Q}}_{(n-1)\times n}\,\underline{T}^{*}_{n\times 1} \tag{A.8}$$

Here

$$\underline{\underline{H}}_{(n-1)\times(n-1)} = \begin{bmatrix} r_2 & q2_2 & 0 & 0 & 0 & \cdots & 0 \\ q1_3 & r_3 & q2_3 & 0 & 0 & \cdots & 0 \\ 0 & q1_4 & r_4 & q2_4 & 0 & \cdots & 0 \\ & & \ddots & \ddots & \ddots & & \\ 0 & \cdots & 0 & q1_{n-2} & r_{n-2} & q2_{n-2} & 0 \\ 0 & \cdots & 0 & 0 & q1_{n-1} & r_{n-1} & q2_{n-1} \\ 0 & \cdots & 0 & 0 & 0 & q1_n & r_n \end{bmatrix}$$

where $q1_i = 3(1-f)GM\left[(w_i^{ss})^2 - \frac{h}{2} w_i^{ss} w_i^{ss}{}'\right]$

$r_i = 3(1-f)GM\left[-2(w_i^{ss})^2 + h^2 w_i^{ss} w_i^{ss}{}'' - h^2 (w_i^{ss}{}')^2\right]$

$q2_i = 3(1-f)GM\left[(w_i^{ss})^2 + \frac{h}{2} w_i^{ss} w_i^{ss}{}'\right]$

$$\underline{\underline{P}}_{(n-1)\times n} = \begin{bmatrix} t_2 & -s_2 & 0 & 0 & 0 & 0 & \cdots & 0 \\ s_3 & t_3 & -s_3 & 0 & 0 & 0 & \cdots & 0 \\ 0 & s_4 & t_4 & -s_4 & 0 & 0 & \cdots & 0 \\ & & \ddots & \ddots & \ddots & & & \\ 0 & \cdots & 0 & s_{n-2} & t_{n-2} & -s_{n-2} & 0 & 0 \\ 0 & \cdots & 0 & 0 & s_{n-1} & t_{n-1} & -s_{n-1} & 0 \\ 0 & \cdots & 0 & 0 & 0 & s_n & t_n & -s_n \end{bmatrix}$$

where $s_i = \frac{1}{2} w_i^{ss}\left[f T_i^{ss} + 3(1-f)GM w_i^{ss}{}'\right]$

$t_i = h\left[f(T_i^{ss} w_i^{ss}{}' - T_i^{ss}{}' w_i^{ss}) + 3(1-f)GM\left\{(w_i^{ss}{}')^2 - w_i^{ss} w_i^{ss}{}''\right\}\right]$

$$\underline{\underline{Q}}_{(n-1)\times n} = \begin{bmatrix} v_2 & -u_2 & 0 & 0 & 0 & 0 & \cdots & 0 \\ u_3 & v_3 & -u_3 & 0 & 0 & 0 & \cdots & 0 \\ 0 & u_4 & v_4 & -u_4 & 0 & 0 & \cdots & 0 \\ & & \ddots & \ddots & \ddots & & & \\ 0 & \cdots & 0 & u_{n-2} & v_{n-2} & -u_{n-2} & 0 & 0 \\ 0 & \cdots & 0 & 0 & u_{n-1} & v_{n-1} & -u_{n-1} & 0 \\ 0 & \cdots & 0 & 0 & 0 & u_n & v_n & -u_n \end{bmatrix}$$

where $u_i = \frac{1}{2} f w_i^{ss} T_i^{ss}$

$v_i = hf\,(T_i^{ss} w_i^{ss}{}' - T_i^{ss}{}' w_i^{ss})$

By the same way, the constitutive relations (3.7) and (3.8) are reduced in a matrix form as follows:

$$\underline{\underline{C}}_{n\times(n-1)} \underline{w}^{*}_{(n-1)\times 1} + \underline{\underline{D}}_{n\times n} \underline{\tau}^{*}_{zz\,n\times 1} = \lambda h \underline{\tau}^{*}_{zz\,n\times 1} \tag{A.9}$$

$$\underline{\underline{E}}_{n\times(n-1)} \underline{w}^{*}_{(n-1)\times 1} + h\underline{\underline{F}}_{n\times n} \underline{\tau}^{*}_{zz\,n\times 1} + \underline{\underline{G}}_{n\times n} \underline{T}^{*}_{n\times 1} = \lambda h \underline{T}^{*}_{n\times 1} \tag{A.10}$$

Here

$$\underline{\underline{C}}_{n\times(n-1)} = \begin{bmatrix} b_2 & -a_2 & 0 & 0 & 0 & \cdots & 0 \\ a_3 & b_3 & -a_3 & 0 & 0 & \cdots & 0 \\ 0 & a_4 & b_4 & -a_4 & 0 & \cdots & 0 \\ & & \ddots & \ddots & \ddots & & \\ 0 & \cdots & 0 & a_{n-2} & b_{n-2} & -a_{n-2} & 0 \\ 0 & \cdots & 0 & 0 & a_{n-1} & b_{n-1} & -a_{n-1} \\ 0 & \cdots & 0 & 0 & 0 & a_n & b_n \\ 0 & \cdots & 0 & 0 & 0 & 0 & 2a_{n+1} \end{bmatrix}$$

where $$a_i = -w_i^{ss}\left(1+\frac{G}{De\tau_{zz,i}^{ss}}\right)$$

$$b_i = 2hw_i^{ss}{}' + \frac{2hGw_i^{ss}{}'}{De\tau_{zz,i}^{ss}} - \frac{hw_i^{ss}\tau_{zz,i}^{ss}{}'}{\tau_{zz,i}^{ss}}$$

$$\underline{\underline{D}}_{n\times n} = \begin{bmatrix} d_2 & -c_2 & 0 & 0 & 0 & \cdots & 0 \\ c_3 & d_3 & -c_3 & 0 & 0 & \cdots & 0 \\ 0 & c_4 & d_4 & -c_4 & 0 & \cdots & 0 \\ & & \ddots & \ddots & \ddots & & \\ 0 & \cdots & 0 & c_{n-1} & d_{n-1} & -c_{n-1} & 0 \\ 0 & \cdots & 0 & 0 & c_n & d_n & -c_n \\ 0 & \cdots & 0 & 0 & 0 & 2c_{n+1} & (d_{n+1}-2c_{n+1}) \end{bmatrix}; \quad \underline{\tau_{zz}^{*}}_{n\times 1} = \begin{Bmatrix} \tau_{zz,2}^{*} \\ \tau_{zz,3}^{*} \\ \tau_{zz,4}^{*} \\ \vdots \\ \tau_{zz,n-1}^{*} \\ \tau_{zz,n}^{*} \\ \tau_{zz,n+1}^{*} \end{Bmatrix}$$

where $$c_i = \frac{w_i^{ss}}{2}$$

$$d_i = 2hw_i^{ss}{}' - \frac{h}{De} - \frac{hw_i^{ss}\tau_{zz,i}^{ss}{}'}{\tau_{zz,i}^{ss}}$$

$$\underline{\underline{E}}_{n\times(n-1)} = \begin{bmatrix} f_2 & -e_2 & 0 & 0 & \cdots & 0 \\ e_3 & f_3 & -e_3 & 0 & \cdots & 0 \\ 0 & e_4 & f_4 & -e_4 & 0 & 0 \\ & & \ddots & \ddots & \ddots & \\ 0 & \cdots & 0 & e_{n-1} & f_{n-1} & -e_{n-1} \\ 0 & \cdots & 0 & 0 & e_n & f_n \\ 0 & \cdots & 0 & 0 & 0 & 2e_{n+1} \end{bmatrix}$$

where $$e_i = \frac{1}{2}\left[w_i^{ss} - \frac{3w_i^{ss}\tau_{zz,i}^{ss}}{T_i^{ss}} - \frac{3Gw_i^{ss}}{DeT_i^{ss}}\right]$$

$$f_i = \frac{3hw_i^{ss}{}'\tau_{zz,i}^{ss}}{T_i^{ss}} + \frac{3hGw_i^{ss}{}'}{DeT_i^{ss}} - \frac{hw_i^{ss}T_i^{ss}{}'}{T_i^{ss}} - hw_i^{ss}{}'$$

$$\underline{\underline{F}}_{n\times n}=\begin{bmatrix} \eta_2 & 0 & 0 & 0 & 0 & \cdots & 0 \\ 0 & \eta_3 & 0 & 0 & 0 & \cdots & 0 \\ 0 & 0 & \eta_4 & 0 & 0 & \cdots & 0 \\ & & \ddots & \ddots & \ddots & & \\ 0 & \cdots & 0 & 0 & \eta_{n-1} & 0 & 0 \\ 0 & \cdots & 0 & 0 & 0 & \eta_n & 0 \\ 0 & \cdots & 0 & 0 & 0 & 0 & \eta_{n+1} \end{bmatrix}$$

where $\eta_i=\dfrac{3\tau_{zz,i}^{ss}w_i^{ss\,\prime}}{T_i^{ss}}$

$$\underline{\underline{G}}_{n\times n}=\begin{bmatrix} p_2 & -g_2 & 0 & 0 & 0 & \cdots & 0 \\ g_3 & p_3 & -g_3 & 0 & 0 & \cdots & 0 \\ 0 & g_4 & p_4 & -g_4 & 0 & \cdots & 0 \\ & & \ddots & \ddots & \ddots & & \\ 0 & \cdots & 0 & g_{n-1} & p_{n-1} & -g_{n-1} & 0 \\ 0 & \cdots & 0 & 0 & g_n & p_n & -g_n \\ 0 & \cdots & 0 & 0 & 0 & 2g_{n+1} & (p_{n+1}-2g_{n+1}) \end{bmatrix};\quad \underline{T}^{\bullet}_{n\times 1}=\begin{Bmatrix} T_2^{\bullet} \\ T_3^{\bullet} \\ T_4^{\bullet} \\ \vdots \\ T_{n-1}^{\bullet} \\ T_n^{\bullet} \\ T_{n+1}^{\bullet} \end{Bmatrix}$$

where $g_i=\dfrac{w_i^{ss}}{2}$

$$p_i=-\frac{h}{De}-\frac{hw_i^{ss}T_i^{ss\,\prime}}{T_i^{ss}}-hw_i^{ss}$$

By multiplying an inverse of $\underline{\underline{H}}_{(n-1)\times(n-1)}$, (i.e., $\underline{\underline{H}}^{-1}_{(n-1)\times(n-1)}$) on both sides of equation (A.8), the axial velocity is expressed in terms of other variables as follows:

$$\underline{w}^{\bullet}_{(n-1)\times 1}=h\underline{\underline{H}}^{-1}_{(n-1)\times(n-1)}\underline{\underline{P}}_{(n-1)\times n}\underline{a}^{\bullet}_{n\times 1}+h\underline{\underline{H}}^{-1}_{(n-1)\times(n-1)}\underline{\underline{Q}}_{(n-1)\times n}\underline{T}^{\bullet}_{n\times 1} \tag{A.11}$$

By substituting (A.11) into (A.6), (A.9), and (A.10), the following set of algebraic equations are derived for the eigenvalue problem:

$$\left[h\underline{\underline{A}}\,\underline{\underline{H}}^{-1}\underline{\underline{P}}+\underline{\underline{B}}\right]_{n\times n}\underline{a}^{*}_{n\times 1}+\left[h\underline{\underline{A}}\,\underline{\underline{H}}^{-1}\underline{\underline{Q}}\right]_{n\times n}\underline{T}^{*}_{n\times 1}=\lambda h\underline{a}^{*}_{n\times 1} \tag{A.12}$$

$$\left[h\underline{\underline{C}}\,\underline{\underline{H}}^{-1}\underline{\underline{P}}\right]_{n\times n}\underline{a}^{*}_{n\times 1}+\left[\underline{\underline{D}}_{n\times n}\right]\underline{\tau^{*}_{zz}}_{n\times 1}+\left[h\underline{\underline{C}}\,\underline{\underline{H}}^{-1}\underline{\underline{Q}}\right]_{n\times n}\underline{T}^{*}_{n\times 1}=\lambda h\underline{\tau^{*}_{zz}}_{n\times 1} \tag{A.13}$$

$$\left[h\underline{\underline{E}}\,\underline{\underline{H}}^{-1}\underline{\underline{P}}\right]_{n\times n}\underline{a}^{*}_{n\times 1}+\left[h\underline{\underline{F}}_{n\times n}\right]\underline{\tau^{*}_{zz}}_{n\times 1}+\left[h\underline{\underline{E}}\,\underline{\underline{H}}^{-1}\underline{\underline{Q}}+\underline{\underline{G}}\right]_{n\times n}\underline{T}^{*}_{n\times 1}=\lambda h\underline{T}^{*}_{n\times 1} \tag{A.14}$$

Equations (A.12)–(A.14) can be combined together to give

$$\begin{bmatrix} \left[h\underline{\underline{A}}\,\underline{\underline{H}}^{-1}\underline{\underline{P}}+\underline{\underline{B}}\right]_{n\times n} & \underline{\underline{0}}_{n\times n} & \left[h\underline{\underline{A}}\,\underline{\underline{H}}^{-1}\underline{\underline{Q}}\right]_{n\times n} \\ \left[h\underline{\underline{C}}\,\underline{\underline{H}}^{-1}\underline{\underline{P}}\right]_{n\times n} & \underline{\underline{D}}_{n\times n} & \left[h\underline{\underline{C}}\,\underline{\underline{H}}^{-1}\underline{\underline{Q}}\right]_{n\times n} \\ \left[h\underline{\underline{E}}\,\underline{\underline{H}}^{-1}\underline{\underline{P}}\right]_{n\times n} & h\underline{\underline{F}}_{n\times n} & \left[h\underline{\underline{E}}\,\underline{\underline{H}}^{-1}\underline{\underline{Q}}+\underline{\underline{G}}\right]_{n\times n} \end{bmatrix} \begin{Bmatrix} \underline{a}^{*}_{n\times 1} \\ \underline{\tau^{*}_{zz}}_{n\times 1} \\ \underline{T}^{*}_{n\times 1} \end{Bmatrix} = \lambda h \begin{Bmatrix} \underline{a}^{*}_{n\times 1} \\ \underline{\tau^{*}_{zz}}_{n\times 1} \\ \underline{T}^{*}_{n\times 1} \end{Bmatrix} \tag{A.15}$$

or

$$\underline{\underline{U}}_{3n\times 3n}\underline{Y}^{*}_{3n\times 1}=\lambda h\underline{Y}^{*}_{3n\times 1} \tag{A.16}$$

Equation (A.15) or (A.16) is a standard form of an eigenvalue problem for which the eignevalue λ is to be determined. In the present study it is solved by the DEVLRG subroutine in the IMSL package.

APPENDIX B
THE MAXIMUM DRAW RATIO

The analytic expression for the maximum attainable draw ratio above which the axial stress becomes infinity is discussed in this section. The maximun draw ratio for the single-phase flow of the generalized UCM fluid was first obtained by Fisher and Denn (1976) which is described as

$$D_r \leq 1 + De^{-1/n} \tag{B.1}$$

When the power-law index n for the shear viscosity is set to 1, the result for the single-phase UCM fluid is obtained.

By a similar approach, Park(1990) obtained the analytic expression for the maximum draw ratio for the two-phase fiber spinning flow:

$$D_r + \frac{k}{2}\ln\left[\frac{\left|D_r - k\right|^3\left|1-k^3\right|}{\left|D_r^3 - k^3\right|\left|1-k\right|^3}\right] - k\sqrt{3}\left\{\tan^{-1}\left(\frac{2D_r + k}{k\sqrt{3}}\right) - \tan^{-1}\left(\frac{2+k}{k\sqrt{3}}\right)\right\} = 1 + \frac{1}{De} \tag{B.2}$$

where $k^3 = 1 - (t_0 f)^{-1}$. If both f and t_0 are set to 1, we may find that (B.2) is reduced to (B.1). Since equation (B.2) is implicit in *Dr*, the maximum draw ratio is calculated numerically once the values of t_0, f (thus *k*) and *De* are specified. The solid lines shown in Figure B are the results of the numerical calculation for f=0.2, 0.5, 1.0 at $t_0 = 10.0$ as a function of *De*. It should be noted that the *Dr* value shown in Figure 34 corresponds to the infinite axial tension. In case of f=0.2 for which the *Dr* vs. *G* curve shows a maximum at a finite value of axial tension, the value of *Dr* which corresponds to the maximum point is the true maximum *Dr* according to the stability analysis of Chapter 3. The true maximum *Dr* calculated from the collection of numerous *Dr* vs. *G* curves for f=0.2 is plotted in dashed line on Figure 34.

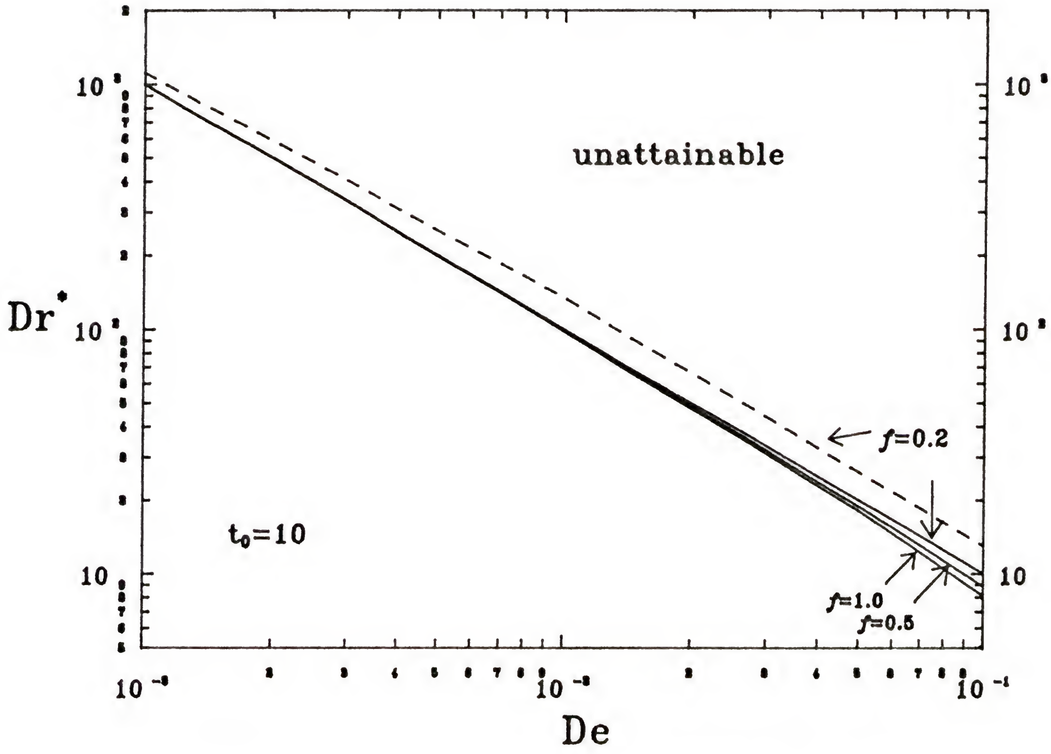

Figure 34. Maximum attainable draw ratio as a function of Deborah number for *f*=0.2, 0.5 and 1.0 at t_0=10.0 (—), and true maximum draw ratio as a function of Deborah number for *f*=0.2 at t_0=10.0 (-----).

APPENDIX C
COMPUTER PROGRAMS

The bicomponent fiber spinning has been simulated by using computer programs. These programs include 1 main program(STABCOEX) and 3 subprgrams (function FUN, subroutine RGKG and subroutine DTRIDAG). There is one additional subprogram which is an IMSL library subroutine (DEVLRG) called by main program. The double precision is used throughout whole computations. The function of each program is described briefly as follows:

STABCOEX:

(1) Solving inverse axial force G use shooting method as Dr is given.

(2) Solving the steady-state solution use Runge-Kutta-Gill method as the parameters are given.

(3) Using linear stability analysis calculate the eigenvalues of disturbanced equations and determine the stability status.

FUN:

The functions of the first order ODE's of equations (2.37), (2.38) and (2.39).

RGKG:

Using Runge-Kutta-Gill method to solve the integration of ODE's.

DTRIDAG:

Solving the inverse of a tridigonal matrix by Thomas algorithm.

DEVLRG:

Solving the eigenvalues λ of eigenvalue problem.

```
ccccccccccccccccccccccccccccccccccccccccccccccccccccccccccccccccccccc
c                                                                   c
c                          Program STABCOEX                         c
c                                 by                                c
c                          Woei-Shyong LEE                          c
c                                                                   c
c                       University of Florida                       c
c                               1993                                c
c                                                                   c
c     This program is designed to solve the two-phase fiber spinning c
c     problem, which is assumed that the skin-layer material is an   c
c     upper-convected Maxwell fluid (UCM) and the core-layer material c
c     is a Newtonian fluid (NWF). It is assumed that the system is an c
c     isothermal, axisymmetrical, uniaxial and neglect the inertia,   c
c     surface tension and gravity. It can solve the draw ratio versus c
c     inverse axial force distribution, the steady-state solution, and c
c     eigenvlues of the disturbanced equations. This program has three c
c     major parts which are:                                          c
c     (1) Solving inverse axial force G use shooting method as Dr is  c
c         given.                                                      c
c     (2) Solving the steady-state solution use Runge-Kutta-Gill      c
c         method as the parameters are given.                         c
c     (3) Using linear stability analysis calculate the eigenvalues of c
c         disturbanced equations and determine the stability status.  c
c     This computation is based on the assumption of no hoop stress,  c
c     that is, E(z)=0 for all z                                       c
c                                                                   c
cccccccccccccccccccccccccccccccccccccccccccccccccccccccccccccccccccc
c
      parameter(ndep=3,ns=7,nspace=4200,n=50)
      implicit double precision(a-h,o-z)
      double precision M
      dimension yy(ns),y(n+1,7),AMX(n,n-1),BMX(n,n),CMX(n,n-1)
      dimension DMX(n,n),EMX(n,n-1),FMX(n,n),GMX(n,n),HMX(n-1,n-1)
      dimension PMX(n-1,n),QMX(n-1,n),HINV(n-1,n-1),V1MX(n-1,n)
      dimension V2MX(n-1,n),W1MX(n,n),W2MX(n,n),W3MX(n,n),W4MX(n,n)
      dimension W5MX(n,n),W6MX(n,n),UMX(3*n,3*n),tria(n-1),trib(n-1)
      dimension tric(n-1),trif(n-1,n-1),RWKSP(100000)
      complex   eval(3*n)
      common /worksp/rwksp
      common/block/f,M,De,G
      data x0,xmax/0.0,1.0/
      external DEVLRG,fun
      call IWKIN(100000)
c
c --- ndep - total number of dependent variables in ODEs
c     ns   - total number of variables
c     x0   - initial value of independent variable
c     h    - increment of independent variable
c     xmax - maximum of independent variable
c
      open(5,file='STABCOEX.DAT',status='old')
      open(6,file='STABCOEX.OUT',status='new')
      nprint = n
      h = (xmax-x0)/nspace
c
c --- Read parameters from data file STABCOEX.DAT --
c
c     f       : Skin flow rate ratio.
c     Dr      : Draw ratio.
c     De      : Deborah number.
c     M       : Shear viscosity ratio of core to skin.
c     G0      : Initial guessed G value (G : inverse axial force)
c     dG0     : Initial setting of discritzed space.
```

```
c     Tauzz0 : Initial extra shear stress at the origin of the fiber.
c     T0     : Initial first normall stress at the origin of the fiber.
c
      read(5,*) f,Dr,De,M,G0,dG0,Tauzz0,T0
      alpha = dlog(Dr)
c
c======================================================================c
c                                                                      c
c (1) This part of the program is solving G when Dr is given by using  c
c     shooting method.                                                 c
c                                                                      c
c======================================================================c
c
      write(*,100) Dr
      G    = G0
      iter = 0
10    iter = iter + 1
      x    = x0
      yy(1) = 1.0
      yy(2) = yy(1)/3./G/M
      yy(3) = Tauzz0
      do i = 1,nspace
        call rgkg(fun,ndep,x,h,yy)
        x = x0+i*h
      end do
      ysavenew = yy(1) - Dr
      write(*,150) G,yy(1)
      if(dabs(ysavenew).le.1.d-6) go to 30
      if(iter.eq.1) go to 20
      ysign = ysavenew*ysaveold
      if(ysign.lt.0.0) dG0 = dG0*0.1
20    if(yy(1).gt.Dr) then
        G = G + dG0
      else
        if(G.eq.dG0) dG0 = dG0*0.1
        G = G - dG0
      end if
      ysaveold = ysavenew
      go to 10
30    write(*,200) G,Dr
c
c======================================================================c
c                                                                      c
c (2) This part of the program use Runge-Kutta-Gill method to find the c
c     steady-state solution of ODEs for two-phase coextrusion fiber    c
c     spinning.                                                        c
c                                                                      c
c======================================================================c
c
c --- Solving steady-state eqs and save the solutions from yy vector
c     to y maxtrix ---
c
c     yy - vector of dependent variables
c        yy(1) = W(ss),   yy(2) = W'(ss),      yy(3) = Tau,zz(ss)
c        yy(4) = W"(ss),  yy(5) = Tau',zz(ss)
c        yy(6) = T(ss),   yy(7) = T'(ss)
c
c     y(i,k) : i : node number
c             k = 1 : W(ss)                 ; ss:steady state
c                 2 : W'(ss)
c                 3 : Tau,zz(ss)
c                 4 : W"(ss)
c                 5 : Tau,zz'(ss)
c                 6 : T(ss)
```

```
c                   7 : T'(ss)
c
       x      = x0
       yy(1) = 1.0
       yy(2) = yy(1)/3./G/M
       yy(3) = Tauzz0
       yy(4) = 1./(3.*(1.-f)*G*M*De) - yy(2)**2/yy(1) + yy(2)
     &       * (2./(3.*(1.-f)*G*M) - f/(1.-f)/M/De/yy(1)
     &       - f*yy(3)/(1.-f)/G/M/yy(1) - 1./De/yy(1))
       yy(5) = (2.*yy(2)*(G+De*yy(3))-yy(3))/De/yy(1)
       yy(6) = yy(1)
       yy(7) = (yy(2)*(3.*(G+De*yy(3))-De*yy(6))-yy(6))/De/yy(1)
       k = 1
       do j = 1,ns
         y(k,j) = yy(j)
       end do
       do i = 1,nspace
         iprint=nspace/nprint*int(i*nprint/nspace)
         call rgkg(fun,ndep,x,h,yy)
         yy(4) = 1./(3.*(1.-f)*G*M*De) - yy(2)**2/yy(1) + yy(2)
     &           * (2./(3.*(1.-f)*G*M) - f/(1.-f)/M/De/yy(1)
     &           - f*yy(3)/(1.-f)/G/M/yy(1) - 1./De/yy(1))
         yy(5) = (2.*yy(2)*(G+De*yy(3))-yy(3))/De/yy(1)
         yy(6) = yy(1)/f - 3.*(1.-f)*G*M*yy(2)/f
         yy(7) = (yy(2)*(3.*(G+De*yy(3))-De*yy(6))-yy(6))/De/yy(1)
         if(i.eq.iprint) then
           k = k + 1
           do j = 1,ns
             y(k,j) = yy(j)
           end do
         end if
         x = x0+i*h
       end do
       write(*,250) f,G,Tauzz0,M,Dr,T0,De,alpha,nspace,n
       write(6,250) f,G,Tauzz0,M,Dr,T0,De,alpha,nspace,n
       do k = 1,n+1
         x = x0 + (k-1)/float(n)
         write(*,300) x,y(k,1),y(k,3),y(k,6)
         write(6,300) x,y(k,1),y(k,3),y(k,6)
       end do
       write(*,350)
       write(6,350)
       do k = 1,n+1
         x = x0 + (k-1)/float(n)
         write(*,400) x,y(k,2),y(k,4),y(k,5),y(k,7)
         write(6,400) x,y(k,2),y(k,4),y(k,5),y(k,7)
       end do
       write(*,450)
c
c=====================================================================c
c                                                                     c
c (3) This part of the program is used to solve all the eigenvalues of c
c     transition equations of two phase coextrusion fiber spinning    c
c     (skin: UCM, core:NWF). The first four largest eigenvalues of    c
c     disturbanced equations are printed out to determine whether the c
c     system is stable or not. The system is stable if all real parts c
c     of eigenvalues are less than zero while the system is unstable  c
c     if at least one real part of eigenvalue is greater than zero. If c
c     the real part of eigenvalue is zero, it is called neutral stable.c
c     An IMSL subroutine DVLRG is called in this program.             c
c                                                                     c
c=====================================================================c
c
c     y(i,k) : i : node number
```

```
c               k = 1 : W(ss)              ; ss:steady state
c                   2 : W'(ss)
c                   3 : Tau,zz(ss)
c                   4 : W"(ss)
c                   5 : Tau,zz'(ss)
c                   6 : T(ss)
c                   7 : T'(ss)
c
      h=1.0/float(n)
c
c --- AMX(n,n-1)*w(n-1,1)+BMX(n,n)*a(n,1)=lambda*h*a(n,1)
c
c --- AMX(n,n-1)
c
      do i = 1,n
        do j = 1,n-1
          AMX(i,j) = 0.0
        end do
      end do
      do i = 2,n+1
        if(i.ge.3.and.i.le.(n-1)) then
          AMX(i-1,i-2) =  0.5*y(i,1)
          AMX(i-1,i-1) =  0.0
          AMX(i-1,i)   = -0.5*y(i,1)
        else
          if(i.eq.2) then
            AMX(i-1,i-1) =  0.0
            AMX(i-1,i)   = -0.5*y(i,1)
          end if
          if(i.eq.n) then
            AMX(i-1,i-2) =  0.5*y(i,1)
            AMX(i-1,i-1) =  0.0
          end if
          if(i.eq.(n+1)) then
             AMX(i-1,i-2) = Dr
          end if
        end if
      end do
c
c --- BMX(n,n)
c
      do i = 1,n
        do j = 1,n
          BMX(i,j) = 0.0
        end do
      end do
      do i = 2,n+1
        if(i.ge.3.and.i.le.n) then
          BMX(i-1,i-2) =  0.5*y(i,1)
          BMX(i-1,i-1) =  0.0
          BMX(i-1,i)   = -0.5*y(i,1)
        else
          if(i.eq.2) then
            BMX(i-1,i-1) =  0.0
            BMX(i-1,i)   = -0.5*y(i,1)
          end if
          if(i.eq.(n+1)) then
            BMX(i-1,i-2) =  Dr
            BMX(i-1,i-1) = -Dr
          end if
        end if
      end do
c
c --- CMX(n,n-1)*w(n-1,1)+DMX(n,n)*Tau(n,1)=lambda*h*Tau(n,1)
```

```
c
c --- CMX(n,n-1)
c
      do i = 1,n
        do j = 1,n-1
          CMX(i,j) = 0.0
        end do
      end do
      do i = 2,n+1
        aelm = -y(i,1)*(1.+G/De/y(i,3))
        belm =  2.*h*y(i,2)+2.*h*G*y(i,2)/De/y(i,3)
     &          -h*y(i,1)*y(i,5)/y(i,3)
        if(i.ge.3.and.i.le.(n-1)) then
          CMX(i-1,i-2) =  aelm
          CMX(i-1,i-1) =  belm
          CMX(i-1,i)   = -aelm
        else
          if(i.eq.2) then
            CMX(i-1,i-1) =  belm
            CMX(i-1,i)   = -aelm
          end if
          if(i.eq.n) then
            CMX(i-1,i-2) = aelm
            CMX(i-1,i-1) = belm
          end if
          if(i.eq.(n+1)) CMX(i-1,i-2) = 2.*aelm
        end if
      end do
c
c --- DMX(n,n)
c
      do i = 1,n
        do j = 1,n
          DMX(i,j) = 0.0
        end do
      end do
      do i = 2,n+1
        celm = 0.5*y(i,1)
        delm = 2.*h*y(i,2)-h/De-h*y(i,1)*y(i,5)/y(i,3)
        if(i.ge.3.and.i.le.n) then
          DMX(i-1,i-2) =  celm
          DMX(i-1,i-1) =  delm
          DMX(i-1,i)   = -celm
        else
          if(i.eq.2) then
            DMX(i-1,i-1) =  delm
            DMX(i-1,i)   = -celm
          end if
          if(i.eq.(n+1)) then
            DMX(i-1,i-2) = 2.*celm
            DMX(i-1,i-1) = delm-2.*celm
          end if
        end if
      end do
c
c --- EMX(n,n-1)*w(n-1,1)+h*FMX(n,n)*Tau(n,1)
c    +GMX(n,n)*T(n,1) = lambda*h*T(n,1)
c
c --- EMX(n,n-1)
c
      do i = 1,n
        do j = 1,n-1
          EMX(i,j) = 0.0
        end do
```

```
       end do
       do i = 1,n
         eelm = 0.5*y(i+1,1)*(1.-3.*y(i+1,3)/y(i+1,6)
     &            -3.*G/De/y(i+1,6))
         felm = 3.*h*y(i+1,2)*y(i+1,3)/y(i+1,6)
     &         +3.*h*G*y(i+1,2)/De/y(i+1,6)
     &         -h*y(i+1,1)*y(i+1,7)/y(i+1,6)-h*y(i+1,2)
         if(i.ge.2.and.i.le.(n-2)) then
           EMX(i,i-1) =  eelm
           EMX(i,i)   =  felm
           EMX(i,i+1) = -eelm
         else
           if(i.eq.1) then
             EMX(i,i)   =  felm
             EMX(i,i+1) = -eelm
           end if
           if(i.eq.(n-1)) then
             EMX(i,i-1) = eelm
             EMX(i,i)   = felm
           end if
           if(i.eq.n) EMX(i,i-1) = 2.*eelm
         end if
       end do
c
c --- FMX(n,n)
c
       do i = 1,n
         do j = 1,n
           FMX(i,j) = 0.0
           if(i.eq.j) FMX(i,j) = 3.*y(i+1,3)*y(i+1,2)/y(i+1,6)
         end do
       end do
c
c --- GMX(n,n)
c
       do i = 1,n
         do j = 1,n
           GMX(i,j) = 0.0
         end do
       end do
       do i = 1,n
         gelm =  0.5*y(i+1,1)
         pelm = -h/De-h*y(i+1,1)*y(i+1,7)/y(i+1,6)-h*y(i+1,2)
         if(i.ge.2.and.i.le.(n-1)) then
           GMX(i,i-1) =  gelm
           GMX(i,i)   =  pelm
           GMX(i,i+1) = -gelm
         else
           if(i.eq.1) then
             GMX(i,i)   =  pelm
             GMX(i,i+1) = -gelm
           end if
           if(i.eq.n) then
             GMX(i,i-1) =  2*gelm
             GMX(i,i)   =  pelm-2*gelm
           end if
         end if
       end do
c
c --- HMX(n-1,n-1)*w(n-1,1)=h*PMX(n-1,n)*a(n,1)+h*QMX(n-1,n)*T(n,1)
c
c --- HMX(n-1,n-1)
c
       do i = 1,n-1
```

```
        do j = 1,n-1
          HMX(i,j) = 0.0
        end do
      end do
      do i = 1,n-1
        qelm1 = 3.*(1.-f)*G*M*(y(i+1,1)**2-0.5*h*y(i+1,1)*y(i+1,2))
        relm  = 3.*(1.-f)*G*M*(-2.*y(i+1,1)**2+h**2*y(i+1,1)*y(i+1,4)
     &         -h**2*y(i+1,2)**2)
        qelm2 = 3.*(1.-f)*G*M*(y(i+1,1)**2+0.5*h*y(i+1,1)*y(i+1,2))
        if(i.ge.2.and.i.le.(n-2)) then
          HMX(i,i-1) = qelm1
          HMX(i,i)   = relm
          HMX(i,i+1) = qelm2
        else
          if(i.eq.1) then
            HMX(i,i)   =  relm
            HMX(i,i+1) =  qelm2
          end if
          if(i.eq.(n-1)) then
            HMX(i,i-1) =  qelm1
            HMX(i,i)   =  relm
          end if
        end if
      end do
c
c --- PMX(n-1,n)
c
      do i = 1,n-1
        do j = 1,n
          PMX(i,j) = 0.0
        end do
      end do
      do i = 1,n-1
        selm = 0.5*y(i+1,1)*(f*y(i+1,6)+3.*(1.-f)*G*M*y(i+1,2))
        telm = h*(f*(y(i+1,6)*y(i+1,2)-y(i+1,1)*y(i+1,7))
     &        +3.*(1.-f)*G*M*(y(i+1,2)**2-y(i+1,1)*y(i+1,4)))
        if(i.eq.1) then
          PMX(i,i)   =  telm
          PMX(i,i+1) = -selm
        else
          PMX(i,i-1) =  selm
          PMX(i,i)   =  telm
          PMX(i,i+1) = -selm
        end if
      end do
c
c --- QMX(n-1,n)
c
      do i = 1,n-1
        do j = 1,n
          QMX(i,j) = 0.0
        end do
      end do
      do i = 1,n-1
        uelm = 0.5*f*y(i+1,1)*y(i+1,6)
        velm = h*f*(y(i+1,6)*y(i+1,2)-y(i+1,1)*y(i+1,7))
        if(i.eq.1) then
          QMX(i,i)   =  velm
          QMX(i,i+1) = -uelm
        else
          QMX(i,i-1) =  uelm
          QMX(i,i)   =  velm
          QMX(i,i+1) = -uelm
        end if
      end do
c
c --- w(n-1,1) = h*HINV(n-1,n-1)*PMX(n-1,n)*a(n,1)
c              + h*HINV(n-1,n-1)*QMX(n-1,n)*T(n,1)
c
c --- Compute HINV(n-1,n-1), inverse of HMX matrix by calling
c     subroutine DTRIDAG
c
      do i = 1,n-1
        if(i.ge.2.and.i.le.(n-2)) then
          tria(i) = HMX(i,i-1)
          trib(i) = HMX(i,i)
          tric(i) = HMX(i,i+1)
        else
          if(i.eq.1) then
            trib(i) = HMX(i,i)
            tric(i) = HMX(i,i+1)
          end if
          if(i.eq.(n-1)) then
            tria(i) = HMX(i,i-1)
            trib(i) = HMX(i,i)
          end if
        end if
        do j = 1,n-1
          trif(i,j) = 0.0
          if(i.eq.j) trif(i,j) = 1.0
        end do
      end do
c
      call DTRIDAG(tria,trib,tric,trif,n-1,HINV)
c
c --- HINV(n-1,n-1)*PMX(n-1,n) --> V1MX(n-1,n)
c
      do i = 1,n-1
        do j = 1,n
          sum = 0.0
          do k = 1,n-1
            sum = sum + HINV(i,k)*PMX(k,j)
          end do
          V1MX(i,j) = sum
        end do
      end do
c
c --- HINV(n-1,n-1)*QMX(n-1,n) --> V2MX(n-1,n)
c
      do i = 1,n-1
        do j = 1,n
          sum = 0.0
          do k = 1,n-1
            sum = sum + HINV(i,k)*QMX(k,j)
          end do
          V2MX(i,j) = sum
        end do
      end do
c
c --- h*AMX(n,n-1)*V1MX(n-1,n) + BMX(n,n)  --> W1MX(n,n)
c
      do i = 1,n
        do j = 1,n
          sum = 0.0
          do k = 1,n-1
            sum = sum + AMX(i,k)*V1MX(k,j)
          end do
          W1MX(i,j) = h*sum + BMX(i,j)
        end do
      end do
c
c --- h*AMX(n,n-1)*V2MX(n-1,n) --> W2MX(n,n)
c
      do i = 1,n
        do j = 1,n
          sum = 0.0
          do k = 1,n-1
            sum = sum + AMX(i,k)*V2MX(k,j)
          end do
          W2MX(i,j) = h*sum
        end do
      end do
c
c --- h*CMX(n,n-1)*V1MX(n-1,n) --> W3MX(n,n)
c
      do i = 1,n
        do j = 1,n
          sum = 0.0
          do k = 1,n-1
            sum = sum + CMX(i,k)*V1MX(k,j)
          end do
          W3MX(i,j) = h*sum
        end do
      end do
c
c --- h*CMX(n,n-1)*V2MX(n-1,n) --> W4MX(n,n)
c
      do i = 1,n
        do j = 1,n
          sum = 0.0
          do k = 1,n-1
            sum = sum + CMX(i,k)*V2MX(k,j)
          end do
          W4MX(i,j) = h*sum
        end do
      end do
c
c --- h*EMX(n,n-1)*V1MX(n-1,n) --> W5MX(n,n)
c
      do i = 1,n
        do j = 1,n
          sum = 0.0
          do k = 1,n-1
            sum = sum + EMX(i,k)*V1MX(k,j)
          end do
          W5MX(i,j) = h*sum
        end do
      end do
c
c --- h*EMX(n,n-1)*V2MX(n-1,n) + GMX(n,n)  --> W6MX(n,n)
c
      do i = 1,n
        do j = 1,n
          sum = 0.0
          do k = 1,n-1
            sum = sum + EMX(i,k)*V2MX(k,j)
          end do
          W6MX(i,j) = h*sum + GMX(i,j)
        end do
      end do
c
```

```
c                         W1MX(n,n)      OMX(n,n)       W2MX(n, n)
c
c --- UMX(3n,3n) =   { W3MX(n,n)      DMX(n,n)       W4MX(n,n)    }
c
c                         W5MX(n,n)    h*FMX(n,n)       W6MX(n,n)
c
      do i = 1,n
        do j = 1,n
          UMX(i,j)           = W1MX(i,j)
          UMX(i,j+n)         = 0.0
          UMX(i,j+2*n)       = W2MX(i,j)
          UMX(i+n,j)         = W3MX(i,j)
          UMX(i+n,j+n)       = DMX(i,j)
          UMX(i+n,j+2*n)     = W4MX(i,j)
          UMX(i+2*n,j)       = W5MX(i,j)
          UMX(i+2*n,j+n)     = h*FMX(i,j)
          UMX(i+2*n,j+2*n)   = W6MX(i,j)
        end do
      end do
c
c --- Call subroutine DEVLRG to compute eigenvalues lambda
c     of UMX(3n,3n) * x(3n,1) = lambda * h * x(3n,1)
c
      call DEVLRG(3*n,UMX,3*n,eval)
c
      write(*,500)
      write(6,500)
      do j = 3*n,3*n-6,-2
        evr = dble(eval(2*j-1))/h
        evi = dble(eval(2*j))/h
        write(*,550) (3*n-j+2)/2,evr,evi
        write(6,550) (3*n-j+2)/2,evr,evi
        if(j.eq.3*n) evalue = evr
      end do
      if(evalue.lt.0.0) then
        write(*,600)
        write(6,600)
      end if
      if(evalue.gt.0.0) then
        write(*,650)
        write(6,650)
      end if
      if(dabs(evalue).le.1.d-6) then
        write(*,700)
        write(6,700)
      end if
      write(*,750)
c
100   format(/1x,' Program is looking for a G value when Dr =',f12.6
     &      //17x,'G',18x,'Dr'/)
150   format(1x,2f20.6)
200   format(/'  Congrulations!, You finally get the solution which is:'
     &       /'  G =',f12.6,' when Dr =',f12.6
     &       /'  Now, program is solving the steady-state solution.'/)
250   format(//3x,'f  =',f12.6,5x,'G     =',f12.6,5x,'Tau,zz(0) =',f12.6
     &        /3x,'M  =',f12.6,5x,'Dr    =',f12.6,5x,'T(0)      =',f12.6
     &        /3x,'De =',f12.6,5x,'alpha =',f12.6,5x,'nsapce    =',i5
     &        /3x,'n  =',i5
     &      ///3x,'The steady-state solution is:'
     &       //10x,'z',11x,'w',20x,'Tau,zz',10x,'T'/)
300   format(2x,2f12.6,12x,2f12.6)
350   format(//10x,'z',10x,'w''',10x,'w"',7x,'Tau,zz''',9x,'T'''/)
400   format(2x,5f12.6)
450   format(/1x,' Now, program is computing the eigenvalues.'
     &       /1x,' Wait a moment ..... Be patient !')
500   format(//1x,' The eigenvalues are:'
     &       //29x,'1,real',14x,'1,imag'/)
550   format(10x,i4,' :',2f20.6)
600   format(/3x,'Stable: all eigenvalues are less than zero.'/)
650   format(/3x,'Unstable: at least one eigenvalue is greater '
     &             'than zero'/)
700   format(/3x,'Neutral Stable: the eigenvalue is close to zero.'/)
750   format(/1x,' Computation is completed. If you want to review the'
     &       /1x,' solution, please input TYPE STABCOEX.OUT'/)
      end
c
c---------------------------------------------------------------------c
c                                                                     c
      function fun(j,n,x,y)
c
c     j   - sequential number of dependent variables
c     n   - total number of dependent variables
c     x   - independent variable
c     y   - vector dependent variables
c
      implicit double precision(a-h,o-z)
      double precision M
      dimension y(n)
      common/block/f,M,De,G
      go to (1,2,3),j
1     fun = y(2)
      return
2     fun = 1./(3.*(1.-f)*G*M*De) - y(2)**2/y(1) + y(2)
     &    * (2./(3.*(1.-f)*G*M) - f/(1.-f)/M/De/y(1)
     &    - f*y(3)/(1.-f)/G/M/y(1) - 1./De/y(1))
      return
3     fun = (2.*y(2)*(G+De*y(3))-y(3))/De/y(1)
      return
      end
c
c---------------------------------------------------------------------c
c                                                                     c
      Subroutine RGKG(f,n,x,h,y)
c
c     This subprogram use Runge-Kutta-Gill method to solve the
c     system of simultaneous first order ordinary differential
c     equations.
c
c     n    - total number of dependent variables
c     x    - independent variable
c     h    - increment of independent variable
c     y    - vector of dependent variables
c
      implicit double precision(a-h,o-z)
      dimension y(n),ybar(50),phi(50)
      double precision k(50,4)
      a=dsqrt(2.d0)
      a=1.0/a
      b=1.0-a
      c=1.0+a
c -- step 1 ---
      do j=1,n
        k(j,1)=f(j,n,x,y)
        ybar(j)=y(j)
        phi(j)=k(j,1)
      end do
c -- step 2 ---
      do j=1,n
```

```
          y(j)=ybar(j)+0.5*h*k(j,1)
        end do
        x=x+0.5*h
        do j=1,n
          k(j,2)=f(j,n,x,y)
          phi(j)=phi(j)+2.0*b*k(j,2)
        end do
c -- step 3 ---
        do j=1,n
          y(j)=ybar(j)+b*h*(a*k(j,1)+k(j,2))
        end do
        do j=1,n
          k(j,3)=f(j,n,x,y)
          phi(j)=phi(j)+2.0*c*k(j,3)
        end do
c -- step 4 ---
        do j=1,n
          y(j)=ybar(j)-a*h*k(j,2)+c*h*k(j,3)
        end do
        x=x+0.5*h
        do j=1,n
          k(j,4)=f(j,n,x,y)
        end do
c -- step 5 ---
        do j=1,n
          y(j)=ybar(j)+h*(phi(j)+k(j,4))/6.0
        end do
        return
        end
c
c-----------------------------------------------------------------------c
c                                                                       c
      Subroutine DTRIDAG(a,b,c,f,n,x)
c
c     This subprogram use Thomas Algorithm to calculate the inverse
c     matrix of a tridigonal matrix.
c
c     n     - total magnitude of x matrix
c     x     - inverse matrix
c     f     - identity matrix
c     a,b,c - tridigonal elements
c
      implicit double precision(a-h,o-z)
      dimension a(n),b(n),c(n),f(n,n),x(n,n)
      do i = 2,n
        b(i) = b(i) - c(i-1)*a(i)/b(i-1)
        do j = 1,n
          f(i,j) = f(i,j) - f(i-1,j)*a(i)/b(i-1)
        end do
      end do
      do j = 1,n
        x(n,j) = f(n,j)/b(n)
        do i = 1,n-1
          x(n-i,j) = (f(n-i,j)-c(n-i)*x(n-i+1,j))/b(n-i)
        end do
      end do
      return
      end
```

Example 1:

```
f  =    0.200000      G     =    0.106984      Tau,zz(0) =   10.000000
M  =    1.000000      Dr    =   20.000000      T(0)      =    1.000000
De =    0.020000      alpha =    2.995732      nsapce    = 4200
n  =   50


The steady-state solution is:

        z           w                          Tau,zz          T

    0.000000    1.000000                    10.000000     1.000000
    0.020000    1.057770                     4.634612     1.601969
    0.040000    1.117991                     2.472781     1.519806
    0.060000    1.184732                     1.603187     1.429720
    0.080000    1.257842                     1.259816     1.402097
    0.100000    1.336898                     1.139957     1.424216
    0.120000    1.421722                     1.120466     1.478581
    0.140000    1.512359                     1.149465     1.553714
    0.160000    1.608999                     1.204371     1.643254
    0.180000    1.711926                     1.275113     1.743965
    0.200000    1.821479                     1.357177     1.854349
    0.220000    1.938046                     1.448618     1.973856
    0.240000    2.062047                     1.548738     2.102465
    0.260000    2.193935                     1.657478     2.240459
    0.280000    2.334193                     1.775130     2.388314
    0.300000    2.483334                     1.902202     2.546640
    0.320000    2.641904                     2.039351     2.716153
    0.340000    2.810478                     2.187349     2.897661
    0.360000    2.989664                     2.347073     3.092063
    0.380000    3.180108                     2.519502     3.300346
    0.400000    3.382485                     2.705714     3.523593
    0.420000    3.597513                     2.906896     3.762987
    0.440000    3.825943                     3.124348     4.019822
    0.460000    4.068568                     3.359497     4.295509
    0.480000    4.326220                     3.613901     4.591590
    0.500000    4.599773                     3.889265     4.909748
    0.520000    4.890142                     4.187454     5.251819
    0.540000    5.198287                     4.510505     5.619808
    0.560000    5.525210                     4.860643     6.015903
    0.580000    5.871959                     5.240298     6.442491
    0.600000    6.239625                     5.652120     6.902177
    0.620000    6.629343                     6.098998     7.397801
    0.640000    7.042294                     6.584083     7.932456
    0.660000    7.479700                     7.110801     8.509510
    0.680000    7.942827                     7.682881     9.132631
    0.700000    8.432981                     8.304374     9.805800
    0.720000    8.951507                     8.979674    10.533344
    0.740000    9.499783                     9.713544    11.319951
    0.760000   10.079224                    10.511135    12.170697
    0.780000   10.691272                    11.378013    13.091071
    0.800000   11.337393                    12.320178    14.086993
    0.820000   12.019073                    13.344086    15.164837
    0.840000   12.737812                    14.456670    16.331454
    0.860000   13.495114                    15.665354    17.594185
    0.880000   14.292486                    16.978072    18.960880
    0.900000   15.131421                    18.403275    20.439907
    0.920000   16.013397                    19.949942    22.040164
    0.940000   16.939861                    21.627579    23.771073
    0.960000   17.912222                    23.446215    25.642585
    0.980000   18.931837                    25.416391    27.665161
    1.000000   19.999999                    27.549140    29.849761
```

```
        z             w'          w"        Tau,zz'         T'

    0.000000    3.115737  -58.246921 -404.351917   90.356387
    0.020000    2.871840   10.215344 -164.862637    1.244689
    0.040000    3.170380   16.815563  -66.227565   -5.736008
    0.060000    3.500486   15.921666  -26.576420   -2.937887
    0.080000    3.806741   14.804915  -10.075412    0.027080
    0.100000    4.097408   14.373479   -2.857730    2.034294
    0.120000    4.385423   14.502957    0.507147    3.308141
    0.140000    4.679900   14.991043    2.216964    4.153921
    0.160000    4.986537   15.702069    3.194899    4.774288
    0.180000    5.308954   16.560006    3.843956    5.284948
    0.200000    5.649649   17.525314    4.347221    5.749155
    0.220000    6.010550   18.578514    4.791534    6.201559
    0.240000    6.393315   19.710779    5.220214    6.661776
    0.260000    6.799487   20.918903    5.656306    7.141637
    0.280000    7.230575   22.202669    6.113180    7.648975
    0.300000    7.688107   23.563482    6.599523    8.189614
    0.320000    8.173644   25.003633    7.121773    8.768423
    0.340000    8.688800   26.525907    7.685345    9.389900
    0.360000    9.235248   28.133352    8.295277   10.058495
    0.380000    9.814723   29.829141    8.956590   10.778807
    0.400000   10.429024   31.616480    9.674492   11.555717
    0.420000   11.080013   33.498534   10.454514   12.394474
    0.440000   11.769617   35.478368   11.302608   13.300771
    0.460000   12.499819   37.558885   12.225219   14.280804
    0.480000   13.272661   39.742770   13.229345   15.341333
    0.500000   14.090235   42.032424   14.322602   16.489731
    0.520000   14.954677   44.429902   15.513275   17.734048
    0.540000   15.868161   46.936832   16.810375   19.083057
    0.560000   16.832888   49.554344   18.223693   20.546315
    0.580000   17.851076   52.282979   19.763855   22.134219
    0.600000   18.924947   55.122600   21.442373   23.858056
    0.620000   20.056714   58.072291   23.271702   25.730060
    0.640000   21.248561   61.130257   25.265282   27.763463
    0.660000   22.502628   64.293707   27.437591   29.972542
    0.680000   23.820987   67.558748   29.804179   32.372661
    0.700000   25.205621   70.920260   32.381707   34.980306
    0.720000   26.658398   74.371781   35.187967   37.813108
    0.740000   28.181040   77.905382   38.241895   40.889864
    0.760000   29.775097   81.511554   41.563573   44.230527
    0.780000   31.441911   85.179090   45.174204   47.856198
    0.800000   33.182583   88.894980   49.096077   51.789078
    0.820000   34.997934   92.644316   53.352504   56.052415
    0.840000   36.888467   96.410210   57.967726   60.670405
    0.860000   38.854327  100.173730   62.966795   65.668079
    0.880000   40.895261  103.913866   68.375416   71.071141
    0.900000   43.010572  107.607513   74.219755   76.905776
    0.920000   45.199084  111.229496   80.526198   83.198414
    0.940000   47.459094  114.752627   87.321078   89.975448
    0.960000   49.788336  118.147810   94.630342   97.262908
    0.980000   52.183948  121.384187  102.479183  105.086087
    1.000000   54.642429  124.429337  110.891612  113.469116

The eigenvalues are:
                          l,real                l,imag

           1 :          -0.293327             13.731118
           2 :          -3.302049             33.178902
           3 :          -4.336087             61.466445
           4 :          -4.994560             69.644864

 Stable: all eigenvalues are less than zero.
```

Example 2:

```
f  =    0.200000      G     =    0.091367      Tau,zz(0) =    10.000000
M  =    1.000000      Dr    =   30.000000      T(0)      =     1.000000
De =    0.020000      alpha =    3.401197      nsapce    = 4200
n  =   50


The steady-state solution is:

       z           w                        Tau,zz        T

    0.000000    1.000000                 10.000000    1.000000
    0.020000    1.066778                  4.721847    1.699080
    0.040000    1.136793                  2.568179    1.611991
    0.060000    1.215584                  1.694314    1.514432
    0.080000    1.303112                  1.348332    1.486551
    0.100000    1.398962                  1.231238    1.515818
    0.120000    1.503018                  1.220327    1.583662
    0.140000    1.615454                  1.263287    1.677692
    0.160000    1.736643                  1.337071    1.791006
    0.180000    1.867088                  1.431344    1.920151
    0.200000    2.007387                  1.541555    2.063661
    0.220000    2.158212                  1.665921    2.221204
    0.240000    2.320296                  1.804068    2.393120
    0.260000    2.494435                  1.956397    2.580175
    0.280000    2.681480                  2.123782    2.783435
    0.300000    2.882342                  2.307430    3.004206
    0.320000    3.097993                  2.508810    3.244007
    0.340000    3.329466                  2.729628    3.504565
    0.360000    3.577857                  2.971825    3.787817
    0.380000    3.844328                  3.237580    4.095928
    0.400000    4.130109                  3.529329    4.431305
    0.420000    4.436498                  3.849787    4.796625
    0.440000    4.764865                  4.201968    5.194854
    0.460000    5.116649                  4.589217    5.629284
    0.480000    5.493361                  5.015244    6.103558
    0.500000    5.896583                  5.484153    6.621710
    0.520000    6.327968                  6.000479    7.188198
    0.540000    6.789236                  6.569233    7.807948
    0.560000    7.282174                  7.195935    8.486388
    0.580000    7.808630                  7.886658    9.229499
    0.600000    8.370509                  8.648076   10.043849
    0.620000    8.969766                  9.487498   10.936645
    0.640000    9.608399                 10.412917   11.915772
    0.660000   10.288440                 11.433049   12.989833
    0.680000   11.011943                 12.557368   14.168190
    0.700000   11.780972                 13.796140   15.460997
    0.720000   12.597589                 15.160453   16.879226
    0.740000   13.463830                 16.662231   18.434686
    0.760000   14.381698                 18.314245   20.140038
    0.780000   15.353133                 20.130107   22.008784
    0.800000   16.379996                 22.124256   24.055255
    0.820000   17.464047                 24.311916   26.294571
    0.840000   18.606914                 26.709044   28.742590
    0.860000   19.810074                 29.332251   31.415828
    0.880000   21.074823                 32.198700   34.331359
    0.900000   22.402251                 35.325978   37.506687
    0.920000   23.793215                 38.731944   40.959592
    0.940000   25.248313                 42.434544   44.707950
    0.960000   26.767859                 46.451604   48.769522
    0.980000   28.351861                 50.800595   53.161722
    1.000000   30.000001                 55.498379   57.901360
    z           w'          w"        Tau,zz'        T'

0.000000    3.648298  -79.860456 -393.700713  105.800633
0.020000    3.315218   13.570954 -163.571379    1.696872
0.040000    3.713942   22.611396  -66.326709   -6.221464
0.060000    4.162238   21.851353  -26.803910   -3.146670
0.080000    4.586831   20.728525  -10.082836    0.207361
0.100000    4.997247   20.455299   -2.571928    2.559011
0.120000    5.409904   20.910145    1.075120    4.123600
0.140000    5.836893   21.853995    3.041136    5.223709
0.160000    6.286208   23.121923    4.256333    6.080123
0.180000    6.763296   24.620213    5.135313    6.822837
0.200000    7.272221   26.299990    5.871948    7.525750
0.220000    7.816345   28.137617    6.562022    8.231595
0.240000    8.398710   30.123139    7.256241    8.966489
0.260000    9.022239   32.253948    7.984031    9.747909
0.280000    9.689845   34.531365    8.764623   10.588976
0.300000   10.404493   36.958783    9.612431   11.500790
0.320000   11.169226   39.540619   10.539757   12.493725
0.340000   11.987179   42.281684   11.558226   13.578184
0.360000   12.861587   45.186784   12.679589   14.765064
0.380000   13.795774   48.260409   13.916203   16.066074
0.400000   14.793153   51.506489   15.281359   17.493960
0.420000   15.857205   54.928160   16.789502   19.062693
0.440000   16.991464   58.527535   18.456426   20.787630
0.460000   18.199497   62.305471   20.299425   22.685656
0.480000   19.484870   66.261315   22.337436   24.775326
0.500000   20.851120   70.392640   24.591167   27.076985
0.520000   22.301716   74.694967   27.083209   29.612886
0.540000   23.840014   79.161473   29.838138   32.407291
0.560000   25.469207   83.782683   32.882595   35.486553
0.580000   27.192270   88.546165   36.245342   38.879180
0.600000   29.011898   93.436217   39.957291   42.615857
0.620000   30.930435   98.433565   44.051486   46.729442
0.640000   32.949803  103.515075   48.563047   51.254902
0.660000   35.071418  108.653501   53.529051   56.229203
0.680000   37.296112  113.817260   58.988347   61.691119
0.700000   39.624038  118.970275   64.981289   67.680972
0.720000   42.054582  124.071883   71.549383   74.240279
0.740000   44.586270  129.076826   78.734836   81.411292
0.760000   47.216680  133.935357   86.579985   89.236438
0.780000   49.942349  138.593458   95.126622   97.757634
0.800000   52.758696  142.993204  104.415189  107.015482
0.820000   55.659947  147.073271  114.483849  117.048340
0.840000   58.639070  150.769614  125.367447  127.891278
0.860000   61.687734  154.016311  137.096350  139.574915
0.880000   64.796279  156.746580  149.695201  152.124169
0.900000   67.953711  158.893961  163.181596  165.556935
0.920000   71.147719  160.393647  177.564726  179.882718
0.940000   74.364726  161.183948  192.844014  195.101267
0.960000   77.589966  161.207851  209.007797  211.201259
0.980000   80.807591  160.414636  226.032105  228.159066
1.000000   84.000817  158.761500  243.879597  245.937695


The eigenvalues are:
                          l,real                l,imag

          1 :            0.297688              14.940623
          2 :           -3.383566              36.623520
          3 :           -5.224641              53.193862
          4 :           -6.271663              68.921562

 Unstable: at least one eigenvalue is greater than zero
```

REFERENCE LIST

Bergonzoni, A. and A.J. DiCresce, "The Phenomenon of Draw Resonance in Polymeric Melts," Polymer Engineering and Science, **January**, pp.45-59 (1966).

Chang, H. and A.S. Lodge, "Comparison of Rubberlike-Liquid Theory with Stress-Growth Data for Elongation of a Low-Density Branched Polyethylene Melt," Rheologica Acta, **11**, pp.127-129 (1972).

Chang, J.C. and M.M. Denn,"An Experimental Study of Isothermal Spinning of A Newtonian and A Viscoelastic Liquid," Journal of Non-Newtonian Fluid Mechanics, **5**, pp.369-385 (1979).

Chang, J.C. and M.M. Denn, "Sensitivity of the Stability of Isothermal Melt Spinning to Rheological Constitutive Assumptions," Rheology, **3**: Applications, pp.9-13 (1980).

Chang, J.C., M.M. Denn and F.T. Geyling, "Effect of Inertia, Surface Tension, and Gravity on the Stability of Isothermal Drawing of Newtonian Fluids," Ind. Eng. Chem. Fundam., **20**, No.2, pp.147-149 (1981).

Christensen, R.E., "Extrusion Coating of Polypropylene," S.P.E. Journal, **18**, pp.751-755 (1962).

Demay, Y. and J.-F. Agassant, "Experimental Study of the Draw Resonance in Fiber Spinning," Journal of Non-Newtonian Fluid Mechanics, **18**, pp.187-198 (1985).

Denn, M.M., "Continuous Drawing of Liquids to Form Fibers," Ann. Rev. Fluid Mech., **12**, pp.365-387 (1980).

Denn, M.M., "Fibre Spinning." In Fiber Spinning in Computational Analysis of Polymer Processing, J.R.A. Pearson and S.M. Richardson, eds., Chap.6, pp.179-279. Applied Science Publishers, London (1983).

Denn, M.M., C.J.S. Petrie and P. Avenas, "Mechanics of Steady Spinning of a Viscoelastic Liquid," AIChE Journal, **21**, No.4, pp.791-799 (1975).

Donnelly, G.J. and C.B. Weinberger, "Stability of Isothermal Fiber Spinning of a Newtonian Fluid," Ind. Eng. Chem. Fundam., **14**, No.4, pp.334-337 (1975).

Fisher, R.J. and M.M. Denn, "Draw Resonance in Melt Spinning," Applied Polymer Symposium, No.27, pp.103-109 (1975a).

Fisher, R.J. and M.M. Denn, "Finite-Amplitude Stability and Draw Resonance in Isothermal Melt Spinning," Chemical Engineering Science, **30**, pp.1129-1134 (1975b).

Fisher, R.J. and M.M. Denn, "A Theory of Isothermal Melt Spinning and Draw Resonance," AIChE Journal, **22**, No.2, pp.236-246 (1976).

Fisher, R.J. and M.M. Denn, "Mechanics of Nonisothermal Polymer Melt Spinning," AIChE Journal, **23**, No.1, pp.23-28 (1977).

Fisher, R.J., M.M. Denn and R.I. Tanner, "Initial Profile Development in Melt Spinning," Ind. Eng. Chem. Fundam., **19**, No.2, pp.195-197 (1980).

Fröberg, C.-E., "Numerical Mathematics, Theory and Computer Application," Benjamin-Cumming, Menlo Park, CA (1985).

Gelder, D., "The Stability of Fiber Drawing Processes," Ind. Eng. Chem. Fundam., **10**, No.3, pp.534-535 (1971).

Geyling, F.T. and G.M. Homsy, "Extensional Instabilities of the Glass Fibre Drawing Process," Glass Technology, **21**, No.2, pp.95-102 (1980).

Gupta, R.K. and R.L. Ballman, "A Study of Spinline Dynamics Using Orthogonal Collocation," Chem. Eng. Commun., **14**, pp.22-33 (1982).

Gupta, R.K. and A.B. Metzner, "Modeling of Nonisothermal Polymer Processes," Journal of Rheology, **26**, No.2, pp.181-198 (1982).

Gupta, R.K., J. Puszynski and T. Sridhar, "Steady Spinning of the Oldroyd Fluid B; I: Theory," Journal of Non-Newtonian Fluid Mechanics, **21**, pp.99-113 (1986).

Han, C.D., "A Study of Coextrusion in a Circular Die," Journal of Applied Polymer Science, **19**, pp.1875-1883 (1975).

IMSL User's Manual, IMSL Math/Library Version 1.0, IMSL Inc., Houston, Texas (1987)

Ishihara, H. and S. Kase, "Studies on Melt Spinning. V. Draw Resonance As a Limit Cycle," Journal of Applied Polymer Science, **19**, pp.557-565 (1975).

Ishihara, H. and S. Kase, "Studies on Melt Spinning. VI. Simulation of Draw Resonance Using Newtonian and Power Law Viscosties," Journal of Applied Polymer Science, **20**, pp.169-191 (1976).

Kase, S., "Studies on Melt Spinning. IV. On the Stability of Melt Spinning," Journal of Applied Polymer Science, **18**, pp.3279-3304 (1974).

Kase, S. and M. Araki, "Studies on Melt Spinning. VIII. Transfer Function Approach," Journal of Applied Polymer Science, **27**, pp.4439-4465 (1982).

Kase, S. and T. Matsuo, "Studies on Melt Spinning. I. Fundamental Equations on the Dynamics of Melt Spinning," Journal of Polymer Science, Part A, **3**, pp.2541-2544 (1965).

Kase, S. and T. Matsuo, "Studies on Melt Spinning. II. Steady-State and Transient Solutions of Fundamental Equations Compared with Experimental Results," Journal of Applied Polymer Science, **11**, pp.251-287 (1967).

Kase, S. and T. Nakajima, "Growth of a Dent on an Isothermal Fluid Filament in Uniaxial Extension, A Spinnability Model in Lagrangian Coordinate," Rheol. Acta., **19**, pp.698-709 (1980).

Keunings, R., M.J. Crochet and M.M. Denn, "Profile Development in Continuous Drawing of Viscoelastic Liquids," Ind. Eng. Chem. Fundam., **22**, No.3, pp.347-355 (1983).

Larson, R.G., "Analysis of Isothermal Fiber Spinning with the Doi-Edwards Constitutive Equation," Journal of Rheology, **27**, No.5, pp.475-496 (1983).

Larson, R.G., Constitutive Equations for Polymer Melts and Solutions, Butterworth, Stoneham, MA (1988).

Lee, W.S. and C.-W. Park, "Draw Resonance in Bicomponent Coextrusion Fiber Spinning," (in review) J.Non-Newtonian Fluid Mech. (1992a)

Lee, W.S. and C.-W. Park, "Experiments on Draw Resonance Instability in Coextrusion Fiber Spinning," Proceedings of 50th Annual Technical Conference, Society of Plastics Engineers, Detroit, Michigan, p2181 (March, 1992b)

Lee, W.S. and C.-W. Park, " A New Processing Method for the Fabrication of Plastic Optical Fibers," NSF Design and Manufacturing Systems Grantees Conference, Atlanta, Georgia (January, 1992c)

Lee, W.S. and C.-W. Park, "Analysis of Draw Resonance in a Two-Phase Extensional Flow," AIChE 1992 Annual Meeting, Miami, Florida (November, 1992d)

Mackay, M.E. and C.J.S. Petrie, "An Unusual Prediction Utilising FENE-P Rheological Models in the Fibre-Spinning Problem," Journal of Non-Newtonian Fluid Mechanics, **41,** 365-373 (1992).

Matovich, M.A. and J.R.A. Pearson, "Spinning A Molten Threadline; Steady-State Isothermal Viscous Flows," I&EC Fundamentals, **8**, No.3, pp.512-520 (1969).

Matsumoto, Y. and D.C. Bogue, "Draw Resonance Involving Rheological Transitions," Polymer Engineering and Science, **18**, No.17, pp.564-571 (1978).

Mewis, J. and C.J.S. Petrie, "Hydrodynamics of Spinning Polymers." In Encyclopedia of Fluid Mechanics, N.P. Cheremisinoff, ed., Vol. 6, Chap.4, Gulf Publishing, Houston (1987).

Miller, J.C., "Swelling Behavior in Extrusion," S.P.E. Trans., **3**, pp.134- 137 (1963).

Minoshima, W. and J.L. White, "A Comparative Experimental Study of the Isothermal Shear and Uniaxial Elongational Rheological Properties of Low Density, High Density and Linear Low Density Polyethylenes," Journal of Non-Newtonian Fluid Mechanics, **19**, pp.251-274 (1986a).

Minoshima, W. and J.L. White, "Instability Phenomena in Tubular Film, and Melt Spinning of Rheologically Characterized High Density, Low Density and Linear Low Density Polyethylenes," Journal of Non-Newtonian Fluid Mechanics, **19**, pp.275-302 (1986b).

Nakamura, K., T. Watanabe, K. Katayama and T. Amano, "Some Aspects of Nonisothermal Crystallization of Polymers. I. Relationship Between Crystallization Temperature, Crystallinity, and Cooling Conditions," Journal of Applied Polymer Science, **16**, pp.1077-1091 (1972).

Nakamura, K., T. Watanabe, T. Amano and K. Katayama, "Some Aspects of Nonisothermal Crystallization of Polymers. III. Crystallization During Melt Spinning," Journal of Applied Polymer Science, **18**, pp.615-623 (1974).

Park, C.-W., "Extensional Flow of a Two-Phase Fiber," AIChE Journal, **36**, No.2, pp.197-206 (1990).

Park, C.-W., "A Study on Bicomponent Two-Layer Slot Cast Coextrusion," Polymer Engineering and Science, **31**, No.3, pp.197-203 (1991).

Pearson, J.R.A. and M.A. Matovich, "Spinning A Molten Threadline; Stability," I&EC Fundamentals, **8**, No.4, pp.605-609 (1969).

Pearson, J.R.A. and Y.T. Shah, "Stability Analysis of the Fiber Spinning Process," Transactions of the Society of Rheology, **16**, No.3, pp.519-533 (1972).

Petrie, C.J.S., "Some Results in the Theory of Melt Spinning for Model Viscoelastic Liquids," Journal of Non-Newtonian Fluid Mechanics, **4**, pp.137-159 (1978).

Petrie, C.J.S., "Elongational Flows," Pitman, San Francisco (1979).

Petrie, C.J.S. and M.M. Denn, "Instabilities in Polymer Processing," AIChE Journal, **22**, No.2, pp.209-236 (1976).

Phan-Thien, N. "A Nonlinear Network Viscoelastic Model," Journal of Rheology, **22**, No.3, pp.259-283 (1978).

Phan-Thien, N., "On the Asymptotic Behaviour of an Oldroyd Fluid B in Steady Spinning Flow," Journal of Non-Newtonian Fluid Mechanics, **25**, pp.129-136 (1987).

Phan-Thien, N. and B. Caswell, "A Nearly-Elongational Flow Analysis of the Fibre Spinning Flow," Journal of Non-Newtonian Fluid Mechanics, **21**, pp.225-234 (1986).

Schultz, W.W. and S.H. Davis, "One-Dimensional Liquid Fibers," Journal of Rheology, **26**, No.4, pp.331-345 (1982).

Schultz, W.W. and S.H. Davis, "Effects of Boundary Conditions on the Stability of Slender Viscous Fibers," Journal of Applied Mechanics, **51**, pp.1-5 (1984).

Shah, Y.T. and J.R.A. Pearson, "On the Stability of Nonisothermal Fiber Spinning," Ind. Eng. Chem. Fundam., **11**, No.2, pp.145-149 (1972a).

Shah, Y.T. and J.R.A. Pearson, "On the Stability of Nonisothermal Fiber Spinning - General Case," Ind. Eng. Chem. Fundam., **11**, No.2, pp.150-153 (1972b).

Shah, Y.T. and J.R.A. Pearson, "Stability of Fiber Spinning of Power-Law Fluids," Polymer Engineering and Science, **12**, No.3, pp.219-223 (1972c).

Spearot, J.A. and A.B. Metzner, "Isothermal Spinning of Molten Polyethylene," Transactions of the Society of Rheology, **16**, No.3, pp.495-518 (1972).

Waters, N.D. and A.M. Keeley, "The Stability of Two Stratified Non-Newtonian Liquids in Couette Flow," Journal of Non-Newtonian Fluid Mechanics, **24**, pp.161-181 (1987).

Ziabicki, A., "Fundamentals of Fibre Formation," John Wiley & Sons, New York (1976).

BIOGRAPHICAL SKETCH

Woei-Shyong Lee was born in I-Lan, Taiwan, Republic of China, on October 25, 1958. He received his B.S. degree in chemical engineering from Chung-Cheng Institute of Technology (CCIT), Taoyuan, Taiwan, R.O.C., in 1981. He was a teaching assistant in the Department of Chemical Engineering at CCIT during 1981~1983. In September 1983, he entered National Taiwan University and earned his M.S. degree in chemical engineering in July 1985. After four years of teaching in the Chemical Engineering Department and the Applied Chemistry Department of CCIT, Mr. Lee joined the graduate program in the Department of Chemical Engineering, the University of Florida, in August 1989. He received his Doctor of Philosophy degree from the Department of Chemical Engineering in August of 1993.

I certify that I have read this study and that in my opinion it conforms to acceptable standards of scholarly presentation and is fully adequate, in scope and quality, as a dissertation for the degree of Doctor of Philosophy.

Chang Won Park

Chang-Won Park, Chair
Assistant Professor of Chemical
Engineering

I certify that I have read this study and that in my opinion it conforms to acceptable standards of scholarly presentation and is fully adequate, in scope and quality, as a dissertation for the degree of Doctor of Philosophy.

Ranganathan Narayanan.

Ranganathan Narayanan, Cochair
Professor of Chemical Engineering

I certify that I have read this study and that in my opinion it conforms to acceptable standards of scholarly presentation and is fully adequate, in scope and quality, as a dissertation for the degree of Doctor of Philosophy.

Lewis E Johns Jr

Lewis E. Johns Jr.
Professor of Chemical Engineering

I certify that I have read this study and that in my opinion it conforms to acceptable standards of scholarly presentation and is fully adequate, in scope and quality, as a dissertation for the degree of Doctor of Philosophy.

Arthur L. Fricke

Arthur L. Fricke
Professor of Chemical Engineering

I certify that I have read this study and that in my opinion it conforms to acceptable standards of scholarly presentation and is fully adequate, in scope and quality, as a dissertation for the degree of Doctor of Philosophy.

James K Walker

James K. Walker
Professor of Physics

This dissertation was submitted to the Graduate Faculty of the College of Engineering and to the Graduate School and was accepted as partial fulfillment of the requirements for the degree of Doctor of Philosophy.

August 1993

for

Winfred M. Phillips
Dean, College of Engineering

Madelyn M. Lockhart
Dean, Graduate School